USGS
science for a changing world

Prepared in cooperation with U.S. Environmental Protection Agency, U.S. Bureau of Land Management, California Department of Fish and Wildlife, California Water Boards - Central Valley Regional Water Quality Control Board, and Cosumnes River Preserve

Mercury on a Landscape Scale—Balancing Regional Export with Wildlife Health

By Mark Marvin-DiPasquale, Lisamarie Windham-Myers, Jacob A. Fleck, Josh T. Ackerman, Collin Eagles-Smith, and Harry McQuillen

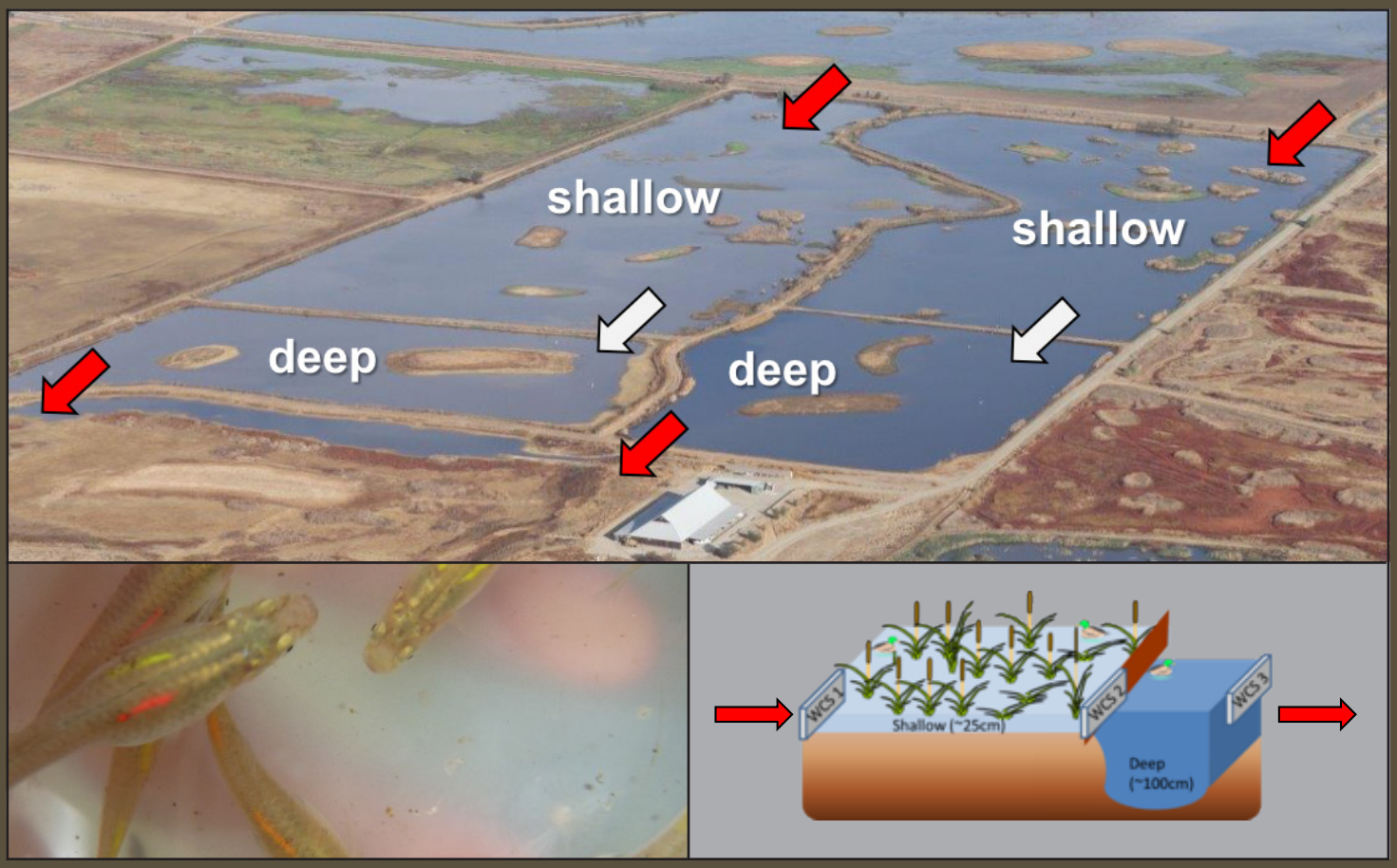

Open-File Report 2018–1092

U.S. Department of the Interior
U.S. Geological Survey

Cover. Upper: Aerial photograph of a portion of the study area (Treatment wetlands 17 and 18), depicting both the upstream shallow cells and downstream deep cells for each of the two experimental wetlands. The arrows indicate the direction of flow (red = inflow and outflow locations; white = location of the weir between the shallow and deep cells). Photograph was taken October 2015 by Tom Palmer, U.S. Bureau of Land Management. Lower: Mosquitofish with elastomer tags. Photograph was taken June 27, 2011 by Josh Ackerman, U.S. Geological Survey, Dixon, California.

Mercury on a Landscape Scale—Balancing Regional Export with Wildlife Health

By Mark Marvin-DiPasquale, Lisamarie Windham-Myers, Jacob A. Fleck, Josh T. Ackerman, Collin Eagles-Smith, and Harry McQuillen

Prepared in cooperation with U.S. Environmental Protection Agency, U.S. Bureau of Land Management, California Department of Fish and Wildlife, California Water Boards - Central Valley Regional Water Quality Control Board, and Cosumnes River Preserve

Open-File Report 2018–1092

U.S. Department of the Interior
U.S. Geological Survey

U.S. Department of the Interior
RYAN K. ZINKE, Secretary

U.S. Geological Survey
James F. Reilly II, Director

U.S. Geological Survey, Reston, Virginia: 2018

For more information on the USGS—the Federal source for science about the Earth, its natural and living resources, natural hazards, and the environment—visit https://www.usgs.gov/ or call 1–888–ASK–USGS (1–888–275–8747).

For an overview of USGS information products, including maps, imagery, and publications, visit https://store.usgs.gov/.

Suggested citation:
Marvin-DiPasquale, M., Windham-Myers, L., Fleck, J.A., Ackerman, J.T., Eagles-Smith, C., and McQuillen, H., 2018, Mercury on a landscape scale—Balancing regional export with wildlife health: U.S. Geological Survey Open-File Report 2018–1092, 93 p., https://doi.org/10.3133/ofr20181092.

ISSN 2331-1258 (online)

Contents

Abstract 1
Introduction 3
Project Goals 5
Hypotheses 5
Field Setting, Preparation and Management 6
  Environmental Setting 6
  Wetland Selection and Field Preparation 7
    Water Management 11
Methods 14
  Field Sampling 14
    Surface Water 15
      Routine Water Samples 15
      Continuous Monitoring Effort 15
      Particulate Flux 16
        Long-Term Seasonal Particulate Flux – Felt Pads 16
        Short-Term Particulate Flux 18
      Water Column Light Extinction Coefficients 21
    Surface Sediment 21
      Collection, Sub-sampling and Preservation 21
    Fish Tagging, Deployment into Cages, and Retrieval 22
  Laboratory Analylses 25
    Initial Processing and Preservation of Routine Water Samples 27
    Total Suspended Solids 28
    Water Isotopes 28
    Sediment Demethylation Incubations 28
    Quality Assurance Results for Sediment and Water Parameters 29
    Total Mercury Determination in Fish 29
  Calculations, Modeling & Statistics 31
    Surface Water 31
      Load Calculations 31
      Mercury Fractions Calculated and Defined 32
      Statistical Models 32
    Sediment 33
      Methylmercury Degradation Potential Rates 33
      MeHg Benthic Diffusive Flux Estimates 33
      Statistical Models 34
    Photodemethylation 35
    Statistical Analysis of Fish 35
Results and Discussion 36
  Surface Water Total Mercury and Methylmercury Concentrations and Loads 36
    Concentrations 37
    MeHg Loads 41
  Particulate Trapping in the Deep Cells 50
    Particulate Trapping via TSS Loads Analysis 51
    Long-Term Seasonal Particulate Flux–Felt Pads 51

Short Term (24 hour) Particulate Flux–Settling Traps 54
Particulate Total Mercury and Methylmercury Removal in the Deep Cells 56
Methylmercury Loss via Photodemethylation 57
Methylmercury Loss via Benthic Microbial Demethylation 59
Methylmercury Benthic Diffusive Flux Estimates 63
Deep Cell MeHg Budget 64
MeHg Box Models 67
Mercury Bioccumulation Studies 73
Fish Body Mass 75
Ancillary Data and Results 76
Hydrology 76
Excitation Emissions Spectra 76
Water Isotopes 79
Surface Sediment Characterization 82
Conclusion 82
Hypotheses Revisited 83
Reflections on Lessons Learned, Challenges Encountered and Going Forward 83
Key Lessons Learned 84
Key Challenges 84
New Question Raised 84
Thoughts for Next Phase Studies and Improved Study Design 85
Acknowledgments 87
References Cited 88
Appendixies 1–10 93

Figures

1. Location maps of the Cosumnes River Preserve study area 6
2. Map and field identification of seasonal wetlands studied 8
3. Design diagrams of treatment and control wetlands 9
4. Photographs of the hydrology and water quality equipment 12
5. Project timeline of field sampling events 14
6. Photographs of long-term particulate settling felt pads 17
7. Maps with field identification showing the location of sediment sampling sites, long-term particle deposition pads, short-term particle flux traps, and inlet/outlet locations in the four deep cells 18
8. Photographs of short-term (24 hour) particulate trapping elevators 19
9. Photographs of field deployment of bioaccumulation study with caged fish 24
10. X–Y plot comparing mosquitofish THg concentration analytical results from the USGS Dixon, Calif. laboratory with the USGS Corvallis, Oreg. Laboratory for the Cosumnes River Preserve mercury study 30
11. Bar plots of MODEL A.2 results for whole water total mercury and methymercury concentration 38
12. Bar plots of MODEL A.2 results for filter-passing total mercury and methylmercury concentration 39
13. Bar plots of MODEL A.2 results for particulate total mercury andmethylmercury concentration 40

14. Bar plots of MODEL A.2 results for filter-passing, particulate, andunfiltered (wholewater) by water control structure type, season, and year 43
15. Bar plots of mean annually integrated THg and MeHG mass loads 44
16. Bar plots of mean annually integrated net change between inlets and outlets for THg and MeHg mass loads within control and treatment wetlands 47
17. Bar plots of mean annually integrated net change for THg and MeHg mass loads in the shallow cells between the check weir and the inlet and deep cells between the outlet and the check weir 49
18. Maps depicting annual particulate deposition (areal basis) within the four deep cells 52
19. Photograph showing an example of turbidity within deep cell D07 53
20. Bar plots of daily total suspended solid (TSS) flux 55
21. Time series plots of areal methylmercury (MeHg) photodegradation monthly average rates in nanograms per square meter per day (ng/m^2/d) for the deep cells 58
22. Bar plots of benthic MeHg degradation potential (MDP) rates 60
23. Bar plots of the net daily rate of change in the ambient MeHg pool 62
24. Box model of MeHg mass loading and within-cell loss (or production) for deep cell D01 68
25. Box model of MeHg mass loading and within-cell loss (or production) for deep cell D07 69
26. Box model of MeHg mass loading and within-cell loss (or production) for deep cell D17 70
27. Box model of MeHg mass loading and within-cell loss (or production) for deep cell D18 71
28. Box model of MeHg mass loading and within-cell loss (or production) for all deep cells 72
29. Geometric means for mosquitofish THg concentrations in micrograms per gram dry weight (µg/g dw) among cage locations (sub-site) within control and treatment wetlands 74
30. Change in mosquitofish body mass in grams (g) from the time of introduction to retrieval 30 days later among cage locations (sub-site) within control and treatment wetlands 75
31. Excitation-Emissions (EEM) Spectra ratio plots for water control structure (WCS) comparisons in treatment wetland T07 78
32. Plot of surface water δ^2H versus δ^{18}O isotopic data 79
33. Contour maps of surface water δ-excess during February 2016 81

Tables

1. Study design, field number and cell characterization of control wetlands and treatment wetlands 10
2. Latitude and longitude data for water control structures 13
3. Latitude and longitude data for deep cell particle trap elevators 21
4. Latitude and longitude data for sediment sampling sites 22
5. Surface water analytical methods used 25
6. Sediment analytical methods used 27
7. Annually integrated total mercury loads 45
8. Annually integrated methylmercury loads 45
9. Mean annual unfiltered surface water MeHg/THg load ratios 46
10. Annually integrated particulate net loss or production within the deep cells 51
11. Annual particulate deposition within the deep cells 53
12. Annually integrated particulate flux to the benthos 56
13. Annually integrated change in particulate total mercury (THg) within the deep cells 56
14. Annually integrated photodemethylation rates for the deep cells 59

15. Annually integrated methylmercury degradation potential in surface sediment of the deep cells 61
16. Annually integrated net change in ambient methylmercury pools in surface sediment of deep cells 63
17. Annually integrated methylmercury benthic diffusive flux in deep cells 63
18. Annually integrated MeHg loads, normalized to area, entering and exiting the deep cells 64
19. Annually integrated net MeHg loss within the deep cells 65
20. Annually integrated percent MeHg loss within the deep cells 66

Conversion Factors

International System of Units to U.S. customary units

Multiply	By	To obtain
	Length	
centimeter (cm)	0.3937	inch (in.)
millimeter (mm)	0.03937	inch (in.)
meter (m)	3.281	foot (ft)
meter (m)	1.094	yard (yd)
	Area	
square meter (m^2)	0.0002471	acre
hectare (ha)	2.471	acre
square meter (m^2)	10.76	square foot (ft^2)
hectare (ha)	0.003861	square mile (mi^2)
	Volume	
liter (L)	33.81402	ounce, fluid (fl. oz)
liter (L)	2.113	pint (pt)
liter (L)	1.057	quart (qt)
liter (L)	0.2642	gallon (gal)
cubic meter (m^3)	264.2	gallon (gal)
cubic meter (m^3)	0.0002642	million gallons (Mgal)
cubic centimeter (cm^3)	0.06102	cubic inch (in^3)
liter (L)	61.02	cubic inch (in^3)
cubic meter (m^3)	0.0008107	acre-foot (acre-ft)
cubic hectometer (hm^3)	810.7	acre-foot (acre-ft)
	Flow rate	
cubic meter per second (m^3/s)	70.07	acre-foot per day (acre-ft/d)
cubic meter per year (m^3/yr)	0.000811	acre-foot per year (acre-ft/yr)
cubic meter per second (m^3/s)	35.31	cubic foot per second (ft^3/s)
liter per second (L/s)	15.85	gallon per minute (gal/min)
	Mass	
gram (g)	0.03527	ounce, avoirdupois (oz)
kilogram (kg)	2.205	pound avoirdupois (lb)
	Density	
gram per cubic centimeter (g/cm^3)	62.4220	pound per cubic foot (lb/ft^3)

Temperature in degrees Celsius (°C) may be converted to degrees Fahrenheit (°F) as °F = (1.8 × °C) + 32.
Temperature in degrees Fahrenheit (°F) may be converted to degrees Celsius (°C) as °C = (°F – 32) / 1.8.

Datum

Horizontal coordinate information is referenced to the World Geodetic System Datum of 1984 (WGS 84)].

Supplemental Information

Transmissivity: The standard unit for transmissivity is cubic meter per day per square meter times meter of aquifer thickness ([m^3/d]/m^2)m. In this report, the mathematically reduced form, meter squared per day (m^2/d), is used for convenience.
Specific conductance is given in microsiemens per centimeter at 25 degrees Celsius (µS/cm at 25 °C).
Concentrations of chemical constituents in water are given in either milligrams per liter (mg/L) or micrograms per liter (µg/L).
Activities for radioactive constituents in water are given in picocuries per liter (pCi/L).
Results for measurements of stable isotopes of an element (with symbol E) in water, solids, and dissolved constituents commonly are expressed as the relative difference in the ratio of the number of the less abundant isotope (^{l}E) to the number of the more abundant isotope of a sample with respect to a measurement standard.
Note to USGS users: Use of hectare (ha) as an alternative name for square hectometer (hm^2) is restricted to the measurement of small land or water areas. Use of liter (L) as a special name for cubic decimeter (dm^3) is restricted to the measurement of liquids and gases. No prefix other than milli should be used with liter.

Abbreviations, Acronyms, and Chemical Notation

Abbreviations

cfs	cubic feet per second
cm	centimeter
cm^3	cubic centimeter
d.w.	dry weight
f	foot
g	gram
g/cm^3	gram per cubic centimeter
ha	hectares
kg	kilogram
L	liter
m	meter
mg	milligram
mL	milliliter
mm	millimeter
µg	microgram
µg/g	microgram per gram
µg/L	microgram per liter
µg/m^2	microgram per square meter
µm	micrometer
ng	nanogram
ng/g	microgram per gram
ng/L	nanogram per liter
ppm	parts per million
<	less than
%	percent

Acronyms

BLM	Bureau of Land Management
CHK-IN	difference in constituent load between the check weir and the inlet or the shallow cells
CRM	certified reference material
CRP	Cosumnes River Preserve
CVRWQCB	Central Valley Regional Water Quality Control Board
DFW	California Department of Fish and Wildlife
DI	deionized water

DO	dissolved oxygen
DOC	dissolved organic carbon
DOM	dissolved organic matter (includes carbon)
dw	dry weight
EEM	excitation-emissions
fDOM	fluorescent dissolved organic matter (includes carbon)
FeRB	iron-reducing bacteria
FNU	formazin nephelometric units
GMWL	global meteoric water line
HPLC	high performance liquid chromatography
IAEA	International Atomic Energy Agency
ICP-MS	Inductively coupled plasma mass spectrometry
LMWL	local meteoric water line
LSM	least squares means
%LOI	loss on ignition (percentage)
MDP	methylmercury degradation potential
OUT-CHK	difference in constituent load between the outlet and the check weir for the deep cells
OUT-IN	difference in constituent load between outlets and inlets
PAR	photosynthetically active radiation
PETG	polyethylene terephthalate
PT	pressure transducer
PVC	polyvinyl chloride
SC	Specific Conductance
SE	standard error
SFB	San Francisco Bay
SPM	suspended particulate matter
SRB	sulfate-reducing bacteria
TMDL	Total Maximum Daily Load
TSS	total suspended solids
USGS	U.S. Geological Survey
WCS	water control structure(s)
WY	water year

Chemical Notation

CH_3OH	methanol
Cl^-	chloride anion
Fe(II)AE	acid extractable ferrous iron
Fe(III)a	amorphous (poorly crystalline) ferric iron
Fe(III)c	crystalline ferric iron
Fe_T	total measured iron ($Fe(II)_{AE}$ + $Fe(III)_a$ + $Fe(III)_c$)
f.MeHg	filtered methylmercury (monomethyl mercury)
f.THg	filtered total mercury
HCl	hydrochloric acid
Hg	mercury
Hg(II)	mercuric ion
K_d	partitioning coefficient
KOH	potassium hydroxide
MeHg	methylmercury (monomethylmercury)
N_2	dinitrogen gas
O_2	molecular oxygen (gas)
p.MeHg	particulate (water column) monomethylmercury
p.RHg	particulate (water column) reactive mercury
p.THg	particulate (water column) total mercury
pw.MeHg	sediment porewater monomethylmercury
SO_4^{2-}	sulfate anion
THg	total mercury

uf.MeHg	unfiltered (whole water) monomethylmercury
uf.THg	unfiltered (whole water) total mercury

Mercury on a Landscape Scale—Balancing Regional Export with Wildlife Health

By Mark Marvin-DiPasquale, Lisamarie Windham-Myers, Jacob Fleck, Josh T. Ackerman, Collin Eagles-Smith and Harry McQuillen

Abstract

The Cosumnes River watershed requires a 57–64 percent reduction in loads to meet the new Delta methylmercury (MeHg) total maximum daily load allocation, established by the Central Valley Regional Water Quality Control Board. Because there are no large point sources of MeHg in the watershed, the focus of MeHg load reductions will fall upon non-point sources, particularly the expansive wetlands considered to be a primary source of MeHg in the region (Wood and others, 2010). Few management practices have been implemented and tested in order to meet load reductions in managed wetlands, but recent efforts have shown promise. This project examines a treatment approach to reduce MeHg loads to the Sacramento-San Joaquin River Delta by creating open-water deep cells with a small footprint at the downstream end of wetlands to promote net demethylation of MeHg and to minimize MeHg and Hg loads exiting wetlands at the Cosumnes River Preserve. Specifically, the deep cells were were located immediately up gradient of the wetland's outflow weir and were deep enough (75–91 centimeter depth) to be vegetation-free. The topographic and hydrologic structure of each treatment wetland was modified to include open-water deep cells so that the removal of aqueous MeHg might be enhanced through (1) particle settling, (2) photo-degradation, and (3) benthic microbial demethylation. These deep cells were, therefore, expected to clean MeHg from surface water prior to its discharge to the Cosumnes River and the downstream Delta.

Our goal was to test whether the implementation of the deep cells within wetlands would minimize MeHg and total Hg export. Further, we sought to test whether continuous flow-through hydrology, would lower MeHg concentrations in resident biota, compared to traditoinal wetland management operations. The dominant practice in seasonal wetlands management is the "fill-and-maintain" approach, in which wetlands are filled with water and the water levels maintained without substantial draining until drawdown. Our approach was to create and characterize replicate treatment wetland complexes, in conjunction with monitoring of hydrologic, biologic, and chemical indicators of MeHg exposure for two full annual cycles within winter-spring flooded seasonal wetlands. In addition to the creation of deep cells within treatment wetlands, hydrology was manipulated so that there was a constant flow-through of water, while the control wetlands utilized the fill-and-maintain approach. Specifically, the treatment wetlands were maintained in a flow-through manner, while the control wetlands were maintained in a fill-and-maintain manner from September through May, to test the hypothesis that the flow of water through the seasonal wetland can lower fish bioaccumulation through dilution of MeHg-concentrated water within the wetland by constant inflows of water into the wetland.

The major tasks of this study included: (1) field design and implementation, (2) water and wetland management, (3) hydrologic monitoring and water quality sampling, (4) MeHg export and load estimates, (5) caged fish experiments for examining MeHg bioaccumulation, (6)

site and process characterization to improve understanding and transferability of results, (7) adaptive management, transferability, and outreach, and (8) reporting of results and conclusions. This report summarizes the key findings of this study, which focuses on MeHg load estimates from control and treatment wetlands, quantification of three MeHg removal mechanisms (particulate settling, benthic demethylation, and photo-demethylation) in the deep cells within the treatment wetlands, and MeHg bioaccumulation in wetland fishes.

Key findings include:

- Over two years of study, mean whole-water MeHg load decreased 37 percent in deep cells, when comparing inlet of check weir flows to outlet.
- Of the 37 percent MeHg load removed within the deep cell, photodegradation accounted for 7 percent and particle flux to the benthos accounted for 24 percent of the mass removed, with the remaining 6 percent apparent MeHg loss unexplained.
- Benthic MeHg degradation did not appear to be a major MeHg removal process in the deep cells, as changes in the ambient MeHg pool over 7-day bottle incubations showed that the surface sediment exhibited net MeHg production in the majority (87 percent) of incubation experiments. In only 13 percent of the incubations (3 out of 24) was net MeHg degradation observed.
- Estimates of benthic diffusive flux of MeHg across the sediment/water interface were small relative to particulate flux and variable (positive or negative), suggesting this is likely a minor term in the overall MeHg budget within the deep cells.
- Although the deep cells served as net MeHg sink overall, MeHg export from the flow-through treatment wetlands (shallow and deep combined) exceeded export from the fill-and-maintain managed control wetlands, because of the differences in hydrologic management between the two wetland types.
- Shallow wetlands under flow-through conditions generated a net export of MeHg.
- Most of the annual MeHg export from the treatment wetlands occurred within the first 3 months of flood up (September to November), shortly after hydrologic management began.
- Despite the effectiveness of the deep cell in lowering MeHg export concentrations, total mercury (THg) concentration did not decrease in biosentinel fish (*Gambusia affinis*, Mosquitofish) between the deep cell inlet and outlet.
- Mosquitofish THg concentrations were higher in treatment wetlands than in control wetlands during the first year of study, likely because of an associated increase in MeHg availability immediately following wetland construction activities. Mosquitofish THg concentrations declined in the treatment wetlands during the second year of study, and fish THg concentrations in treatment wetlands were no different from those in the control.
- Similarly, the increased hydrologic flow rates in the treatment wetlands did not lower fish THg concentrations nor aqueous MeHg concentrations in the shallow cells, suggesting that MeHg flux from the sediment to water column exceeded the flow-through flushing rate in the shallow portion of the treatment wetlands.
- Reductions in MeHg concentrations of surface water and fish may require higher flow rates than used in the study to achieve the region's regulatory goals. However, the flow rates necessary may not be feasible for these managed wetlands because of limited water supply and the associated costs for water and pumping.
- The use of deep cells in seasonal wetlands were effective in lowering MeHg exports under continuous water flow-through hydrology. However, fill-and-maintain hydrology

had lower exports overall, because of a single major drainage event at the end of the flood season.

- Future studies focused on limiting MeHg export should consider combining deep cells with the fill-and-maintain or fill-and-trickle hydrologic management approach.

Introduction

The Central Valley Regional Water Quality Control Board (CVRWQCB) is gathering information in order to review methylmercury (MeHg) total maximum daily load (TMDL) for the Sacramento-San Joaquin River Delta. The Cosumnes River watershed has been identified as a seasonal hotspot for total mercury (THg) and MeHg production and discharge to the Delta (Marvin-DiPasquale and others, 2007; Wood and others, 2010; Eagles-Smith and others, 2014). The watershed contains vast floodplains, managed wetland habitats, and rice agriculture, which are all habitat types known to contribute to increases in MeHg in the environment (Zillioux and others, 1993; Ackerman and Eagles-Smith 2010; Windham-Myers and others, 2014a). There are ongoing and planned efforts to restore additional wetland habitats in the Cosumnes River watershed that may further increase MeHg loading to the Delta.

In the Delta MeHg TMDL, a 57–64 percent reduction in current loads from the Cosumnes River watershed is proposed (Wood and others, 2010). Wetlands and rice agriculture are thought to be potentially significant MeHg production sites in the Delta (Windham-Myers and others, 2014a). Approximately 40 percent of the aqueous MeHg present in the Delta is estimated to be produced in place, with roughly 50 percent contributed from sediments in open-water habitats (for example, channels) and 50 percent from wetlands (Wood and others, 2010). The production of MeHg is facilitated by sulfate-reducing bacteria (SRB) and iron-reducing bacteria (FeRB) that are active largely in the sediment zone (Gilmour and others, 1992; Fleming and others, 2006; Kerin and others, 2006). The inorganic Hg(II)-methylation process is largely controlled by the activity of those bacteria (limited by sulfate, ferric iron, and/or organic matter) and by the availability of inorganic Hg(II) to these bacteria. The role of wetland plants (both type and density) is a critical factor mediating MeHg production by the bacteria in sediments (Windham-Myers and others, 2009; Windham-Myers and others, 2014b). Since Hg forms strong bonds with dissolved organic matter (DOM; Gasper and others, 2007), the type, production and flux of DOM from wetlands and rice agriculture in the Delta may also influence both THg and MeHg production, discharge, bioaccumulation and transport.

Past mining activities in the upper portion of the watershed have resulted in extensive Hg contamination within the Cosumnes River and the fluvial plain of the lower watershed. The abundance of restored and managed wetlands and floodplains within the lower Cosumnes River watershed facilitates MeHg production, resulting in elevated discharges to the Sacramento-San Joaquin River Delta (Marvin-DiPasquale and others, 2007; Wood and others, 2010). The floodplains and wetlands are also important because they serve as habitats for rearing native fishes, support wintering migratory birds and breeding birds, and improving overall ecosystem function and services of the area (Jeffres and others, 2008; Seavy and others, 2009). Therefore, it is critical to protect and expand these wetland habitats while also reducing contamination to resident biota and MeHg export to the downstream environments of the Sacramento-San Joaquin River Delta.

The goals of the current project were two-fold:

- To test a promising management strategy—the inclusion of deep cells—for altering wetland topography (and thus hydrology) to limit MeHg discharge to the Delta and reduce MeHg bioaccumulation within fish using this portion of the wetland; and

- To examine if the manipulation of hydrologic flow through the wetland complex can decrease bioaccumulation in fish.

Three primary mechanisms of MeHg removal within the deep cells were investigated:

1. Photodegradation,
2. Particulate settling, and
3. Microbial demethylation in the benthos.

This study comes at a critical time when the need for strategies to limit MeHg transport and bioaccumulation in the Delta have been identified (McCord and Heim, 2015). The 2003 Mercury Strategy for the Bay-Delta Ecosystem (Wiener and others, 2003) explicitly called for the "Quantification of effects of ecosystem restoration on methylmercury exposure" and the "Identification and testing of potential management approaches for reducing methylmercury contamination". This 2003 call to action was recently revisited in a series of meetings held in Sacramento, California during 2016, and while some progress has been made, there was general consensus that much more needs to be done with respect to these two points. We are aware of only one other effort to look at the effectiveness of adding deep cells at the downstream end of seasonal wetland habitats as a way of decreasing MeHg export to the downstream Delta, a study at the Yolo Wildlife Area being carried out by researchers at the Moss Landing Marine Laboratory (MLML) and others. One key difference between the two study efforts is habitat hydrology; the MLML study is being conducted in constructed ponds that are permanently flooded with fill-and-maintain conditions, while our study considers deep-water cells included within the existing seasonal wetlands that are typically flooded from September to May.

Initial funding for this study was obtained as part of a 2013 Clean Water Act 319(h) Implementation grant awarded to Bureau of Land Management (BLM) in collaboration with the U.S. Geological Survey (USGS; CA State Agreement# 13-504-255). This funding supported two field seasons of study for:

- Creation of deep cells within four treatment wetlands at Cosumnes River Preserve (CRP);
- Management and monitoring of hydrology (stage) and basic water quality parameters (conductivity, pH, dissolved oxygen, and temperature) in the four treatment and four control wetlands;
- Measurement of particulate and filter-passing THg and MeHg in surface water at the water control structures (inlets and outlets) of the treatment and control wetlands;
- Calculation of filtered and filter-passing THg and MeHg loads and net export;
- Calculation of MeHg photodegradation based upon established relations between photosynthetic active radiation (PAR) and dissolved MeHg concentration;
- Initial site characterization with respect to sediment THg and MeHg concentrations; and
- Conducting caged fish experiments to assess Hg bioaccumulation in biosentinel western mosquitofish (*Gambusia affinis*) within wetland habitats critical for fish and wildlife.

Additional funding from the California Department of Fish and Wildlife (DFW) Ecosystem Restoration Program (Grant #: E1483002) allowed for the measurement of additional processes and characterization that could not to be supported with the Clean Water Act 319(h) funds. The additional activities supported by the DFW funding included:

- Direct measurement of MeHg degradation potential rates (via stable isotope amendment assays) in deep cell surface sediment;
- Assessment of seasonal particulate vertical flux and trapping in the deep cells via the use of felt deposition pads;
- Assessment of short-term (24 hour) particulate vertical flux and trapping in the deep cells via the use of settling traps;
- Assessment of hydraulic residence time;

- Additional sediment samples for better characterization of Hg species concentration and organic content;
- A 20 percent increase in caged fish analysis for improved statistics to test site differences;
- An increase in the number of sampling events (from 4 to 7 per year) for surface water dissolved and particulate THg and MeHg to increase statistical power to assesses Hg species loads;
- Surface water dissolved organic carbon characterization; and
- Surface water particulate characterization in terms of chlorophyll and particulate organic carbon and nitrogen content.

This report provides a synthesized summary of the key results of this study, as supported by both funding sources.

Project Goals

The overall goal of this study was to test whether the implementation of deep cells at the downstream end of seasonal wetland habitats would minimize MeHg export while also lowering Hg in resident biota, compared to current wetland management operations (fill, maintain and drain) by performing the following:

- Construction of treatment wetlands (deep cell at the downstream end of a seasonal wetland) and water managed as a continuous flow-through condition in four seasonal wetlands within Cosumnes River Preserve. The deep cell footprint was built to be approximately 20 percent of the surface area of the adjacent seasonal wetland.
- Quantification of particulate and dissolved THg and MeHg load and export through both treatment wetlands (with deep cell and water managed as continuous flow through) and control wetlands (no deep cell construction and water managed in a traditional a fill-and-maintain mode) over two years of seasonally flooding (September to May) at all water control structures (WCS) in both treatment and control wetlands.
- Determination if treatment wetlands reduced Hg bioaccumulation in biosentinel fish caged at specific locations within wetlands.
- Quantification of the aqueous MeHg removal processes and rates within the deep cells: photodemethylation, benthic microbial demethylation, and particle settling.

Hypotheses

The study hypotheses (HYP) detailed below are those explicitly tested with the data collected over the two years of study.

- HYP 1: The presence of deep cells will reduce the load of MeHg and THg exported from the shallow portion of the treatment wetlands.
- HYP 2: The presence of deep cells at the downstream end of seasonal wetlands will reduce THg bioaccumulation in caged fish at the outlet of the deep cell relative to upstream WCS in the seasonal wetland and the outlet of the control wetlands.
- HYP 3: The hydrologic flow-through management approach will result in lower surface water MeHg concentrations in treatment wetlands compared to control wetlands with fill-and-maintain water management.
- HYP 4: The hydrologic flow-through management approach will result in lower biota (*Gambusia*; caged fish) THg concentrations in shallow treatment wetlands, compared to the fill-and-maintained water management approach in control wetlands.

- HYP 5: The hydrologic flow-through management approach will result in increased surface water MeHg and THg loads from the shallow portion of the treatment wetlands compared to the fill-and-maintain control wetlands.

Field Setting, Preparation and Management

This study focused on approximately 80 hectares (ha) of seasonally flooded and managed wetland fields within the CRP. The CRP is located at the lower southwestern end of the Cosumnes River watershed, which drains 198,900 ha of the western Sierra Nevada (fig. 1). A brief description of the CRP environmental setting, the field preparation for the study, and the hydrologic management of treatment and control wetland cells follows.

Environmental Setting

The CRP encompasses more than 20,000 ha of wetland, upland, and agricultural land. The Preserve is owned by a consortium of seven land-owning partners (The Nature Conservancy, BLM, DFW, Sacramento County, California Department of Water Resources, Ducks Unlimited, and the California State Lands Commission), and is managed by BLM for the protection of a continuous riparian corridor extending from the Cosumnes River headwaters to the Sacramento-San Joaquin Delta. The Preserve is composed of a mosaic of habitats that include floodplains, vernal pool grasslands, seasonal and permanent wetlands, valley oak (*Quercus lobata*) woodlands, and wildlife-compatible agriculture (such as rice fields). This diversity of habitats supports an abundance of native and non-native plants, fish, and wildlife including thousands of migratory and wintering waterbirds and several special status species, such as sandhill cranes [*Grus canadensis*], giant garter snake [*Thamnophis gigas*], western pond turtle [*Actinemys marmorata*], and native fish species. It is also an especially important habitat for breeding birds.

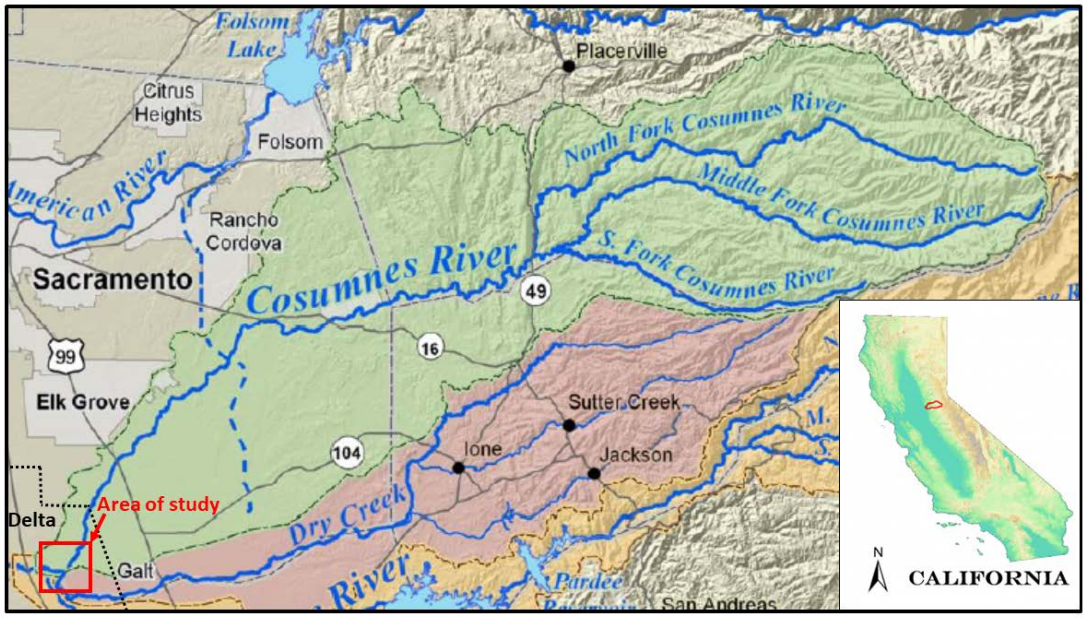

Figure 1. Location map showing the general location of the Cosumnes River Preserve study area (red square) within the Cosumnes River watershed. The inset map shows the location of Cosumnes River watershed (red outline) on the western edge of the Sacramento-San Joaquin Delta and Central Valley in California, USA.

Wetland Selection and Field Preparation

Eight managed freshwater wetland fields at the CRP were selected for the study (fig. 2), each with an approximate area of 10 ha. A stratified approach was used to assign four of the eight seasonal wetlands as control wetlands (C# fields: C02, C06, C09 and C13) and four as treatment wetlands (T# fields: T01, T07, T17 and T18). Treatment wetlands were divided into two spatial components (cells) separated by the construction of an earthen check levee,an internal levee between the shallow cell and deep cell in a treatment wetland that restricted the flow of water from the shallow cell to the deep cell through a single conduit. The original shallow vegetated zone (S# cells: S01, S07, S17 and S18) represented approximately 80 percent of the treatment wetland area. The deep cells (D# cells: D01, D07, D17 and D18), which were cleared of vegetation and scraped to a depth of up to 1 meter (m) to maintain open-water conditions, represented approximately 20 percent of the treatment wetland (figs. 2 and 3). Ultimately, the wetland areas selected for deep cell were those with the most efficient slope configuration. The acreage and average depth of each wetland is summarized in table 1. All deep cells were constructed to the extent possible to have a similar volume of water within the deep cell as within the upstream, shallow cell portion of the treatment wetland (table 1). Thus, the deep and shallow cells within each treatment wetland were designed to have nearly equal water residence time within each cell component despite different surface acreages. Engineering surveys confirmed the configuration and water volumes of each cell within treatment wetlands.

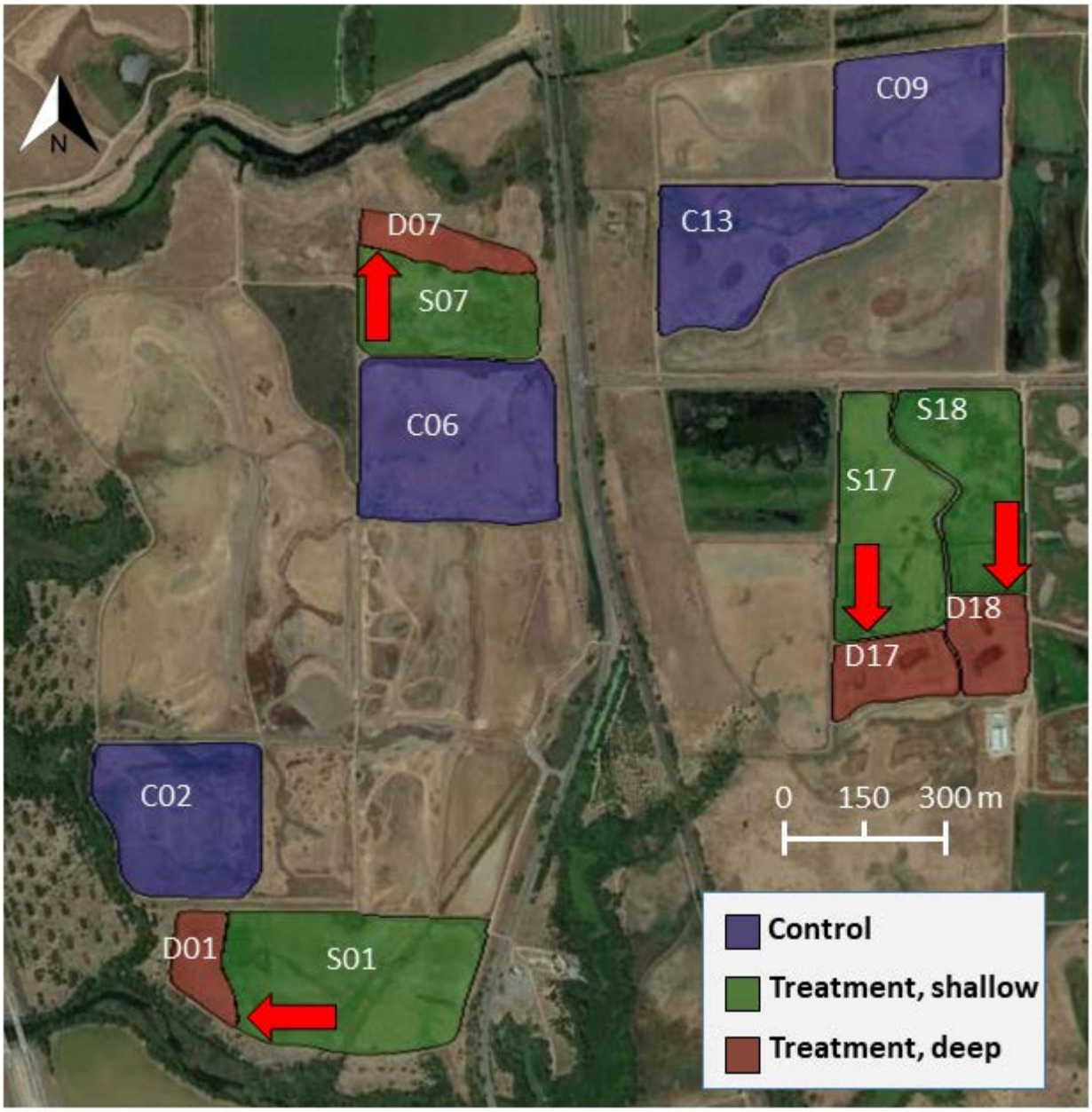

Figure 2. Map and field identification of seasonal wetlands studied within the Cosumnes River Preserve. Control wetlands (C##) are shown in purple and the treatment wetlands are shown in red/green. Each treatment Wetland consisted of two sections, one shallow cell (S##, in green) and one deep cell (D##, in red), with the shallow cells representing 80 percent of the total area of each treatment wetland. The red arrows indicate the direction of flow within the treatment wetlands, from the shallow to the deep cells.

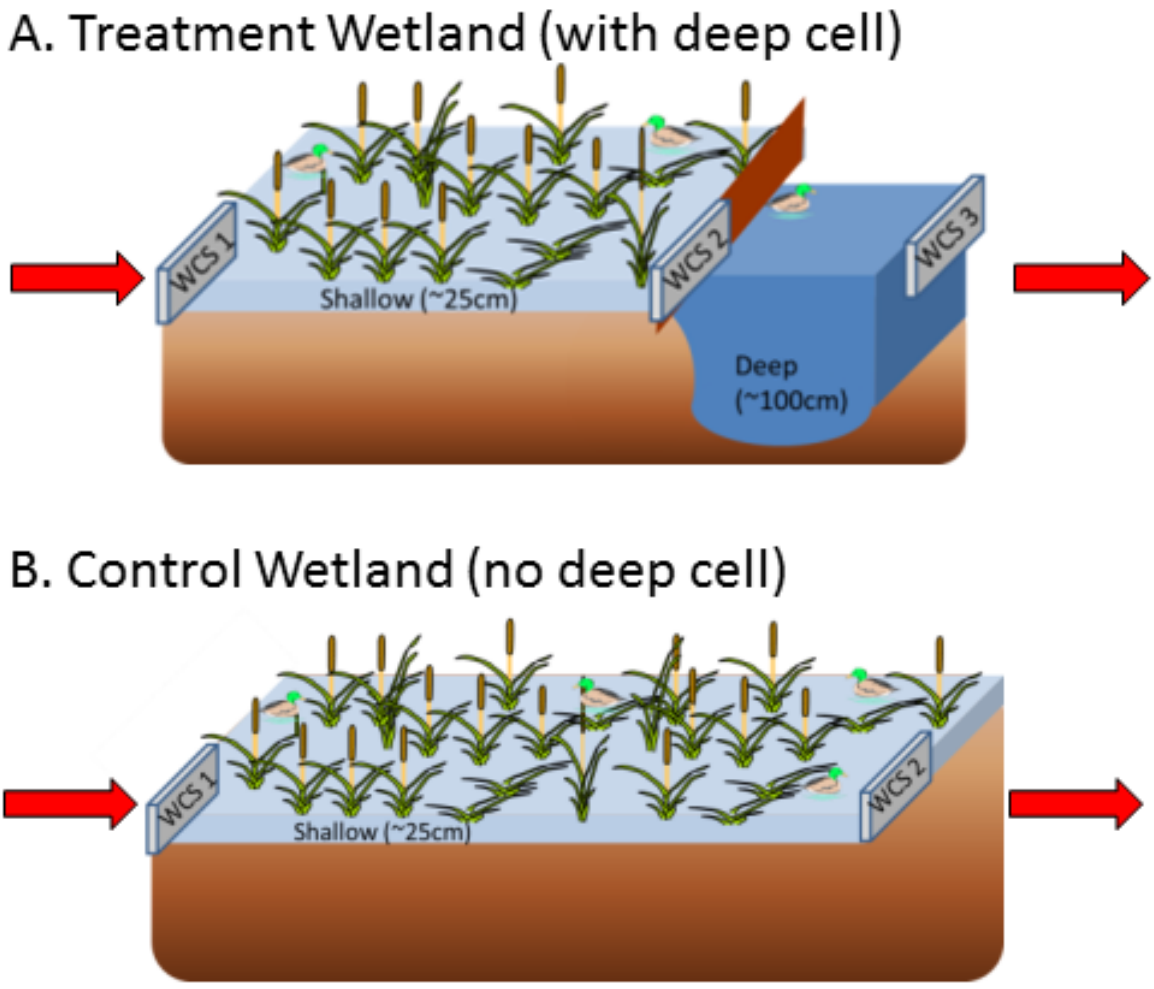

Figure 3. Design diagrams of *A*, treatment and *B*, control wetlands in the Cosumnes River Preserve mercury study area. *A*, Water control structures (WCS) for monitoring hydrologic and constituent loads are shown as: WCS1 (inlet), WCS 2 (check levee weir for treatment wetland and outlet for control wetland), and WCS3 (outlet for treatment wetland). The red arrows indicate the direction of water flow.

Cells varied slightly with respect to water depth during the flooded period and management practices during the dry period (extent of area scraped, mowed, or disced; table 1). Vegetation management (discing and mowing) conducted during the dry (nonflooded) season were applied similarly to each of the shallow cells within treatment wetlands and control wetlands during both study years. Because of soil scraping and removal required to achieve the target water depths, deep cells were barren of vegetation at the time of flood up during study Year 1 (September 2014). During summer 2015, and prior to the flood up at the beginning of study Year 2, any vegetation in the deep cells was mowed to a height of 6 inches.

Table 1. Study design, field number and cell characterization of control wetlands and treatment wetlands in the Cosumnes River Preserve mercury study.
[D, deep; S, shallow; C, control; NA, not applicable; cm, centimeter; ft, foot; cfs, cubic feet per second]

Wetland type	Field number	Cell code	Total area (acres)[1]	Area scraped (acres)	Area mowed (acres)	Area disked (acres)	Average depth (cm)[2]	Average volume (acre ft)[2]	Target outflow (cfs)[3]	Dominant vegetation[4]
Treatment	1	D01	4.7	4.5	NA	NA	65	10.0	0.5	barren
Treatment	1	S01	27.5	NA	13.6	11.7	30	27.0	NA	*Crypsis schoenoides* (swamp timothy)
Treatment	7	D07	4.9	7.0	NA	NA	65	10.5	0.4	barren
Treatment	7	S07	12.1	NA	7.1	5.9	31	12.3	NA	*Ludwigia peploides* (floating primrose-willow)
Treatment	17	D17	6.5	8.2	NA	NA	54	11.5	0.5	barren
Treatment	17	S17	18.8	NA	9.5	10.2	24	15.0	NA	*Crypsis schoenoides* (swamp timothy)
Treatment	18	D18	6.4	5.8	NA	NA	65	14.0	0.5	barren
Treatment	18	S18	16.8	NA	9.7	8.2	44	24.0	NA	*Crypsis schoenoides* (swamp timothy)
Control	2	C02	20.2	NA	8.3	7.0	37 (27)	15.3	0	*Schoenoplectus acutus* (tule rush)
Control	6	C06	27.7	NA	10.6	9.7	19 (6)	20.3	0	*Crypsis schoenoides* (swamp timothy)
Control	9	C09	17.6	NA	13.5	6.1	27 (20)	19.6	0	*Crypsis schoenoides* (swamp timothy)
Control	13	C13	22.2	NA	17.1	7.7	16 (6)	24.8	0	*Crypsis schoenoides* (swamp timothy)

[1]Total acreage and acreage scraped for each deep cell was calculated from the engineering drawings, and accounted for within-cell islands.

[2]Average depth and volume for cells in treatment wetlands are based on engineering drawings and operation stage assessment. Depths and volumes for control wetlands represent the average of six measurements routinely taken at the fixed sediment collection sampling sites, with the standard deviation given in parentheses ( ).

[3]Target outflows associated with treatment wetlands were controlled at the outlet water control structure of the deep cells and are based on a target of 2 cm of water flow over that water control structure.

[4]Vegetation data collected at the initiation of the study (August 2014), prior to initial flood up.

Water Management

Annual managed flooding of the CRP wetlands occurs from mid-September through May to provide habitat for wintering migratory waterfowl, and is similar in hydrologic regime to to flooding of unmanaged seasonal wetlands regionally. Water management associated with each wetland was achieved with WCS (inlets, outlets, weirs; fig. 4). Control wetlands each had one inlet and one outlet WCS. Treatment wetlands had a total of three WCS, including the inlet to the shallow cell, the outlet to the deep cell, and the weir associated with the check levee that separated the shallow cell from the deep cell (fig. 3). The location of each WCS is given in table 2. These WCS provided quantifiable control over the hydrologic flow into and out of each cell type. Manipulations of flow at WCS by BLM staff for the purpose of water management were recorded and implemented in consultation with the science team.

Figure 4. Photographs of the hydrology and water quality equipment used during the Cosumnes River Preserve mercury study. *A*, and *B*, source water inlets; *C*, check levee weir outfitted with water quality sonde; *D*, outlet water control structure and stage gauge (indicated by red arrow); *E*, rain gauge; *F*, fluorometer deployment (indicated by yellow arrow).

Water delivery began on September 15th for both Year 1 (Water year [WY] 2014–15) and Year 2 (WY 2015–16) of the study. Flows were maintained until flooding was at the desired depths. In Year 1, flooding rates and timing were moderated as needed until the maintenance flow rates were determined. Once determined, these flow rates were continued for the 8 month flooded period. The shallow cells within treatment wetlands and control wetlands were flooded to similar depths (average of 25 centimeters [cm]) but were exposed to different flow regimes, as follows:

- Control Wetlands (Year 1): Standard CRP wetland management approach of fill-and-maintain water delivery with target depths of 25 cm. This standard approach needs only periodic water flows to maintain a steady water table despite losses to seepage and evapotranspiration.
- Control Wetlands (Year 2): Slow flow-through water delivery with target depths of 25 cm from September through December, then switching to the standard CRP wetland management approach of fill-and-maintain water delivery from December to May with target depths of 25 cm.
- Treatment Wetlands (both Year 1 and Year 2): Slow flow-through water delivery with target depths of 25 cm in the shallow cell and >75 cm depths in the deep cells, with maintenance of approximately 2.5 cm of flow over the outlet weirs of the deep cells at all times from September through May.

After more than 8 months of flooded conditions, all eight study wetlands were drained on May 1, 2015, and again on May 18, 2016, according to CRP's Annual Wetland Operations Plan. All wetlands were drained of surface water over approximately 7 days each years. During Summer 2015, the CRP implemented land management actions including mowing any sparse vegetation in the deep cells to a height of 6, clearing WCS and drains, reinforcing valves, and rebuilding coffer dams within swales as needed. Shallow cells experienced minimal maintenance during the summers of 2015 and 2016, with only selected operations to inhibit cocklebur (*Xanthium* spp) recruitment. CRP also collected vegetation data in the wetlands along the same transects that were used during summer 2014 prior to the start of the study.

Table 2. Latitude and longitude data for water control structures (WCS) in the Cosumnes River Preserve mercury study area.

[Location data referenced to WGS84 Datum in decimal degrees (ddd.dddddd). Lat, latitude; Long, longitude; NA, not applicable]

Field	Inlet			Check weir		Outlet	
	Type	Lat	Long	Lat	Long	Lat	Long
2	Control	38.267180	-121.446421	NA	NA	38.269664	-121.449489
6	Control	38.276214	-121.440070	NA	NA	38.273940	-121.443999
9	Control	38.281644	-121.429862	NA	NA	38.279559	-121.433541
13	Control	38.279219	-121.431594	NA	NA	38.279095	-121.437420
1	Treatment	38.266636	-121.442331	38.265585	-121.446667	38.265225	-121.447671
7	Treatment	38.276463	-121.443937	38.277783	-121.442067	38.278315	-121.441318
17	Treatment	38.275698	-121.432518	38.271700	-121.431500	38.270109	-121.433359
18	Treatment	38.275702	-121.429878	38.272300	-121.430100	38.270502	-121.430609

Methods

The methods used for the field sampling of surface water, sediment and biota, and the subsequent laboratory sub-sampling regime, sample preservation and analytical methods are detailed below.

Field Sampling

The primary field sampling components of the study consisted of:

- Surface water sampling,
- Sediment sampling,
- Short-term particulate flux measurements,
- Long-term (flooded period) particulate flux measurements, and
- Caged fish Hg bioaccumulation studies.

The field sampling timeline for each of these components, as well as wetland flood up and drawdown periods, are graphically presented in fig. 5 and detailed below.

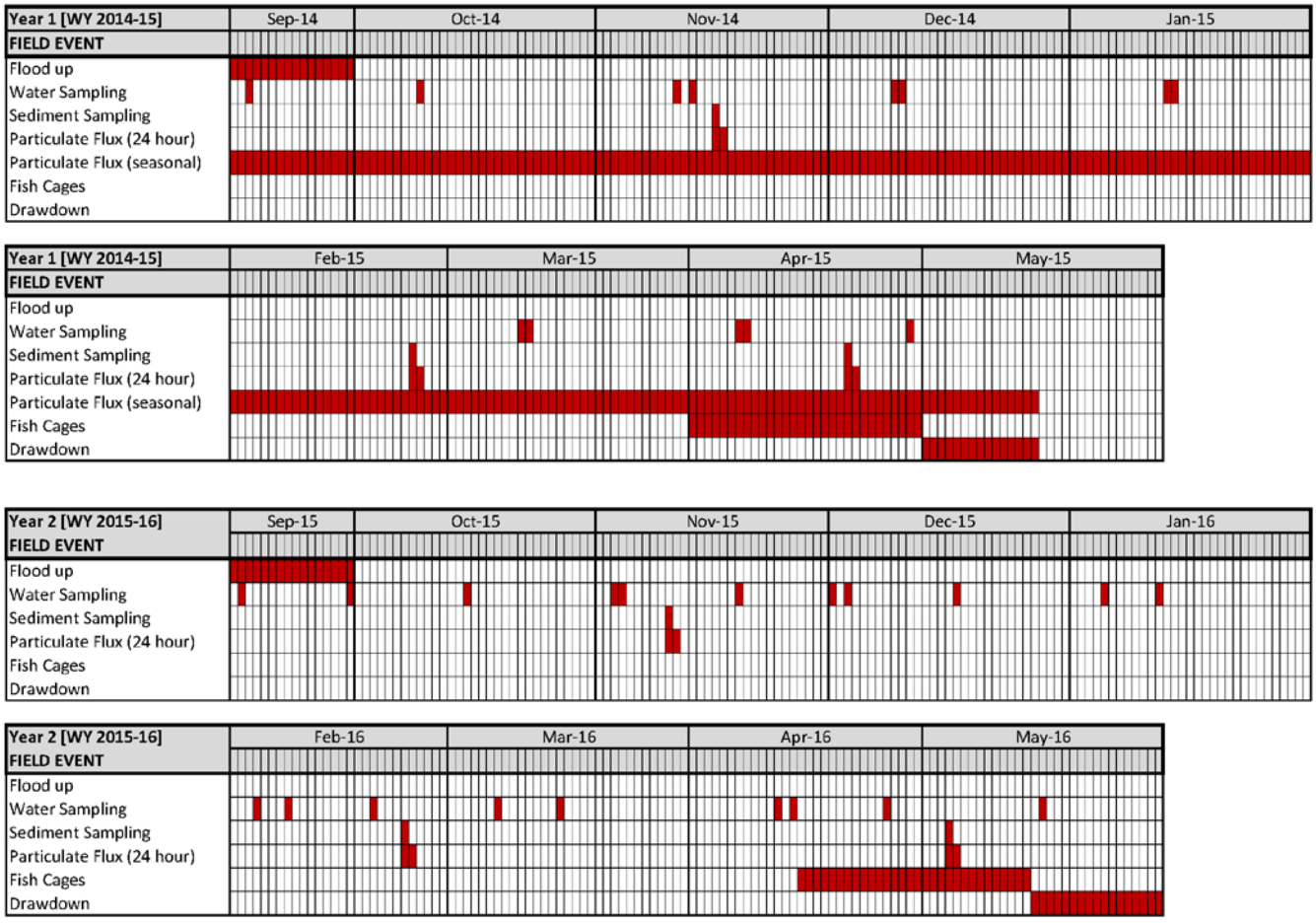

Figure 5. Project timeline of field sampling events for the Cosumnes River Preserve mercury study during the flooded period (September 15–May 31) for sampling Year 1 (Water year [WY] 2014–15) and Year 2 (WY 2015–16).

Surface Water

Field sampling and measurements associated with surface water consisted of multiple components, and include: a) routine samples collected at the WCS for both Hg and non-Hg constituents, b) continuously monitored parameters, and c) seasonal and daily particulate flux measurements.

Routine Water Samples

Routine surface-water samples were collected at the inlets and outlets of each wetland cell approximately every five weeks during the flooded period for each location for the following constituents: total suspended solids (TSS), particulate total Hg (p.THg), particulate MeHg (p.MeHg), particulate reactive Hg (p.RHg), filter-passing (dissolved) THg (f.THg), filter-passing MeHg (f-MeHg), chloride (Cl^-) and sulfate (SO_4^{2-}). Sampling at the inlet hydrants (fig. 4) began each year within a week of initial irrigation (September 15). Sampling was staggered to capture the most representative water flows at each WCS and to account for water residence time, with 8 collection events per year. Specifically, inlets were sampled during flood up when outlets were dry. Conversely, check weirs and outlets were sampled during drawdown after inflow had ceased, with initial sampling at the check weirs and outlets conducted approximately two to five weeks following the initial irrigation, shortly after the water reached the WCS. During the fully flooded period, samples from all WCS were collected concomitantly.

Samples were collected by immersing a 2 liter (L) clean and sterile polyethylene terephthalate (PETG) bottle in the water column without disturbing the bottom substrate. During sample collection, the bottle opening was covered with acid-cleaned, 1-millimeter (mm) nylon mesh netting to omit large particles and algal clumps from the sample. In some cases, water depth was too shallow to immerse the bottle without disturbing the bottom substrate, so multiple dips of the cap were used to fill the bottle. Once the sample was collected, the bottles were capped, labeled, double-bagged, and placed on ice in a dark cooler for transport to the laboratory for processing. Ancillary water-quality parameters (pH, temperature, specific conductance [SC], dissolved oxygen [DO]) were measured directly using a field-deployed *YSI EXO2 multisonde* equipped with optical sensors for chlorophyll-a, turbidity, and fluorescent dissolved organic matter in addition to the measurements listed above (fig. 4). All surface-water samples were collected during controlled, managed flooding conditions.

Additional samples for water isotope analysis were collected during three sampling events (February, March and April of 2016) in all twelve study cells during Year 2 to document flow paths and residence time of source water within each cell. Surface-water samples were collected at the inlets, outlets, and an additional six evenly distributed locations in each cell, by immersing a prelabeled 30 milliliter (mL) high-density polyethylene plastic bottle below the surface of the water. The bottles were filled to the top with no head space and sealed tightly for transport back to the laboratory for storage until analysis could be performed. Additional field data documented for each surface water isotope sample included the time and location, surface water depth, and surface water temperature for cross-validation.

Continuous Monitoring Effort

Prior to the beginning of irrigation (September 15) each year, pressure transducers (PT) were deployed at the 20 WCS and left in place until the fields were drained by removing the boards at the check weirs and outlets at the end of the flooded period (late April to mid-May). The height of water spilling over the outlet WCS of each wetland cell was calibrated approximately bi-weekly using a ruler (measured to the nearest 1/16 inch) to establish a stage-flow relations for each WCS. Initial calibrations

of the stage-flow relations were performed using a high-sensitivity optical flow meter and manual measurements of water depth at the WCS relative to the land surface and the location of flow. Twelve of the PT included integrated conductivity cells, allowing salt budgets to be calculated for five fields (C06, C09, T07, T18, D01) thus validating model estimates of hydraulic residence times (HRT). Water depth at each deep cell outlet WCS was verified using polyvinyl chloride (PVC) staff gages located near the outlet WCS (fig. 4).

A fluorometer was deployed at the deep cell outlet WCS of T07 during Year 1 of the study to generate multiple week-long high-frequency measurements of turbidity and fluorescent dissolved organic matter (fDOM) to better understand temporal variability in these systems. In Year 2, two fluorometers were deployed in the T07 field, one at the outlet WCS and one at the check weir WCS to observe differences in temporal variability between the checks and outlets.

Particulate Flux

In addition to a load-based estimate of particulate trapping in the deep cells provided by comparing the total suspended solids (TSS) loads measured at the check WCS and the deep cell outlet WCS, two additional independent approaches were employed to explicitly assess particulate flux to the benthos (sediment zone) within the deep cells. The goal of the first of these two approaches was to integrate the particulate flux for the full flooding season, using settling pads deployed for the full study period of Year 1. The goal of the second approach was to assess short-term particulate flux using settling traps deployed for only 24 hours. These two approaches are described in detail below.

Long-Term Seasonal Particulate Flux – Felt Pads

To determine the spatial pattern and mass of particulate settling from flood up (September) to drawdown (May), 60 sediment settling plates (felt pads) were distributed regularly within each of the four deep cells. Settling plates consisted of 33 cm by 33 cm ceramic tiles with a 30 cm by 30 cm polyethylene felt square secured to the top with binder clips (fig. 6). Each felt pad was prelabeled, pre-weighed to ±0.01gram (g), and stored in a ziplock bag until field deployment. The settling plates were deployed in a predetermined grid in all four deep cells during September 1–3, 2014, approximately 2 weeks prior to flood up on September 15, 2015 (fig. 7). Latitude and longitude was recorded for each settling plate, and their location was flagged with a small red surveyors flag. Just prior to flood up, eight blank pre-flood felt pads were collected by BLM staff, to determine the extent of dust settling that might have occurred during the 2 weeks between pad deployment and flooding. The remaining 232 settling pads were left in place for roughly 8 months to record total sediment accumulation during the flooding period, which ended with drawdown (initiated on May 1st, 2015). Felt pads were retrieved on field visits once the cells were sufficiently dry for access (May 14, 2015 for D07, May 21, 2015 for D17 and D18, and June 10, 2015 for D01). The majority of felt pads were successfully retrieved (96 percent). Each pad was visibly examined, folded on themselves, and individually bagged. Field technicians made notes and ranked their organic buildup on a scale of 1–4 (1, free of visible algal/plant material; 2, less than 50 percent covered with visible algal/plant material; 3, more than 50 percent, but not fully covered with visible alga/plant material; 4, fully covered with visible alga/plant material). All 223 felt pads were refrigerated and returned to the laboratory for freeze-drying (lyophilization), and reweighing. The final mass was subtracted from the initial mass to calculate an areal rate of sediment deposition. A subsample of freeze-dried sediment (~2–3 g) was carefully scraped from the felt pads and placed in a crucible for combustion to estimate the organic content of the deposited material.

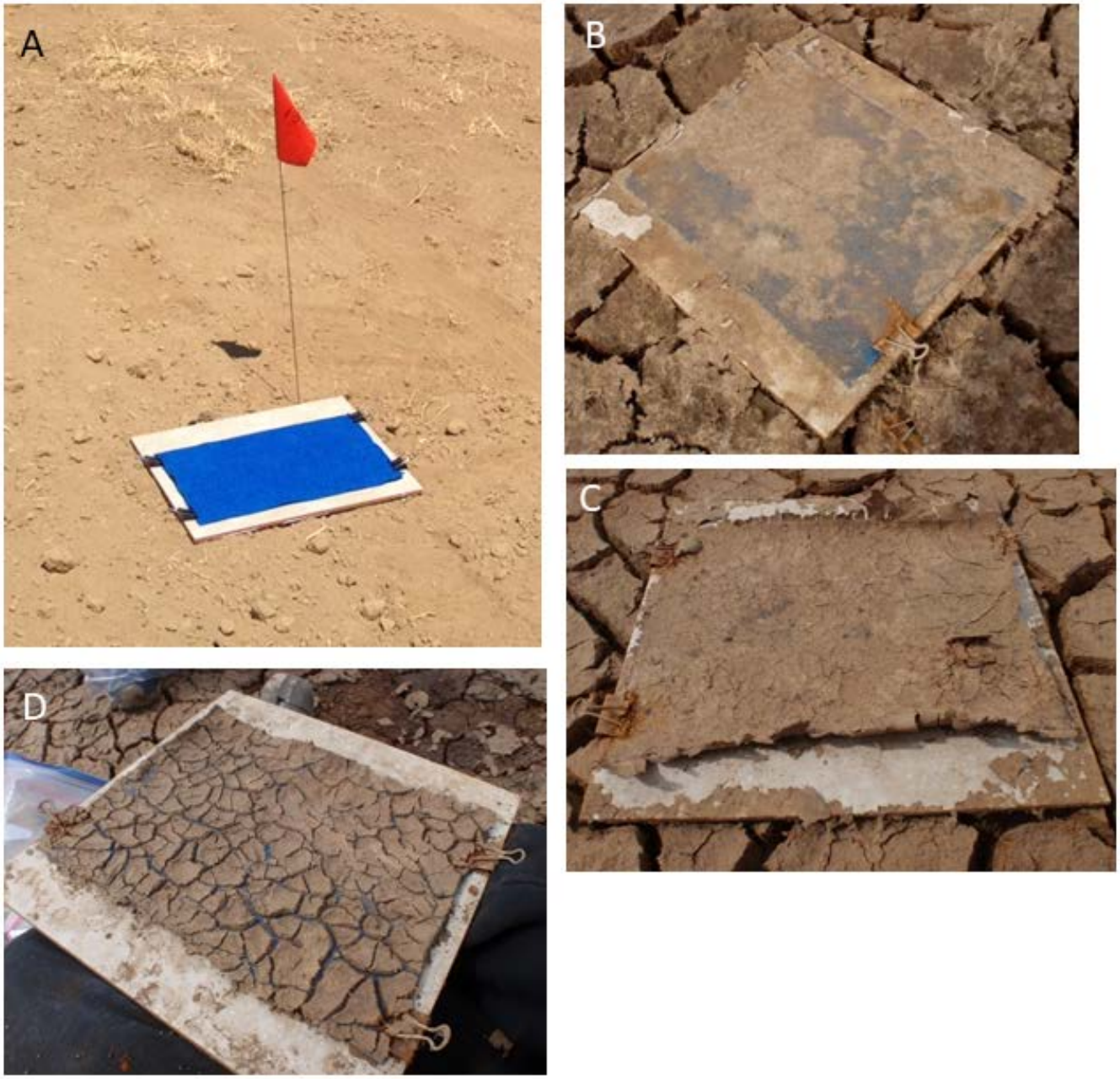

Figure 6. Photographs of long-term particulate settling felt pads used in the Cosumnes River Preserve mercury study. *A*, Felt pad deployment and flagging (pre-flooding); *B–D*, Felt pads after flooding season (~8 months) and drawdown period with evidence of *B*, minor; *C*, moderate; and *D*, heavy deposition.

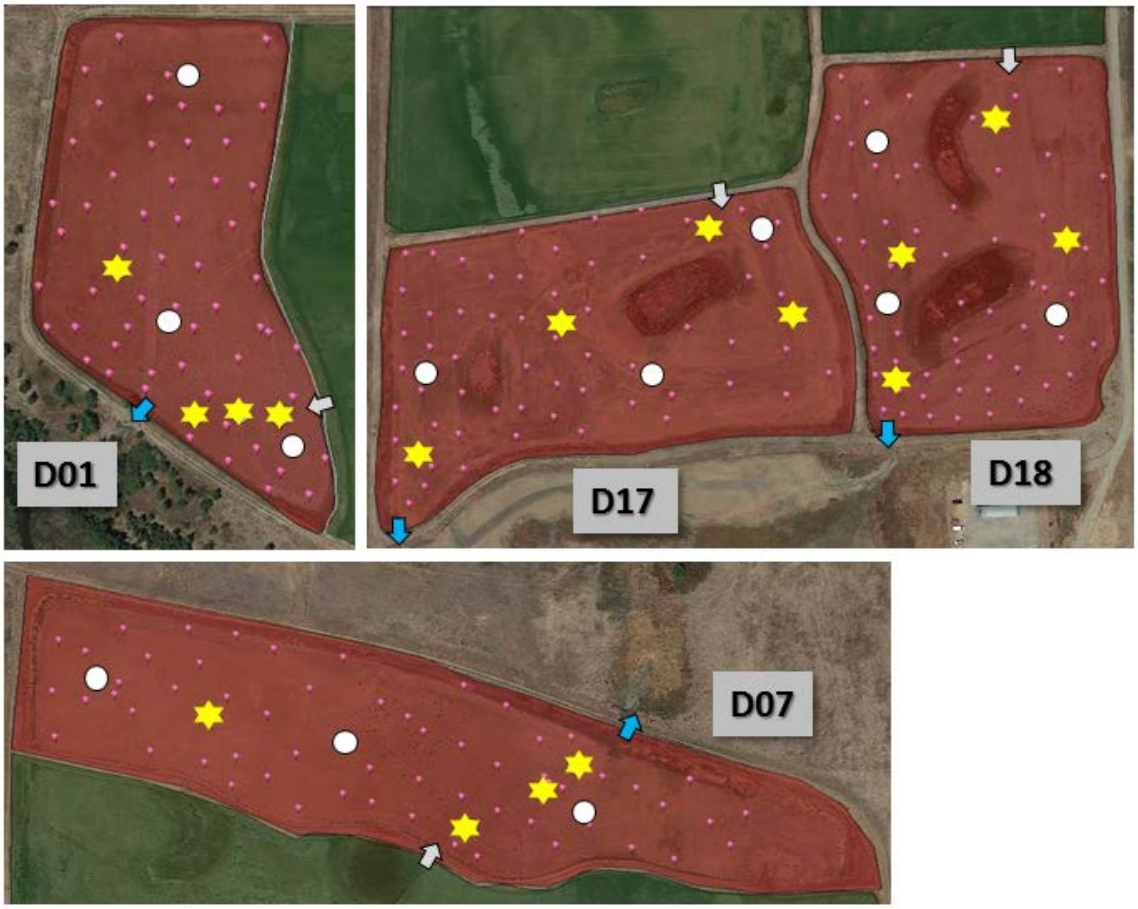

Figure 7. Maps with field identification showing the location of sediment sampling sites, long-term particle deposition pads, short-term particle flux traps, and inlet/outlet locations in the four deep cells of the Cosumnes River Preserve mercury study. Sediment sampling sites are indicated by white circles. Long-term particle deposition pad locations (60 per deep cell) are indicated by pink markers. Short-term particle flux traps are depicted by yellow stars. Water control structure inlets and outlets are depicted by white and blue arrows, respectively.

Short-Term Particulate Flux

Short-term (24 hour) particulate flux measurements were made at four fixed locations per deep cell (fig. 7, table 3), and coincided with the surface sediment sampling efforts conducted during the early season (November), mid-season (February) and late season (April/May) flooding period, during both study years (fig. 5). Prior to flood up in September 2014, particulate trap deployment and retrieval elevators were installed at each fixed sampling site (fig. 8). Each elevator consisted of a landing pad made of cement backerboard (1 by 1 m) set on leveled ground; a central shaft composed of PVC pipe that extended 0.3 m below the marsh surface and 2 m above the marsh surface and stabilized by four guide wires; a height adjustable plastic grated platform (0.7 x 0.7 m) reinforced around the edges with PVC piping; four Mason jar holders constructed of acrylonitrile butadiene styrene (ABS) pipe (15 cm length with a 10 cm inside diameter) secured to the grated platform with cable ties; a pulley system to raise and lower the platform; and a boat mooring station, composed of metal stakes on either end with PVC pipe across the top, offset 0.5 m from the central shaft to allow for a boat to pull alongside the elevator, without bumping into it, and tie up for deployment and retrieval of particulate traps.

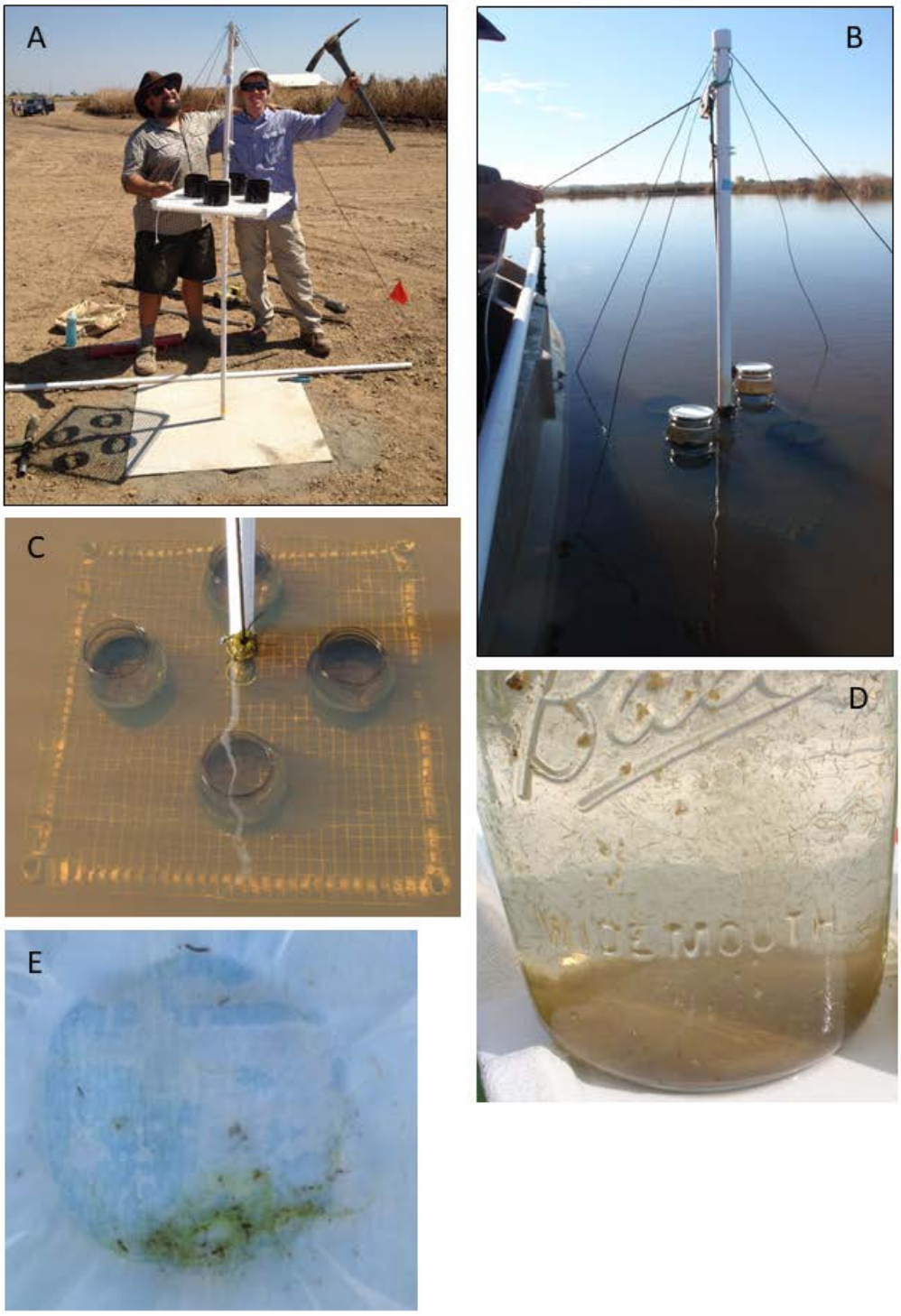

Figure 8. Photographs of short-term (24 hour) particulate trapping elevators used in the Cosumnes River Preserve mercury study. *A*, Elevator construction (pre-flooding); *B*, Particle trap retrieval via boat; *C*, Particle traps just below the water surface; *D*, single settling trap with particulates after 24 hour deployment; and *E*, Filtration removal of <210 micrometer (µm) particulates during initial sample processing after trap retrieval.

While it was originally conceived that the settling traps would be deployed for approximately 2 weeks, initial testing demonstrated extremely high sediment trapping rates and biofilm growth on the jar interiors over a two week deployment period. Subsequently, the approach was standardized to 24 hour deployment periods, which allowed for more than adequate particulate trapping (fig. 8*D*) without the complication of biofilm formation.

The day prior to each deployment, the landing pads and adjustable grated platforms were cleaned of any algal growth that may have accumulated. Since this activity resuspended previously settled particulates, the actual deployment was not initiated until the following day after the water column had cleared. Quart-size Mason jars were used for settling traps and were completely filled with deionized (DI) water from the laboratory and capped. Upon deployment, four jars were placed into the four jar holders for each elevator and lowered to just below the water/air interface while still capped and filled with DI water. The caps were then gently removed and the grated platform was slowly lowered until it rested on the landing pad, being extremely cautious to not disturb any particulates that may have resettled on the landing pad since the previous days cleaning. The jars were then retrieved 24 hours later in a reverse manner, slowly and carefully raising off of the platform until the jar openings were just below the water/air interface and then recapping before removing from the ABS holders. For each trap deployment event and for each study cell, a single blank trap was collected immediately prior to the full deployment. The blank consisted of deploying a single jar at one of the four elevators per deep cell for a period of 5 minutes and then retrieving as described above. This blank was used to verify that the act of deployment and retrieval caused little if any appreciable disturbance of sediment accumulated on the landing pad, and to account for any particulates captured from the water column during the deployment and retrieval. The deep cell specific constituent concentrations (for example, THg, MeHg, TSS) associated with this blank trap were minimal and were subtracted from those measured in the traps deployed for 24 hours from that same study cell. Immediately prior to the jar deployment at each elevator station, measurements of surface water (approximately 10–15 cm below the surface) temperature, SC, pH, algal pigments, and fDOM were taken using a YSI EXO2 water quality sonde.

After retrieval, the settling traps were processed and subsampled the same day (within 2–4 hours) at an indoor CRP facility. All four settling traps from a single elevator were first prefiltered through 210 micron (µm) acid-cleaned nylon mesh, to remove any large zooplankton and (or) clumps of filamentous algae (fig. 8*E*), and composited into a single sample in an acid-cleaned 4 L PETG container. Three types of particulate subsamples were then collected on preweighed 0.3 µm glass-fiber filters (Advantec) from each composite; particulate total mercury (p.THg), particulate monomethylmercury (p.MeHg), and particulate carbon (PC)/particulate nitrogen (PN. The precise amount of composite water filtered was recorded in each case, and the 4 L PETG container was shaken immediately prior to all subsample removals to ensure homogeneity. Standard trace metal cleaning techniques were used during all aspects of sample collection (Lewis and Brigham, 2004). All filters were frozen immediately after collection, and remained frozen until analysis.

Table 3. Latitude and longitude data for deep cell particle trap elevators in the Cosumnes River Preserve mercury study area.

[Location data referenced to WGS84 Datum in decimal degrees (ddd.dddddd). Lat, latitude; Long, longitude]

Cell	Elevator	Lat	Long
D01	E1	38.265210	-121.446955
D01	E2	38.265220	-121.447153
D01	E3	38.265214	-121.447377
D01	E4	38.265784	-121.447751
D07	E1	38.277987	-121.441982
D07	E2	38.278116	-121.441659
D07	E3	38.278196	-121.441516
D07	E4	38.278383	-121.443154
D17	E1	38.271441	-121.431687
D17	E2	38.270991	-121.432545
D17	E3	38.270390	-121.433396
D17	E4	38.271030	-121.431190
D18	E1	38.271920	-121.430029
D18	E2	38.271323	-121.430566
D18	E3	38.270732	-121.430611
D18	E4	38.271388	-121.429584

Water Column Light Extinction Coefficients

For the purposes of calculating photodemethylation rates, and empirically verifying calculations of photosynthetically active radiation, (PAR) extinction based on water quality (dissolved organic carbon [DOC] and turbidity; Fleck and others, 2014), light extinction profiles for the entire water column were directly measured in all four deep cells during winter and spring of 2016. Interior sites were profiled adjacent to the short-term particulate trap elevators, four per cell in all four deep cells for a total of 16 profiles, during February 2016. Water quality data was simultaneously collected using the YSI-EXO2 sonde to obtain the water quality information (fDOM and turbidity) used in the model validation. From January–April 2016, thirty additional light extinction profiles were collected at outlets in coordination with water sample collections, including field YSI-EXO2 sonde measurements. Light measurements were taken using a calibrated LiCor LI-192SA Underwater Quantum Sensor just above the water surface and below the water surface at 10 cm intervals to the bottom of the water column.

Surface Sediment

Collection, Sub-sampling and Preservation

Surface sediment (top 0–2 cm) was initially collected from all study cells during early September pre-flood period during Year 1, to establish starting concentrations of THg, MeHg and organic content as percent loss-on-ignition (%LOI). Subsequently, surface sediment was collected from the deep cells during the early season (November), mid-season (February) and late season (April/May) flooding period, during both study years (fig. 5). In addition, shallow cells and control cells were sampled during the flooded period during November 2014 and April 2015 of Year 1 and during May 2016 of Year 2.

In deep cells, sediment was collected from a boat using an extended pole corer with polycarbonate core tubes, and included four cores per fixed sampling site. The cores were immediately extruded on-shore, with the top 0–2 cm interval being transferred to acid-cleaned glass Mason jars. The jars were completely filled to exclude atmospheric oxygen and then stored chilled until further sub-sampling at the USGS laboratory (Menlo Park, CA) the following day. In shallow and control cells, the

0–2 cm interval was collected by hand using a 2 cm polycarbonate core ring, and similarly transferring to acid-cleaned Mason jars, chilled and sub-sampled the following day. Fixed sampling sites for surface sediment included three in each deep cell (fig. 7) and two in each shallow cell and control cell. The specific sampling locations and dates for surface sediment are given in table 4. In-field measurements included sediment temperature, pH and oxidation-reduction potential, as previously described (Lutz and others, 2008).

Table 4. Latitude and longitude data for sediment sampling sites in the Cosumnes River Preserve mercury study area.

[Location data referenced to WGS84 Datum in decimal degrees (ddd.dddddd). The month/year that sediment was sampled at each site is indicated by 'X'. Sediment sampling during September 2014 occurred during the pre-flood up period, while all other sampling events occurred during the flooded period. For control (C##) and shallow (S##) cells, it is noted if the sediment site sampled was either mowed (M) or disced (D) prior to flood up. Lat, latitude; Long, longitude]

Cell label	Sediment site	Lat	Long	9/2014	11/2014	2/2015	4/2015	11/2015	2/2016	5/2016
C02	SED.1 D	38.26921	-121.44859	X	X		X			X
C02	SED.2 M	38.26726	-121.44843	X	X		X			X
C06	SED.1 D	38.27594	-121.44357	X	X		X			X
C06	SED.2 M	38.27531	-121.44008	X	X		X			X
C09	SED.1 D	38.28114	-121.43034	X	X		X			X
C09	SED.2 M	38.27957	-121.43141	X	X		X			X
C13	SED.1 D	38.27731	-121.43713	X	X		X			X
C13	SED.2 M	38.27865	-121.43300	X	X		X			X
S01	SED.1 D	38.26640	-121.44690	X	X		X			X
S01	SED.2 M	38.26654	-121.44327	X	X		X			X
S07	SED.1 D	38.27794	-121.44395	X	X		X			X
S07	SED.2 M	38.27665	-121.44220	X	X		X			X
S17	SED.1 D	38.27409	-121.43341	X	X		X			X
S17	SED.2 M	38.27291	-121.43336	X	X		X			X
S18	SED.1 D	38.27439	-121.42961	X	X		X			X
S18	SED.2 M	38.27282	-121.42947	X	X		X			X
D01	SED.1	38.26651	-121.44751	X	X	X	X	X	X	X
D01	SED.3	38.26561	-121.44756		X	X	X	X	X	X
D01	SED.4	38.26522	-121.44713	X	X	X	X	X	X	X
D07	SED.1	38.27843	-121.44357	X	X	X	X	X	X	X
D07	SED.3	38.27825	-121.44234		X	X	X	X	X	X
D07	SED.4	38.27812	-121.44163	X	X	X	X	X	X	X
D17	SED.1	38.27066	-121.43338	X	X	X	X	X	X	X
D17	SED.3	38.27079	-121.43235		X	X	X	X	X	X
D17	SED.4	38.27132	-121.43136	X	X	X	X	X	X	X
D18	SED.1	38.27164	-121.43059	X	X	X	X	X	X	X
D18	SED.3	38.27109	-121.43060		X	X	X	X	X	X
D18	SED.4	38.27113	-121.42973	X	X	X	X	X	X	X

Fish Tagging, Deployment into Cages, and Retrieval

During spring of 2015 (April 1) and 2016 (April 14), we deployed 32 cages, each containing 30 western mosquitofish (*Gambusia affinis*). Each year, approximately 2,000 western mosquitofish were obtained from Sacramento-Yolo Mosquito and Vector Control District's aquaculture facility, where they were fed as much as they wanted to eat and treated for diseases prior to release. Fish were taken from

holding tanks within the rearing facility and placed into aerated 180 L coolers filled with rearing-facility well water. Fish were immediately transported to the field site where they were acclimated to site water in a mobile aquaculture facility for approximately 24 hours prior to processing.

Acclimating the fish involved a continuous 30 percent per hour titration of water from wetland inlet pumps into aerated holding tanks containing rearing-facility well water. After 3 hours, fish were transferred into one of three 1,900 L holding tanks, which received a continuous flow of fresh water from the wetland inlet pumps. Continuous flow was achieved by gravity flow from a central 1,900 L distribution tank. The central distribution tank was refilled every 6–8 hours by pumping water from a 7,600 L water tender, which was filled directly at a wetland inlet valve on-site. The acclimation and distribution tanks were continuously aerated. All fish were held for approximately 18–20 hours in the acclimation tanks prior to processing.

After acclimating for 18–20 hours, each fish was individually removed from the acclimation tank and placed in a buffered 100 milligram per liter (mg/L) MS-222 solution until they became sedated. To control for potential sex differences in THg concentrations, we selected only females for use in this study. We then weighed each female fish to the nearest 0.001 g on a digital balance (fresh wet mass) and measured them to the nearest millimeter on a fish board. We then marked each individual fish with a combination of colored elastomer tags (Northwest Marine Technology, Inc., Shaw Island, Wash.) placed in up to three locations on each fish. Specifically, tags were placed along the dorsal muscle on either the left or right of the fish, as well as at the base of the caudal fin. The combination of four colors and up to three tag locations allowed us to uniquely identify each of the 30 individual fish within each cage. After tagging, we placed each fish in a recovery tank until it regained consciousness, at which point we moved the fish into a labeled flow-through 19 L holding cage within the acclimation pools. Each holding cage was designated for deployment to a specific field location. After all fish were tagged, we held them overnight and deployed them into their specific cage the following day. Any mortalities prior to a deployment (<1 percent) were replaced with newly tagged fish that had the same tag sequence (fig. 9).

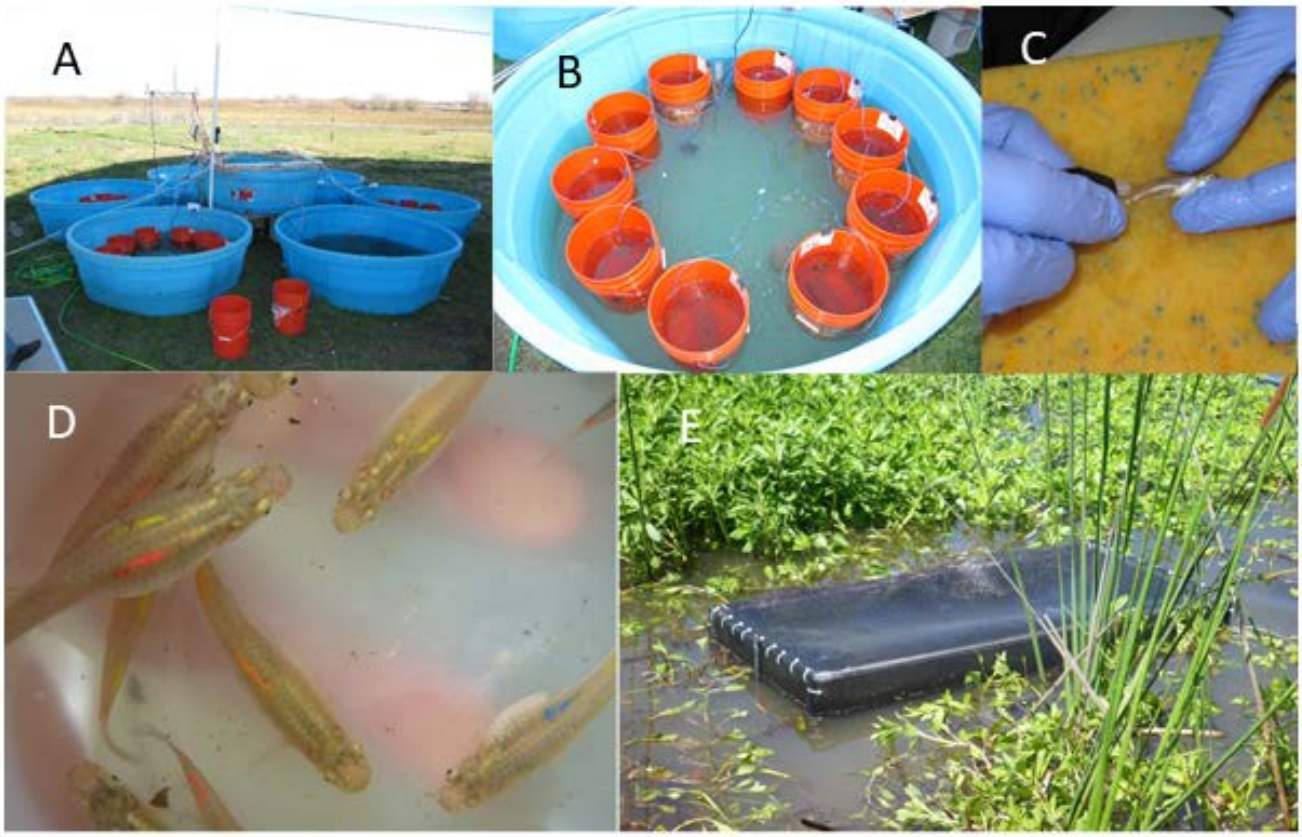

Figure 9. Photographs of field deployment of bioaccumulation study with caged fish in the Cosumnes River Preserve mercury study. *A*, Holding pools; B, Mobile aquaculture; C, Mosquitofish being tagged with elastomer tags along dorsal fin; D, Mosquitofish with elastomer tags; and E, Cage deployed in wetland.

Each fish was then deployed into the field in a 120 × 55 × 55 cm (357 L) cage constructed from 3.175 mm mesh polypropylene aquaculture netting. Cages were placed in 4 locations within each of the 4 control wetlands and 4 experimental wetlands. Within the experimental wetlands, cages were placed within 15 m of the following WCS (table 2):

- Shallow cell inlet,
- Shallow cell side of check weir,
- Deep cell side of check weir, and
- Deep cell outlet.

Cages were similarly collocated with WCS in the control wetlands, except for 2 cages placed in the center of each control wetland were not separated by a check berm. In 2015, three fish cages were also placed in the source water canals in order to determine background mercury bioaccumulation in those canals. Cages were placed 2–3 days prior to fish introduction. In total, 2,010 mosquitofish were introduced into 67 different cages (32 wetland cages each year and 3 canal cages during Year 2).

After deployment, fish in cages were held under field conditions for 30 days, and cages were checked weekly to ensure water levels remained stable and there was no disturbance to cages. After 30 days of exposure, fish were retrieved from the cages. Upon removal, all collected fish were stored on ice in the field and in a refrigerator until they could be measured. The same day fish were retrieved, each fish was weighed and measured as described during tagging. Each fish was identified using the

sequencing of fish tags. Each mosquitofish was individually bagged, labeled, and frozen at -20°C until mercury determination. To determine baseline THg concentrations in fish at the time of introduction, 80 female mosquitofish were randomly selected from our stock population at the time of each introduction (2015 and 2016) and stored frozen in polyethylene bags at -20°C until processing and mercury determination.

Laboratory Analylses

The vast majority of laboratory analysis conducted on surface water and sediment samples as part of the current study have been previously detailed. Table 5 and table 6 summarize the specific analytes assayed for surface water and sediment, respectively, along with their short name (abbreviation/code) used in this report, analyte units, the analytical laboratory, detection limits (where appropriate) and the associated references where more details regarding methods can be found. In cases where the specific assay conditions were unique to this study and/or modifications were made relative to the method(s) cited, additional detailed is provided below.

Table 5. Surface water analytical methods used in the Cosumnes River Preserve mercury study.

[mmol/L, millimole per liter; mg/L, milligram per liter; ng/L, nanogram per liter; ng/g, nanogram per gram; µg/L, microgram per liter; g/cm^3, µS/cm, microsiemens per centimeter; L/mg m, liters per milligram per meter; °C, degrees celsius; FNU, formazin nephelometric units; QSE, Quinine Sulfate equivalents; pg, picogram; ppm, parts per million; RFU, relative fluorescent units; AU, absorbance units; RU, Raman units; USGS, U.S. Geological Survey; NRP-WR, National Research Program–Western Region (Menlo Park, CA); CA-WCS, California Water Science Center; ND, not determined; NA, not applicable]

Analyte name	Analyte notation	Analyte units	Analytical laboratory	Method detection limit	Method reporting limit	Reference(s)
Sulfate	SO_4^{2-}	(mmol/L)	USGS, NRP-WR	0.02 mmol/L	0.05 mmol/L	(U.S. Environmental Protection Agency, 2007a)
Chloride	Cl^-	(mmol/L)	USGS, NRP-WR	0.06 mmol/L	0.25 mmol/L	(U.S. Environmental Protection Agency, 2007a)
Filter-passing methylmercury	f.MeHg	(ng/L)	USGS, NRP-WR	0.26 pg (absolute mass as Hg) at the level of the autoanalyzer	0.30 pg (absolute mass as Hg) at the level of the autoanalyzer	(U.S. Environmental Protection Agency, 2001; DeWild and others, 2002)
Filter-passing total mercury	f.THg	(ng/L)	USGS, NRP-WR	0.14 ng/L at the level of the Tekran 2600 autoanalyzer	0.53 ng/L at the level of the Tekran 2600 autoanalyzer	(U.S. Environmental Protection Agency, 2002)
Particulate methylmercury	p.MeHg	(ng/L) or (ng/g) dry wt.	USGS, NRP-WR	0.26 pg (absolute mass as Hg) at the level of the autoanalyzer	0.30 pg (absolute mass as Hg) at the level of the autoanalyzer	(Marvin-DiPasquale and others, 2011)
Particulate total mercury	p.THg	(ng/L) or (ng/g) dry wt.	USGS, NRP-WR	0.14 ng/L at the level of the Tekran 2600 autoanalyzer	0.53 ng/L at the level of the Tekran 2600 autoanalyzer	(Olund and others, 2004)

Analyte name	Analyte notation	Analyte units	Analytical laboratory	Method detection limit	Method reporting limit	Reference(s)
Chlorophyll (lab)	Chl.a	(µg/L)	USGS, NRP-WR	N.D.	0.7 mg/m^3	(Strickland and Parsons, 1972)
Total suspended solids	TSS	(mg/L)	USGS, NRP-WR	ND	2 mg/L or 0.3 mg/filter	See: Methods / Laboratory Analyses / Total Suspended Solids
Particulate organic carbon	POC		USGS, NRP-WR	0.010 mg	0.02 mg	(Kendall and others, 2001)
Particulate nitrogen	PN		USGS, NRP-WR	0.002 mg	0.004 mg	(Kendall and others, 2001)
13C-carbon, particulate organic carbon	δ^{13}C-POC	(per mil)	USGS, NRP-WR	NA	NA	(Kendall and others, 2001)
15N-nitrogen, particulate nitrogen	δ^{15}N-PN	(per mil)	USGS, NRP-WR	NA	NA	(Kendall and others, 2001)
Specific conductivity (via EXO)	SC	(µS/cm)	USGS, CA-WSC	0.1 uS/cm	ND	(YSI, 2012)
pH (via EXO)	pH	unitless	USGS, CA-WSC	NA	NA	(YSI, 2012)
Temperature (via EXO)	TEMP	(C°)	USGS, CA-WSC	NA	NA	(YSI, 2012)
Dissolved oxygen (via EXO)	DO	(mg/L)	USGS, CA-WSC	0.01 mg/L	ND	(YSI, 2012)
Turbidity (via EXO)	TURB	(FNU)	USGS, CA-WSC	0.01 FNU	ND	(YSI, 2012)
fDOM (via EXO)	fDOM	(QSE)	USGS, CA-WSC	0.07 ug/L	ND	(YSI, 2012)
Chlorophyll (via EXO)	Chl.a	(RFU)	USGS, CA-WSC	0.01 RFU	ND	(YSI, 2012)
Water isotopes, deuterium	δ^{2}H	per mil	USGS, CA-WSC		ND	(Downing and others, 2016)
Water isotopes, oxygen	δ^{18}O	per mil	USGS, CA-WSC		ND	(Downing and others, 2016)
Dissolved organic matter concentration (carbon-basis)	DOC	(mg/L)	USGS, CA-WSC	0.03 mg/L	0.3 mg/L	(Potter and Wimsatt, 2005)
Specific UV Absorption @ 254nm	$SUVA_{254}$	(L/mg m)	USGS, CA-WSC	NA	NA	(U.S. Environmental Protection Agency, 2005; Weishaar and others, 2003)
Absorbance spectra (250–600 nm)	A	AU (per cm)	USGS, CA-WSC	various, see ref		(Hansen and others, in press)
Fluorecence spectra (ex 240–400, em290–600)	Various	RU	USGS, CA-WSC	various, see ref		(Hansen and others, in press)
Excitration emissions spectra (EEMS)	EEMS	RU	USGS, CA-WSC	NA	NA	(Poulin and others, 2014)

Table 6. Sediment analytical methods used in the Cosumnes River Preserve mercury study.

[ng/g, nanogram per gram; 1/d, per day; %, percent; g/cm^3, grams per cubic centimeter; mL PW/cm^3, milliliters of porewater per cubic centimeter; <, less than; µm, micrometers; mv, millivolts; mg/L, milligram per liter; pg, picogram; mmol/L, millimole per liter; USGS, U.S. Geological Survey; NRP-WR, National Research Program–Western Region (Menlo Park, CA)]

Analyte name	Analyte notation	Analyte units	Analytical laboratory	Method detection limit	Method reporting limit	Reference(s)
Total mercury	THg	(ng/g) dry wt.	USGS, NRP-WR	0.14 ng/L at the level of the Tekran 2600 autoanalyzer	0.53 ng/L at the level of the Tekran 2600 autoanalyzer	(Olund and others, 2004)
Methylmercury	MeHg	(ng/g) dry wt.	USGS, NRP-WR	0.26 pg (absolute mass as Hg) at the level of the autoanalyzer	0.30 pg (absolute mass as Hg) at the level of the autoanalyzer	(Marvin-DiPasquale and others, 2011)
Methylmercury degradation rate constant	k_{deg}	(1/d)	USGS, NRP-WR	NA	0.0073 d^{-1}	See: Methods / Laboratory Analyses / Sediment Demethylation Incubations Text
Percent dry weight	%.dw	(% of wet weight)	USGS, NRP-WR	1% of wet wt.	3% of wet wt.	(American Public Health Association, 1981a; Marvin-DiPasquale, Alpers, and Fleck, 2009)
Percent loss on ignition	%.LOI	(% of dry weight)	USGS, NRP-WR	0.3% dry wt.	0.9% dry wt.	(U.S. Environmental Protection Agency, 1981b; Marvin-DiPasquale, Alpers, and Fleck, 2009)
Bulk density (laboratory)	BD	(g/cm^3 wet sediment)	USGS, NRP-WR	0.04 g/cm^3 wet sed	0.12g/cm^3 wet sed	(Marvin-DiPasquale, Alpers, and Fleck, 2009)
Porosity (laboratory)	POR	(mL PW/cm^3 wet sediment)	USGS, NRP-WR	0.02 mL PW/cm^3 wet sed	0.06 mL PW/cm^3 wet sed	(Marvin-DiPasquale, Alpers, and Fleck, 2009)
Sand/silt break	GS	(% <64 µm)	USGS, NRP-WR	2.6%	7.8%	(Matthes, Sholar, and George, 1992)
Oxidation-reduction potential	ORP	(mv)	USGS, NRP-WR	NA	NA	(Lutz, Brigham, and Marvin-DiPasquale, 2008)
pH	pH	standard units	USGS, NRP-WR	NA	NA	(Lutz, Brigham, and Marvin-DiPasquale, 2008)
Porewater Sulfate	pw.SO4	(mmol/L)	USGS, NRP-WR	0.02 ppm	0.05 ppm	(U.S. Environmental Protection Agency, 2007a)
Porewater chloride	pw.Cl	(mmol/L)	USGS, NRP-WR	0.06 ppm	0.25 ppm	(U.S. Environmental Protection Agency, 2007a)

Initial Processing and Preservation of Routine Water Samples

Upon arrival at the laboratory, the water samples were logged and organized for splitting into aliquots for each selected analysis. Collection bottles were shaken to homogenize the sample and aliquots of 30 to 120 mL poured quickly into clean Teflon® filter towers loaded with pre-weighed 0.3

um glass fiber filters. Additional aliquots were added to the filter apparatus until the filters were loaded and flow slowed to a drip under vacuum. Three filters were loaded for each sample for analysis of TSS retained on the 0.3um filter pad. After weighing, the filters were labeled for p.THg, p.MeHg and p.RHg analysis. Filters were stored frozen until further analysis. The filtrate that passed through the 0.3 um glass fiber filters was retained in two 125 mL PETG bottles for respective analysis of the dissolved Hg fractions (f.THg and f.MeHg). A 60 mL split of the filtrate was also retained and stored refrigerated until subsequent analysis of Cl^- and SO_4^{2-}.

Total Suspended Solids

Preweighed filters associated with surface water p.MeHg and p.THg were reweighed after these particulate-laden filters were freeze-dried. The difference between initial and final filter weight was calculated to determine TSS for the volume of sample passed through each filter. This approach was used for surface water samples collected as part of the routine assessment of loads, and for the samples collected as part of the short-term particulate flux measurements.

Water Isotopes

Water isotopes were measured using a cavity ring-down spectrometer (Picarro L2130-i CRDS). After correction with standards, water isotope values (δ^2H, $\delta^{18}O$) are expressed relative to the Vienna Standard Mean Ocean Water-Standard Light Antarctic Precipitation (VSMOW-SLAP) scale in per mil (‰). Secondary standards, previously calibrated against certified primary reference standards from the International Atomic Energy Association (IAEA), were run to develop a linear regression equation for normalizing the water isotope data to the VSMOW-SLAP scale. Two working standards, DI water and Kona Deep drinking water (Kona), were used to perform instrument calibration checks every 4 hours during the analytical runs. To characterize the relation between δ^2H and $\delta^{18}O$ in global precipitation, we used the Global Meteoric Water Line (GMWL) of Craig (1961). To characterize the isotopic signature of local precipitation, we constructed a local meteoric water line (LMWL) using data collected over the previous decade from 19 stations in the San Francisco Bay-Delta (341 samples) and 2 Sacramento River stations (Keswick and Freeport; 32 samples) (Downing and others, 2016).

Sediment Demethylation Incubations

Sediment MeHg degradation potential (MDP) rates were measured in bottle incubations amended with ^{201}Hg stable isotope enriched methylmercury ($Me^{201}Hg$), using an approach somewhat similar to that used previously for ^{14}C radioisotope enriched methylmercury ($^{14}CH_3Hg$) incubations (Marvin-DiPasquale and others, 2000; Marvin-DiPasquale and Agee, 2003; Marvin-DiPasquale and others, 2003). Stable isotope enriched $Me^{201}Hg$ was synthesized from inorganic $^{201}Hg(II)$ methylated with methylcobalamin (Rouleau and Block, 1997). After extraction into high performance liquid chromatography (HPLC) grade methylene chloride and back-extraction into water, the final concentrated $Me^{201}Hg$ solution was 588 nanograms per milliter (ng/mL; as Hg), with an enriched isotope purity of 96.2 percent ^{201}Hg, preserved in 1 percent trace metal clean HCl.

For each round of incubations, the concentrated $Me^{201}Hg$ solution was diluted to 30 ng/mL (as Hg), in diluted phosphate buffer, to create a working stock with a final pH of 2.2. Sediment collected from the field the previous day was subsampled (3.00±0.05 g) into 13 cm^3 crimp sealed incubation bottles under anaerobic conditions using a N_2 flushed glove bag. For each field site, three subsamples were collected. The incubation bottles were preincubated for 4 hours at a temperature that was ±1°C of the mean sediment temperature determined in the field for that sampling event, which ranged from

11.4–26.4°C for the six sampling events. After preincubation, each incubation bottle was injected with 0.1 mL of the $Me^{201}Hg$ working stock, resulting in a final target sediment amendment of approximately 1 ng $Me^{201}Hg$ per g of wet sediment. Between each set of three incubation bottles amended with the $Me^{201}Hg$ solution, a 50 microliter (µL) subsample of the injection solution was added to a 20 mL screw-top vial containing 5 mL of 0.5 percent HCl, with this sample being ultimately used to verify amendment concentrations added. One of the three incubation bottles from each set was then immediately flash frozen in a bath of dry ice and ethanol, and then transferred to the -80°C freezer. This sample represents a site-specific killed control. The remaining two incubation bottles for each site were returned to the incubator and maintained at the predetermined temperature for 7 days. After the incubation period, all of the incubation bottles are similarly flash frozen and stored at -80°C until futher processing. Upon thawing, the previously incubated samples were assayed for $Me^{201}Hg$ via isotope dilution inductively coupled plasma mass spectrometry (ICP-MS), after extraction with potassium hydroxide and methanol (KOH/CH_3OH) as described by Marvin-DiPasquale and others (2011).

Quality Assurance Results for Sediment and Water Parameters

A summary of the quality assurance metrics associated with laboratory analysis of sediment and water parameters is provided in appendix 1.

Total Mercury Determination in Fish

Each frozen fish was initially thawed to room temperature and rinsed with DI water, blotted dry. We then dried each fish to a constant mass at 50°C for approximately 48 hours until completely dried. After drying, we removed fish from the oven and cooled them to room temperature in a desiccator, and weighed them again on an analytical balance to obtain a dry weight for each individual fish. Samples were then homogenized to a fine powder using stainless steel scissors and porcelain mortar and pestle. After processing, homogenized fish samples were stored in a desiccator until Hg determination.

MeHg concentrations are highly correlated with THg concentrations in mosquitofish, with 94 percent of the THg comprised of MeHg (Ackerman and Eagles-Smith, 2010). We therefore used THg concentrations as an index of MeHg concentrations. We determined THg concentrations in mosquitofish on a whole-body basis. THg concentrations were determined at the USGS Dixon Field Station Environmental Mercury Laboratory (Dixon, California) or USGS Contaminant Ecology Research Lab (Corvallis, Oregon) on a Nippon MA-3000 Direct Mercury Analyzer (Nippon Instruments North America, College Station, Texas) or Milestone DMA-80 Direct Mercury Analyzer (Milestone, Monroe, Connecticut) following Environmental Protection Agency Method 7473 (U.S. Environmental Protection Agency, 2007b), using an integrated sequence of drying, thermal decomposition, catalytic conversion, and then amalgamation, followed by atomic absorption spectroscopy. Because we used two different labs to determine THg concentrations in fish, we had each lab analyze 50 percent of the fish retrieved from every cage to eliminate the potential for any bias. Additionally, we calculated the geometric mean THg concentrations for each lab's fish samples and correlated these values among all cages; we found a very strong correlation (linear coefficient of determination (R^2)=0.99, probability (p)<0.0001) and an intercept of 0.001 and slope of 1.02 indicating that the two labs produced comparable data (fig. 10).

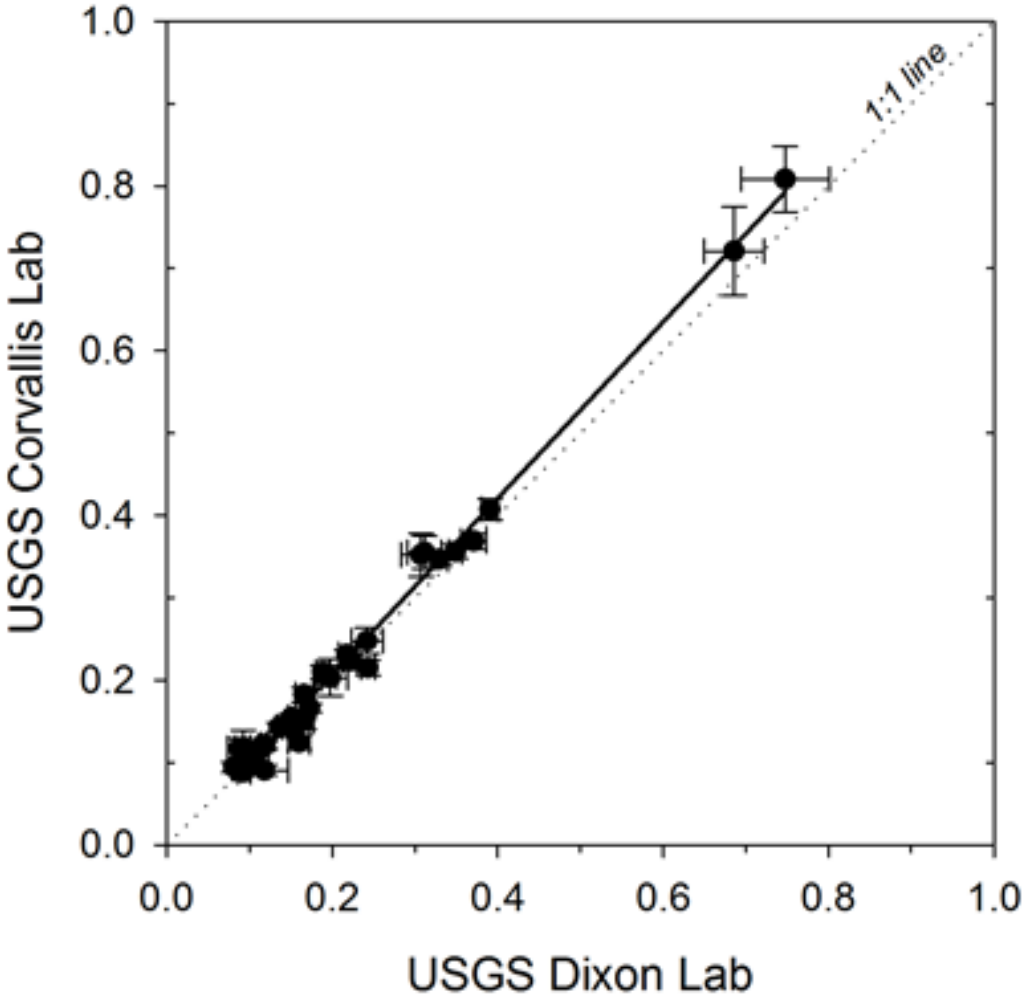

Figure 10. X–Y plot comparing mosquitofish THg concentration analytical results from the USGS Dixon, Calif. laboratory with the USGS Corvallis, Oreg. Laboratory for the Cosumnes River Preserve mercury study. The geometric means (± standard error) are shown, with half of the fish samples from each cage assayed. The dashed 1:1 line is depicted and the results indicate a high correlation between the two laboratories. Units are micrograms per gram dry weight.

Quality assurance measures included analysis of a certified reference material (CRM; either dogfish muscle tissue [DORM] or lobster hepatopancreas [TORT] certified by the National Research Council of Canada, Ottawa, Canada or fish tissue [IAEA-407] certified by International Atomic Energy Agency), system blank, method blank, continuing calibration verification, and duplicate with each set of approximately 10 samples, and two spiked duplicates with each batch of approximately 70 samples. Recoveries (mean ± standard deviation) were 98.8±2.7 percent (number of samples [*n*]=190) for CRM's, 99.2±3.0 percent (*n*=182) for continuing calibration verifications, and 101.6±2.0 percent (*n*=72) for matrix spikes. Relative percent difference averaged 3.6±4.0 percent (*n*=165) for duplicates and 0.8±0.5 percent (*n*=36) for matrix spike duplicates.

Calculations, Modeling & Statistics

All linear least squares statistical models developed and used for examining surface water and sediment results employed JMP statistical software (version 11.2.1, SAS Institute, Inc.). The significance level for a Type-II error was set at a probability (P) level of $P<0.05$ in all cases. Each parameter being tested was first assessed for normality of distribution. In cases where the data was not normally distributed, a natural logarithm (LN) transformation of the data was modeled, with final reported results being back-transformed with standard errors estimated using the Delta method (Seber 1982).

Surface Water

Load Calculations

Surface water loads were calculated two ways to help evaluate sensitivity to error in the integration of the flow and concentration measurement. In the first method, we developed hourly time series of flow using stage-discharge relations at the WCS using in place PT calibrated with manual measurements. Hydrant flow was estimated and calibrated using several methods. During full flow of the hydrant, flow rates were estimated using a distance-flow rate table for a horizontal pipe opening (Schwankl and others, 2007) and (or) bucket tests when flow rates were able to be effectively captured in a 5 gallon pail (<300 gallons per minute) and verified using a Sontek flowtracker where possible. Stage-discharge relations for the weirs were developed using the in place depth measurements from the PT correlated with manual measurements of depth over each weir and converted to flow using the engineering equation for flow over a rectangular weir (U.S. Bureau of Reclamation, 2001; Heald, 2002):

$$Q = C*(L-0.2 \times H)*H^{1.5} \quad (1)$$

where Q=flow in cubic feet per second, L=length of weir opening in feet, H=head on weir in feet and C=weir coefficient, assigned as 3.207 based on calibrated results for similar weir systems (Bachand and others, 2014).

The resulting hourly flow records were then integrated with water concentrations measured in the laboratory and interpolated to a corresponding hourly record for each WCS to generate an hourly loading rate. Load rate=concentration (ng/L) x flow (L/hour). That hourly loading rate was then integrated over time to determine a cumulative mass loading over the flooded period. Loads were determined first for the conservative tracer chloride (Cl), measured in laboratory samples, and the quasi-conservative tracer, specific conductance (SC), measured in place hourly at a subset of locations.

The second method used only manual measurements to estimate loads. The manual measurements of water level at the inlets and outlets were averaged on a monthly timescale and integrated with the lab-based concentration measurements to generate a load value for each month during the flooded period. All loads were then corrected using the Cl balance. Where possible, the two methods were compared. In both cases, the measurements ended prior to the field drainage, a quick (approximately one week) drawdown of the field by pulling all of the boards at the outlets over two or three days. The export load from the drawdown event was estimated using the volume of the field multiplied by the concentration measured in the field in the day prior to the pulling of the boards and then added to the loads calculated for the period of flow. For constituents that had both filter-passing (dissolved) and filter-retained (particulate) results, the load calculations were conducted separately and then added together for a total constituent load for the flooded period.

Mercury Fractions Calculated and Defined

There are a number of ways THg and MeHg data can be calculated and expressed, each of which is informative in its own right. In this report we express surface water particulate forms of THg and MeHg both on a volumetric basis (p.THg.vol and p.MeHg.vol, respectively, units in ng/L) and on a gravimetric basis (p.THg.mass and p.MeHg.mass, respectively, units in ng/g). While filter-passing (f.THg and f.MeHg) and particulate (p.THg.vol and p.MeHg.vol) fractions are separated upon suface water collection and assayed independently, they can be added back together to back-calculate what the unfiltered THg (uf.THg) and unfiltered MeHg (uf.MeHg) volumetric (ng/L) concentrations were in the original sample. In addition, f.MeHg, p.MeHg and uf.MeHg can all be expressed as a percentage of the THg in each of their respective fractions, leading to %f.MeHg, %p.MeHg and %uf.MeHg. Finally, it is often useful to consider the relative partitioning of THg and MeHg between the suspended particulate phase and the aqueous (dissolved, filter-passing) phase. This is typically expressed as a partitioning coefficient (k_d) for each species:

$$k_d[THg]=(p.THg.mass*1{,}000)/f.THg \quad (2)$$

and

$$k_d[MeHg]=(p.MeHg.mass*1{,}000)/f.MeHg \quad (3)$$

where k_d[THg] and k_d[MeHg] (units=L/kg); p.THg and p.MeHg (units=ng/g); 1000 multiplier from g to kg; f.THg and f.MeHg (units=ng/L).

Statistical Models

Linear least squares multi-variable statistical models were used to analyze the bulk of the surface water, sediment and biota data collected in this study. The benefit of this approach is that it allows for multiple statistical questions to be asked simultaneously for individual model terms while controlling for (taking into account) the variability in the other model terms. It also allows for examining potential interactions between main model terms (for example the interaction between season and WCS type).

Surface water parameters given in table 5 were statistically analyzed with a linear mixed-effects model (MODEL A.1) of the general form:

$$Y = WCS.Type+YEAR+SEASON+WCS.Type*YEAR+WCS.Type*SEASON+FIELD_{[random]} \quad \text{(MODEL A.1)}$$

where Y=any surface water parameter; YEAR=study Year 1 (WY2014–15=September 2014–April 2015), study Year 2 (WY2015–16=September 2015–May 2016); SEASON=early (September to November), mid (December to Februrary), late (March to May); WCS.Type (control inlet [C.in], control outlet [C.out], treatment inlet [T.in], treatment check weir [T.chk], treatment outlet [T.out]); WCS.Type*YEAR=interaction term; WCS.Type*SEASON=interaction term; $FIELD_{[random]}$=all individual control and treatment wetlands (field ID's) as a random variable.

For Hg specific data, in cases where the WCS.Type*YEAR interaction term was significant, an abbreviated form of MODEL A.1 (MODEL A.2) was used for data subset by individual YEAR:

$$Y_{[YEAR]} = WCS.Type+SEASON+WCS.Type*SEASON+FIELD_{[random]} \quad \text{(MODEL A.2)}$$

where $Y_{[YEAR]}$=any surface water parameter subset by study Year (WY2014–15, WY2015–16); WCS.Type, SEASON, WCS.Type*SEASON and $FIELD_{[random]}$ as per MODEL A.1.

In cases where the WCS.Type*SEASON interaction term was significant for MODEL A.1, and there was a desire to more completely resolve the differences among WCS.Type for each season (both Year 1 and Year 2 data included), statistics were rerun for data subset by individual seasons according to MODEL B:

$$Y_{[SEASON]}=WCS.Type+FIELD_{[random]} \quad \text{(MODEL B)}$$

where $Y_{[SEASON]}$=any surface water parameter subset by season (September to November, December to February, March to May); WCS.Type and $FIELD_{[random]}$ as per MODEL A.1.

In cases where the WCS.Type*YEAR interaction term was significant, and there was a desire to more completely resolve the differences among WCS.Type for each by Year , statistics were rerun for data subsets by individual sampling years according to MODEL C:

$$Y_{[Year]}=WCS.Type+FIELD_{[random]} \quad \text{(MODEL C)}$$

Where: $Y_{[Year]}$=any surface water parameter subset into either study Year 1 (WY2014–15) or study Year 2 (WY2015–16); WCS.Type and $FIELD_{[random]}$ as per MODEL A.1.

Temporally integrated (full flooded season) loads data, associated with filtered and dissolved THg and MeHg fractions, were modeled as:

$$Y_{[load.WCS]}=FIELD.type+YEAR+FIELD.type*YEAR+FIELD_{[random]} \quad \text{(MODEL D)}$$

where $Y_{[load.WCS]}$=temporally integrated (full flooding season) surface water mass (in mg) loads fractions (for example f.THg, p.THg, f.MeHg, p.MeHg, uf.THg, uf.MeHg) calculated for cell specific WCS (inlets and outlets) or the difference in these load fractions between WCS in series (i.e. outlets minus checks [OUT–CHK], checks minus inlets [CHK-IN], outlets minus inlets [OUT-IN]); FIELD.type=control or treatment) to examine the net change in a given Hg fraction within a study cell; YEAR, FIELD.type*YEAR, and $FIELD_{[random]}$, as per MODEL A.1.

Sediment

Methylmercury Degradation Potential Rates

Rate constants associated with the $Me^{201}Hg$ degration incubations were calculated as:

$$k_{deg}= -\ln(1–(Me^{201}Hg_{kc} –Me^{201}Hg_{t=f})/Me^{201}Hg_{t=0})/t \quad (4)$$

where k_{deg} = the MeHg degradation rate constant (d^{-1}); $Me^{201}Hg_{kc}$ = the concentration of $Me^{201}Hg$ (in ng/g wet sediment) in the killed control sample; $Me^{201}Hg_{t=f}$ = the concentration of $Me^{201}Hg$ (in ng/g wet sediment) in the incubated sample at the end of the incubation (time=final); $Me^{201}Hg_{t=0}$ = the theoretical $Me^{201}Hg$ concentration (in ng/g wet sediment) at the beginning of the incubation (time=0) based on the $Me^{201}Hg$ amendment; t = time (days).

The methylmercury degradation potential (MDP) rate is then calculated as:

$$MDP=MeHg_{ambient}–MeHg_{ambient} * EXP(-k_{deg} * t) \quad (5)$$

where $MeHg_{ambient}$ = the independently measured ambient surface sediment MeHg concentration (in ng/g wet sediment), and where t is set for 1 day.

MeHg Benthic Diffusive Flux Estimates

While MeHg benthic flux was not directly measured in this study, it was estimated in an attempt to better refine the deep cell MeHg loads budgets. To do this, we needed to first estimate what the porewater f.MeHg concentration might have been in the 0–2 cm surface sediment interval sampled. A large dataset (*n*=74) of previously published (Marvin-DiPasquale and others, 2009; Chalmers and others, 2013) distribution coefficients (k_d), measured in stream bed sediment (nine unique steam settings across the United States), was statistically analyzed for its mean and non-parametric quartile distribution. The summary statistics are as follows (k_d units: L/kg): mean±standard error, 4,980±955; 25 percent quartile= 606; 50 percent quartile (median)=1,706; 75 percent quartile=5,188.

Porewater f.MeHg concentrations were then back calculated for every deep cell sediment sampling site and event (table 4), according to equation. 6:

$$pw.MeHg=1{,}000 * sed.MeHg/k_d \quad (6)$$

where pw.MeHg=porewater MeHg concentration (ng/L), sed.MeHg=bulk sediment MeHg concentration (ng/g, dry wt.), and k_d=partitioning coefficient (in L/kg) for the 25 percent, median (50 percent), and 75 percent percentile k_d values given above. This provided three estimates of pw.MeHg concentration for each one of the original sed.MeHg concentrations actually measured.

Temperature corrected MeHg diffusion coefficients were then calculated for each sediment sampling site and date, based on the sediment temperature at the time of collection, according to equation 7 (Lerman, 1979):

$$D_{T1} = D_{T2} * (1 + 0.048 * \Delta t) \quad (7)$$

where D_{T1}=diffusion coefficient (in square centimeters per second [cm^2/s]) at temperature T1; D_{T2}=diffusion coefficient (cm^2/s) at temperature T2=0.000013 cm^2/s at 25°C for MeHgCl (Gill and others, 1999); Δt=temperature difference (T1–T2) in °C.

Each pw.MeHg concentration was then paired with a monthly average surface water f.MeHg concentration (measured at the deep cell outflow WCS), based on the sediment deep cell identification and sampling date. Temperature corrected diffusive MeHg flux was then calculated according to Fick's Law, equation 8:

$$F=D_{T1}*(\delta C/\delta x)/1{,}000*60*60*24*100*100 \quad (8)$$

where F=diffusive flux for MeHg ($ng/m^2/d$); δC=pw.MeHg–f.MeHg=porewater MeHg minus surface water f.MeHg (in mg/L); δx=diffusion gradient distance (in cm) between porewater and surface water=3 cm (assumed). For each deep cell and sampling event, an average (± standard error) daily MeHg flux was then calculated based on *n*=3 fixed sediment sampling sites per deep cell. These daily flux rates were then integrated for the full flooded season for each deep cell and sampling Year.

Statistical Models

Sediment parameters given in table 6 were statistically analyzed with a linear mixed-effects model designed to compare the subset of sediment parameters that were collected from both treatment and control wetlands on four sampling events (Year 1=Sept.2014 (pre-flood), Nov.2014, April.2015; Year 2=May.2016). The form of the model (MODEL E) was:

$$Y_{sed}=CELL.Type+EVENT+CELL.Type*EVENT+CELL_{[random]} \quad (MODEL\ E)$$

where Y_{sed}=any sediment parameter; CELL.Type=control, shallow (treatment), deep (treatment); EVENT=Sept.2014 (pre-flood), Nov.2014, April.2015, May.2016; CELL.Type* EVENT=interaction term; $CELL_{[random]}$=all each individual study cell as a random variable.

To examine sediment parameters specifically focused on the results for the four individual deep cells while under flooded conditions, which were sampled on six events (early, mid and late season during both study years, table 4), the following model (MODEL F) was used:

$$Y_{sed}=CELL.ID+YEAR+SEASON+CELL.ID*YEAR+CELL.ID*SEASON \quad (MODEL\ F)$$

where Y_{sed}=any sediment parameter; CELL.ID=D01, D07, D17, D18; YEAR=WY2014–15, WY2015–16; SEASON=Fall (Nov.), Winter (Feb.), Spring (April/May); CELL.ID* YEAR=interaction term; CELL.ID* SEASON=interaction term.

To examine the effect of shallow field management approaches to vegetative growth (mowing vs discing) during the non-flooded season on sediment MeHg concentrations during the flooded season, the following model (MODEL G) was used:

$$Y_{sed}=VEG+EVENT+VEG*EVENT+CELL_{[random]} \quad (MODEL\ G)$$

where Y_{sed}=any sediment parameter; VEG=mowed or disced (shallow treatment cell and control cell vegetation management practice at specific sediment sampling locations); EVENT=Sept.2014 (pre-flood), Nov.2014, April.2015, May.2016; VEG* EVENT=interaction term; $CELL_{[random]}$=all each individual study cell as a random variable.

Photodemethylation

Photodemethylation, the photo-reactive degradation of water column MeHg (photodegradation), was modeled on a monthly and cell-specific basis using previously established relations (Fleck and others, 2014), based on net radiation and initial MeHg concentrations (Fleck and others, 2014). Photosynthetically available radiation (PAR) is commonly used as index of ultraviolet (UV) radiation as it is measured more often and is proportional to UV. Although it is true that there are different demethylation rates for the specific wavelength ranges, the rates we are using were derived from exposure to the full spectrum of solar radiation—the use of PAR is simply a subset of the spectrum used to represent the full spectrum in the derived regressions from our previous paper (Fleck and others, 2014).

$$LN[MeHg]_{LOSS}=LN[MeHg]_{INITIAL}*k_{pd}*PAR_{[cc]} \quad (9)$$

where $LN[MeHg]_{Loss}$ = the natural logarithm of the photodegraded MeHg concentration (normalized to ng/m^2); $LN[MeHg]_{initial}$ = the initial ambient water column MeHg concentration (normalized to ng/m^2) based on and the average filter-passing MeHg concentration (in ng/L) converted to an areal basis and limited to the depth of maximal light penetration (Z_{max}, see equation 13 below) specific for each month and study cell; k_{pd} = the photodegradation rate constant of 0.0075 m^2/mol (Fleck and others, 2014); PAR[cc] = the corrected cumulative PAR (mol/m^2). Monthly and study cell specific values of $PAR_{[cc]}$ were calculated as:

$$PAR_{[cc]}=(-2.43 * K_{ext}+0.42)*PAR_{[cd]} \quad (10)$$

where K_{ext} = the monthly and cell specific light extinction coefficient (units: cm^{-1}) calculated from monthly averaged cell specific DOC and turbidity data (see equation 11 below), $PAR_{[cd]}$ = the cumulative daily PAR for each month using a summation of total daily PAR values from the California Irrigation Management Information System (CIMIS) Station #70 for Manteca, San Joaquin Valley (University of California Agriculture and Natural Resources, 2016). CIMIS data, in units of Langleys of radiation per day, were converted on an areal basis to mols of PAR per m^2.

Monthly and cell specific K_{ext} values were modeled based on monthly and cell specific average values of DOC (in mg/L) and turbidity (in formazin nephelometric units [FNU]) measured at outlet WCS, according to equation 11, which was developed from directly measured light profiles paired with concurrently measured turbidity and fDOM (converted to DOC) data (n=32, R^2 = 0.84) collected during this study:

$$K_{ext}=0.0013*DOC+0.00087*Turbidity+0.0141 \quad (11)$$

The surface water fDOM (in FNU) data measured with the EXO water quality sonde, co-collected with the above light depth profiles, were converted to DOC (in mg/L) according to:

$$DOC=0.116*fDOM+0.823 \quad (12)$$

Equation 12 was derived from n=183 paired observations of fDOM and DOC collected throughout the study from check and outlet WCS, after excluding data pairs where the fDOM/DOC ratio were less than a value of 5. The R^2 value for Equation 12 was 0.67.

The depth of maximal light penetration (Z_{max}), necessary for calculating $LN[MeHg]_{initial}$ in Equation 9 above, was calculated from K_{ext} according to:

$$Z_{max}= -LN(0.05)/k_{ext} \quad (13)$$

Statistical Analysis of Fish

We compared THg concentrations in mosquitofish using linear mixed-effect models in two main analyses. First, we tested whether THg concentrations in mosquitofish differed among experimental treatments. In this test, log_e-transformed THg concentration in mosquitofish was the dependent variable and treatment (experimental wetland or control wetland), subsite (cage location within wetland), year

(2015 or 2016), body mass at introduction (wet mass), change in fish mass from introduction to retrieval, and the interactions treatment × subsite, treatment × year, year × subsite, and treatment × subsite × year were fixed effects, and wetland identification and cage identification were random effects. The random effect variables insured that individual fish would be nested within their specific cage and wetland.

Second, we tested whether mosquitofish mass change after introduction into cages for 30 days differed among experimental treatments. In this test, mosquitofish body mass change (wet body mass at retrieval – wet body mass at introduction) was the dependent variable and treatment (experimental wetland or control wetland), subsite (cage location within wetland), year (2015 or 2016), body mass at introduction (wet mass), and the interactions treatment × subsite, treatment × year, year × subsite, and treatment × subsite × year were fixed effects, and wetland identification and cage identification were random effects.

In each test, we dropped nonsignificant interaction terms and used Tukey's Honest Significant Difference test to examine differences among pair-wise comparisons. We used the Satterthwaite method to estimate the degrees of freedom. We reported model-based, least squares mean (LSM) ± standard error (SE) THg concentrations based on back-transformed LSM ± SEs. SEs were approximated using the delta method (Seber, 1982). Mean ± standard deviation for percent moisture in mosquitofish was 73.9±0.02 percent (n=1,711) which can be used to convert reported dry weight concentrations into wet weight concentrations.

Results and Discussion

The overarching drivers of the current study were to investigate two proposed wetland management strategies that could at least partially ameliorate MeHg export from, and bioaccumulation within, managed wetlands. Specifically asking the questions: (a) Does the inclusion of a deep cell (open water) in a wetland reduce MeHg export? and (b) Does managing a wetland under continuous flow-through conditions reduce Hg bioaccumulation in fish compared to a control wetland that is managed under fill-and-maintain conditions? In addressing the first question, three modes of MeHg removal were studied in the constructed deep-water cells: particle settling, photodemethylation, and microbial degradation in the surface sediment. To address the second question, caged fish experiments were employed.

Surface Water Total Mercury and Methylmercury Concentrations and Loads

A central focus of this study was to examine how the inclusion of deep cells in a wetland setting managed under flow-through conditions impacted net THg and MeHg export from the wetland complex. This question is composed of two parts: (a) the effect of flow-through versus fill-and-maintain wetland management practices overall, and (b) the effect of the deep cell on removing MeHg coming in from the adjacent upstream shallow cell. To begin to resolve these two issues we highlight here the observed changes in Hg species concentration data collected at the various WCS throughout the flooded period during two years of study, as well as the Hg species loads data temporally integrated for each of the two flooded periods studied. The complete study dataset for surface water filter-passing, particulate and unfiltered (whole water) concentrations of THg and MeHg, as well as calculated THg and MeHg partitioning coefficients (k_d), are provided in appendix 2.

Concentrations

Appendix 3 summarizes the LSM and Tukey comparison results for all surface water constituent data using MODEL A.1, which simultaneously tests differences between the two study years (WY2014–15, WY2015–16), among three seasons (September to November, December to February, March to May), and among the five types of WCS (control cell inlets and outlets, shallow treatment cell inlet, treatment field check weir, deep cell outlet), as well as tests for interaction effects between WCS.Type*SEASON and WCS.Type*YEAR. Eight out of the 13 Hg-related metrics summarized in appendix 3 had significant WCS.Type*SEASON interactions (f.THg, f.MeHg, p.THg.vol, p.MeHg.mass, p.MeHg.vol, uf.THg, uf.MeHg, k_d[THg], %f.MeHg, %p.MeHg, %uf.MeHg), while only five out of the 13 had significant WCS.Type*YEAR interactions (p.THg.vol, p.MeHg.vol., uf.THg, k_d[THg], %f.MeHg).

Where WCS.Type*SEASON interactions were found to be significant in MODEL A.1, statistical difference among WCS for each SEASON grouping were further resolved using MODEL B with the LSM and Tukey results being summarized in appendix 4. Where WCS.Type*YEAR interactions were found to be significant in MODEL A.1, statistical difference among WCS for each study YEAR were further resolved using MODEL C with those results being summarized in appendix 5. In addition, at a more granular level of analysis of surface water Hg species in particular, MODEL A.2 compares all WCS.Type*SEASON interactions for each YEAR, individually.

Focusing on unfiltered (whole water) Hg fractions, MODEL A.1 indicated significant differences in uf.THg by WCS.type ($F_{4,42.56}$=55.7, p<0.001), YEAR ($F_{1,286}$=16.6, p<0.001), and modestly by SEASON ($F_{2,286}$=2.84, p=0.06). However, interaction terms WSC.type*YEAR ($F_{4,286}$=4.07, p=0.003) and WSC.type*SEASON ($F_{8,286}$=8.3, p<0.001) were also significant, indicating that differences in uf.THg concentrations among WCS varied both by SEASON and by YEAR. In the case of uf.MeHg, MODEL A.1 showed significant differences by WCS.type ($F_{4,43.85}$=43.6, p<0.001), YEAR ($F_{1,287}$=4.72, p=0.031), SEASON ($F_{2,288}$=43.66, p<0.001) and WSC.type*SEASON ($F_{8,287}$=7.41, p<0.001), but not by WSC.type*YEAR ($F_{4,287}$=1.95, p=0.103), indicating that differences in uf.MeHg concentration among WCS varied by SEASON, but not by YEAR. The spatial and temporal trends in uf.THg and uf.MeHg concentrations are graphically illustrated in fig. 11 (LSM results of MODEL A.2, with each YEAR modeled separately). Similarly, plots for f.THg and f.MeHg are shown in fig. 12, and plots for p.THg and p.MeHg are shown in figure 13. The tabular summary of surface water Hg concentration data corresponding to figures 11–13, along with the Tukey results for each model term, is summarized in appendix 6.

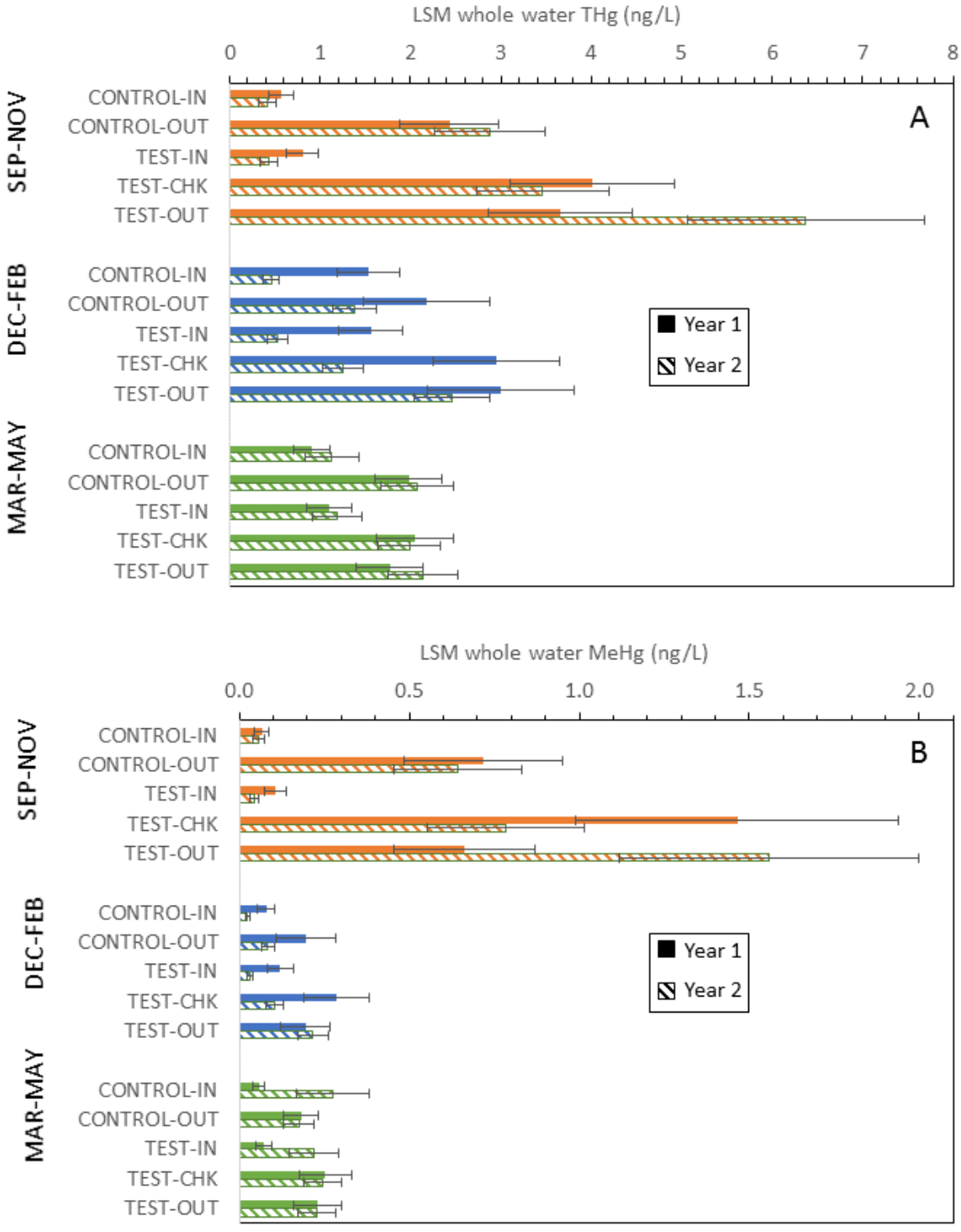

Figure 11. Bar plots of MODEL A.2 results from the Cosumnes River Preserve mercury study depicting least square means (LSM) for *A*, whole water total mercury (THg); and *B*, methymercury (MeHg) concentration, by water control structure type, season, and year. Data was modeled by each year individually. See appendix 6 for Tukey rankings. Error bars reflect standard errors. ng/L, nanogram per liter.

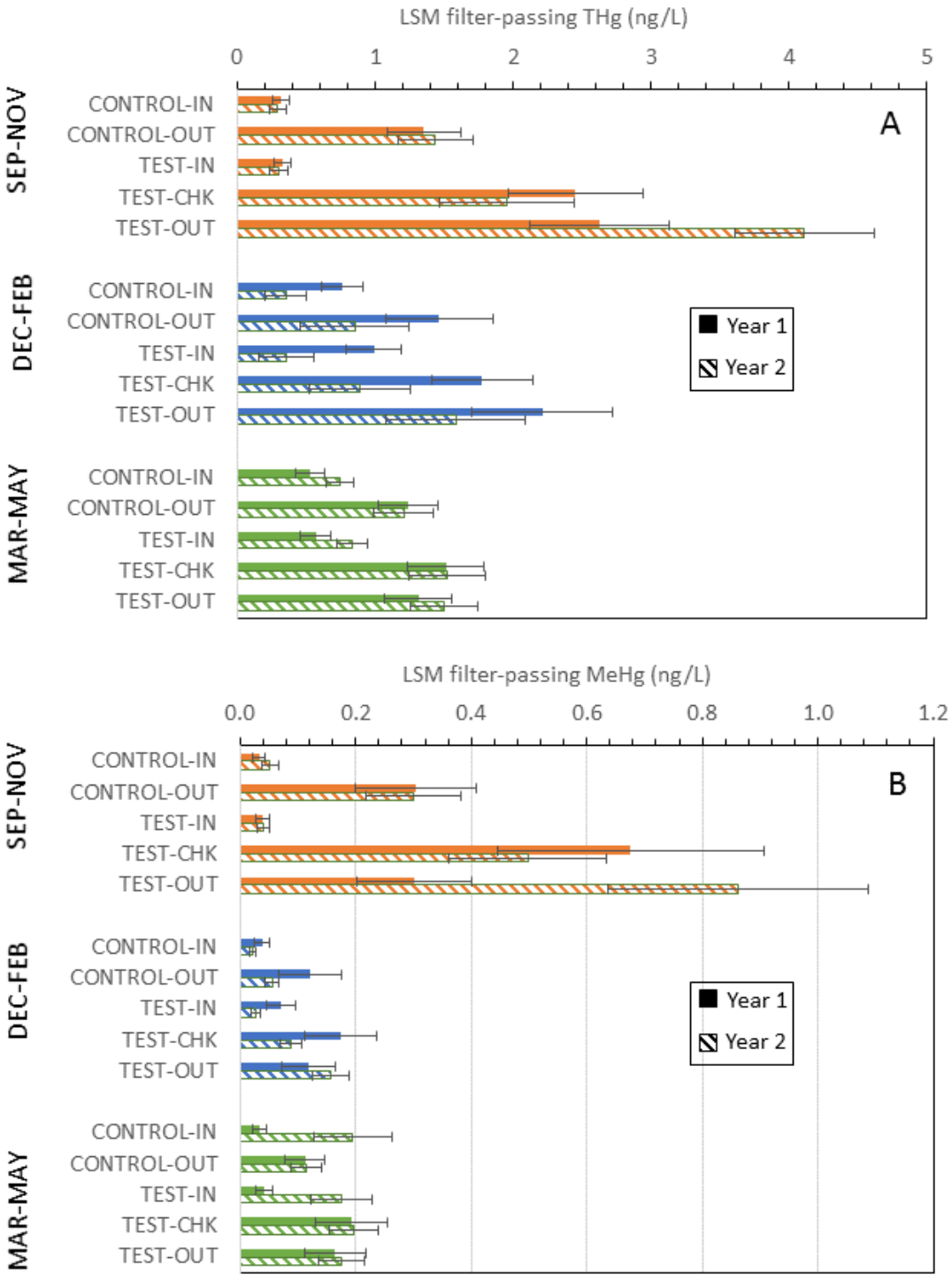

Figure 12. Bar plots of MODEL A.2 results from the Cosumnes River Preserve mercury study depicting least square means (LSM) for *A*, filter-passing total mercury (THg); and *B*, methylmercury (MeHg) concentration, by water control structure type, season, and year. Data was modeled by each year individually. See appendix 6 for Tukey rankings. Error bars reflect standard errors. ng/L, nanogram per liter.

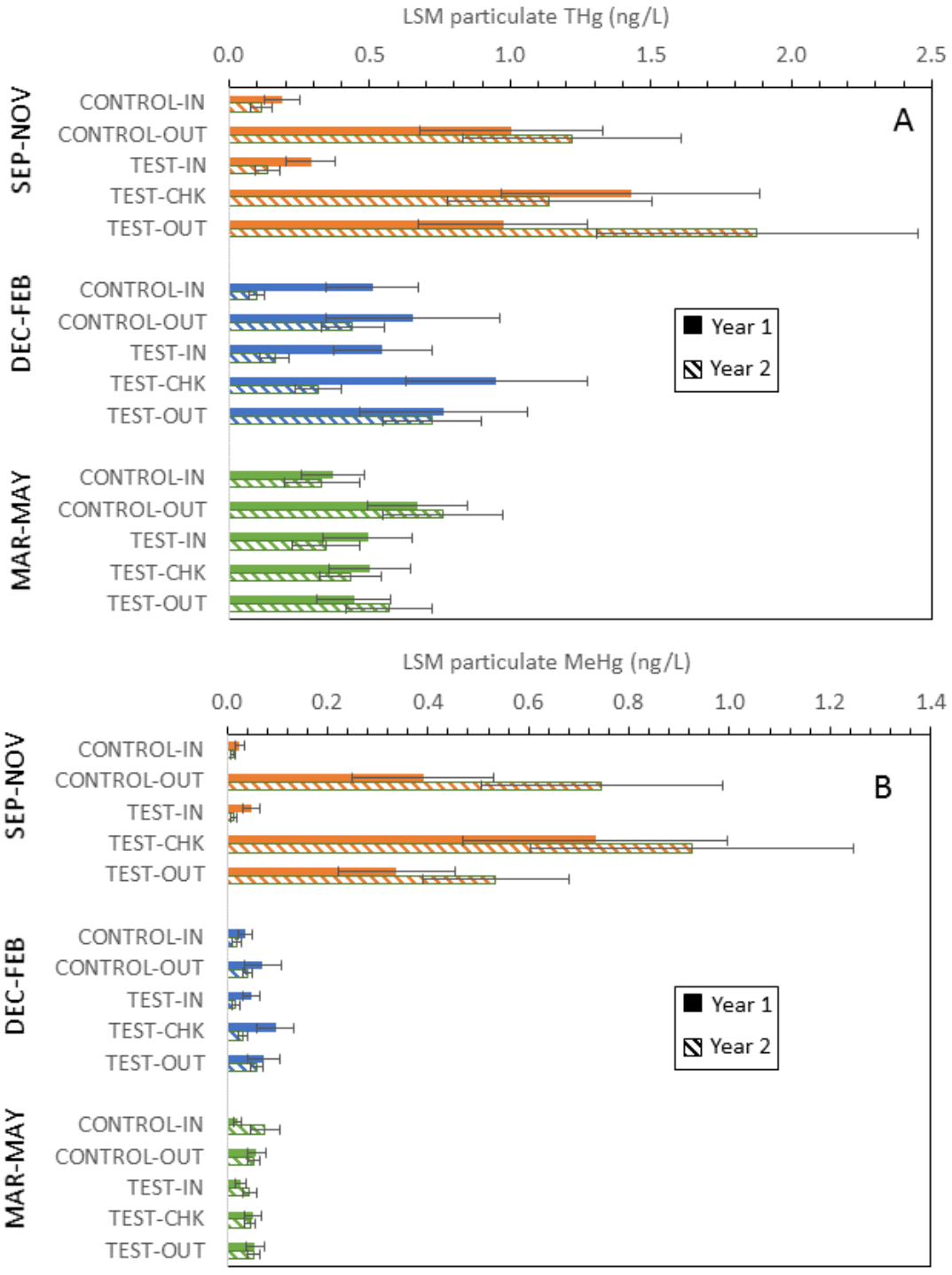

Figure 13. Bar plots of MODEL A.2 results from the Cosumnes River Preserve mercury study depicting least square means (LSM) for *A*, particulate total mercury (THg); and *B*, methylmercury (MeHg) concentration, by water control structure type, season, and year. Data was modeled by each year individually. See appendix 6 for Tukey rankings. Error bars reflect standard errors. ng/L, nanogram per liter.

Relevant observations resulting from this temporal/spatial statistical analysis of surface water Hg concentration data include:

- In control wetlands, the significant increase in concentrations of uf.THg and uf.MeHg (fig. 11), f.THg and f.MeHg (fig. 12), and p.THg and p.MeHg (fig. 13), from the inlets to the outlets, was most pronounced and consistent (both years) during the SEP–NOV period (appendix 6).
- In the shallow portion of the treatment wetlands, the significant increase in concentrations of uf.THg and uf.MeHg (fig. 11), f.THg and f.MeHg (fig. 12), and p.THg and p.MeHg (fig. 13), from inlets to the check weirs, was also most pronounced and consistent (both years) during the SEP–NOV period (appendix 6).
- In the deep portion of the treatment wetlands, there were no significant difference in either uf.THg or uf.MeHg concentrations, between the check weirs and the outlets, for any season or year, with the sole exception of an increase from check to outlet for uf.THg during DEC–FEB/Year 2 (fig. 11, appendix 6).
- In the deep portion of the treatment wetlands, there were no significant difference in either f.THg or f.MeHg concentrations, between the check weirs and the outlets, for any season or year, with the two exceptions of an increase from check to outlet for f.THg during SEP–NOV/Year 2 and DEC–FEB/Year 2 (fig. 12, appendix 6).
- In the deep portion of the treatment wetlands, there were no significant difference in either p.THg or p.MeHg concentrations, between the check weirs and the outlets, for any season or year (fig. 13, appendix 6).

It is clear from figs. 11–13 that the fall period (September to November), following initial flood up, is particularly significant in terms of elevated THg and MeHg concentrations (all fractions) within both the control wetlands and the shallow cell portion of the treatment wetlands. This could reflect either new MeHg production or the release of MeHg trapped in previously dry soil into the overlying water in the period soon after flood up. The spatial and temporal similarity of this trend for both THg and MeHg suggests that the early season MeHg peak is at least partially the result of a release of previously stored MeHg, as has been suggested in other studies (Marvin-DiPasquale, Alpers, and Fleck 2009; Marvin-DiPasquale and others, 2014).

We also statistically tested whether water supply (pumps associated with inlet WCS) varied with respect to THg and MeHg concentrations entering the control and shallow treatment cells. The only significant differences found occurred at the inlet WCS for both f.THg and f.MeHg, with a significant interaction between supply and year for both Hg species (f.THg: $F_{2,90.8}$=7.05, p=0.0014; f.MeHg: $F_{2,87}$=6.94, p=0.0016) indicating that the differences among pumps was not consistent between years. Further, f.THg and f.MeHg concentrations at the pumps (inlets) were comparatively low (n=116; mean and SE: uf.THg = 0.63±0.05 ng/L; uf.MeHg = 0.09±0.01 ng/L) when compared with concomitant values at check and outlet WCS. In short, pump 1 (feeding fields 2 and 7) had higher concentrations for both Hg species during Year 1, whereas pumps 3 and 4 (feeding fields 9, 13, 17, and 18) had higher concentrations for both Hg species during Year 2. Pump 2 (feeding fields 1 and 6) was most consistent between years for all fractions.

MeHg Loads

Loads are a function of both concentration and hydrologic flow rate. Thus, we would anticipate (and did observe) some of the highest MeHg loads of the study at the check weir of the treatment welands (outflow from the shallow cell to the deep cell) during the September to November period (fig. 14), because of the elevated concentratons at these WCS during this period (as discussed in Concentrations) and the flow-through conditions imparted on the treatment wetlands as part of the study

design. In contrast, we would anticipate no significant change in MeHg loads between the inflow and outflow WCS of the control wetlands, and low MeHg loads at the control outlets compared to the treatment wetland check weirs, during the same September to November period, because of the fill-and-maintain management stategy employed for the control wetlands. This anticpated trend was indeed observed during Year 1 (fig. 14, appendix 6). However, during Year 2 there was a significant increase in both p.MeHg and uf.MeHg load between the inlet and outlet WCS for the control wetlands during September to November, which was driven by a temporary change to flow-though operation of the control wetlands during the September to December, 2015 period. In addition, there was no significant difference in p.MeHg and uf.MeHg loads between control wetland outlets and treatment wetland check weirs during September to November of Year 2. After fill-and-maintain management was re-established for the control wetlands (December 2015) both December–February and March–May periods of Year 2 exhibited significantly higher f.MeHg, p.MeHg and uf.MeHg loads at the treatment check weir compared to the control outlet, demonstrating the critical effect of flow on MeHg export from shallow wetland cells.

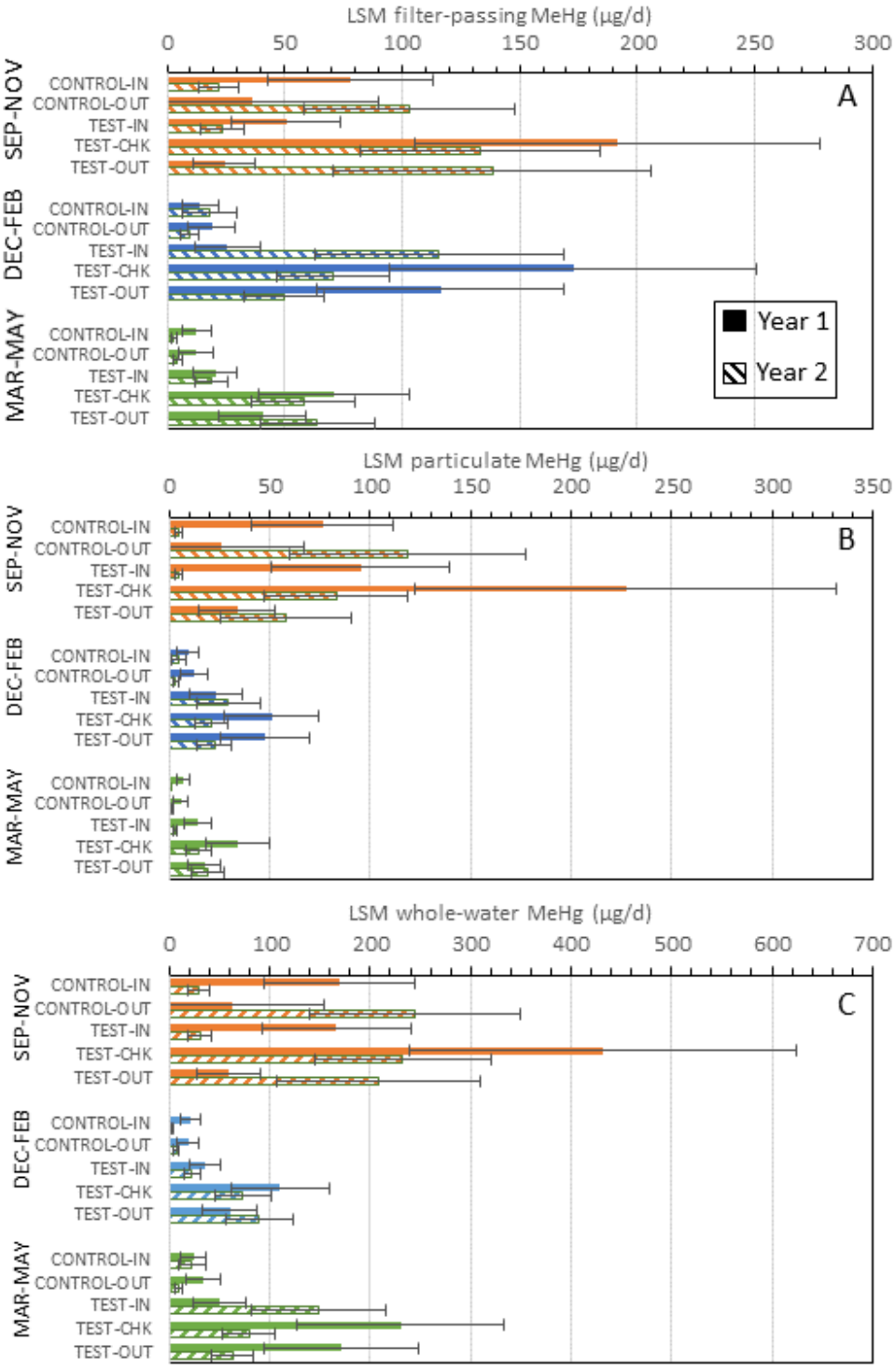

Figure 14. Bar plots of MODEL A.2 results from the Cosumnes River Preserve mercury study depicting least square mean (LSM) loads for *A*, filter-passing; *B*, particulate; and *C*, unfiltered (wholewater) by water control structure type, season, and year. Data was modeled by each year individually. See appendix 6 for Tukey rankings. Error bars reflect standard errors. µg/d, microgram per day.

When calculating the total cumulative mass loading over the entire flooded period for each field and each year, it is possible to assess the mass balance of each cell and pond complex. Tables 7 and 8 summarize annually integrated mass loads of THg and MeHg, respectively, for each study cell during both study years. The mean values for the four control wetlands and four treatment field, by study year and by WCS, are graphically illustrated for filtered, particulate, and unfiltered THg and MeHg (fig. 15).

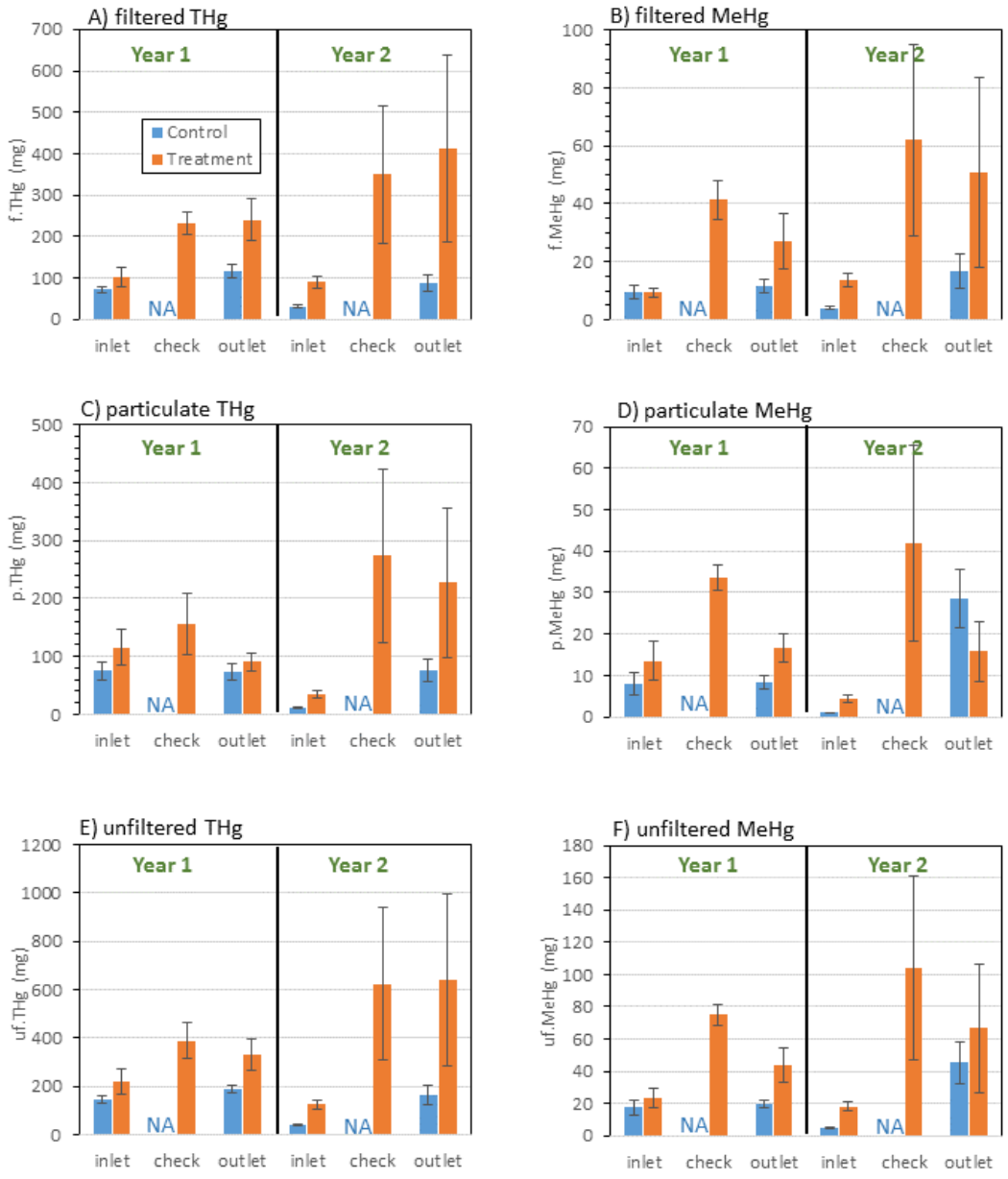

Figure 15. Bar plots of mean annually integrated THg and MeHG mass loads from the Cosumnes River Preserve mercury study by water control structure, wetland type, and study year. Hg fractions represent *A*, filter-passing THg; *B*, filter-passing MeHg; *C*, particulate THg; *D*, particulate MeHg; *E*, unfiltered THg; and *F*, unfiltered MeHg. Error bars reflect standard errors. NA, not applicable; mg, milligram.

Table 7. Annually integrated total mercury loads from the Cosumnes River Preserve mercury study by study year and water control structure (inlet, check weir, outlet) for the four treatment and control wetlands.

[f.THg, filtered total mercury; p.THg, particulate total mercury; T##, treatment wetland identification; C##, control wetland identification; Year 1, Water Year 2014–15; Year 2, Water Year 2015–16; mg, absolute milligrams of THg; NA, not applicable; AVG, average; SE, standard error]

Field	Year 1						Year 2					
	Inlet		Check		Outlet		Inlet		Check		Outlet	
	f.THg	p.THg	f.THg	p.THg	f.THg	p.THg	f.THg	p.THg	f.THg	p.THg	f.THg	p.THg
T01	83	60	288	181	382	115	103	36	838	714	1,086	609
T07	172	190	221	85	155	81	55	23	150	74	147	46
T17	68	69	260	294	254	118	117	50	271	204	263	139
T18	86	144	159	64	172	47	84	31	139	104	152	116
AVG	102	116	232	156	241	90	90	35	350	274	412	228
SE	24	31	28	53	52	17	13	6	166	149	226	129
C02	86	63	NA	NA	79	67	39	11	NA	NA	145	131
C06	70	121	NA	NA	126	51	24	13	NA	NA	72	62
C09	55	71	NA	NA	100	113	28	11	NA	NA	54	35
C13	74	47	NA	NA	157	61	33	11	NA	NA	82	76
AVG	71	76			116	73	31	12			88	76
SE	6	16			17	14	3	1			20	20

Table 8. Annually integrated methylmercury loads from the Cosumnes River Preserve mercury study by study year and water control structure (inlet, check weir, outlet) for the four treatment and control wetlands.

[f.THg, filtered total mercury; p.THg, particulate total mercury; T##, treatment wetland identification; C##, control wetland identification; Year 1, Water Year 2014–15; Year 2, Water Year 2015–16; mg, absolute milligrams of THg; NA, not applicable; AVG, average; SE, standard error]

Field	Year 1						Year 2					
	Inlet		Check		Outlet		Inlet		Check		Outlet	
	f.MeHg	p.MeHg	f.MeHg	p.MeHg	f.MeHg	p.MeHg	f.MeHg	p.MeHg	f.MeHg	p.MeHg	f.MeHg	p.MeHg
T01	8	8	38	37	54	17	19	4	161	113	149	37
T07	11	27	61	32	25	26	8	2	26	16	22	7
T17	6	5	29	40	14	15	16	6	37	21	14	10
T18	13	14	37	26	15	9	12	5	24	18	19	9
AVG	9	14	41	34	27	17	14	4	62	42	51	16
S.E.	2	5	7	3	9	4	2	1	33	24	33	7
C02	15	16	NA	NA	17	4	5	1	NA	NA	34	43
C06	9	5	NA	NA	7	7	5	1	NA	NA	11	31
C09	4	4	NA	NA	8	11	3	1	NA	NA	6	9
C13	10	7	NA	NA	14	11	3	1	NA	NA	16	31
AVG	10	8			12	8	4	1			17	29
S.E.	2	3			2	2	1	0			6	7

There was a clear increase in mean annually integrated uf.THg mass load within the shallow portion of the flow-through treatment cells (between inlets and checks) during both study years, with no further significant increase or decrease within the deep portion of the treatment cells (between the check and outlets) (fig. 15*E*). The increase between the inlets and check weir was more pronounced during Year 2 as compared to Year 1. This general trend was apparent in both the f.THg (fig. 15*A*) and p.THg (fig. 15*C*) fractions. In contrast, there was no appreciable increase in uf.THg mass loads between inlets and outlets for the fill-and-maintain control sites during Year 1, and a modest increase during Year 2 (fig. 15*E*) when the control sites were managed as flow-through for the September to December period, prior to being reverted back to fill-and-maintain for the remainder of Year 2. These same spatial trends for the control sites were generally reflected in the f.THg (fig. 15*A*) and p.THg (fig. 15*C*) fractions.

There was also a clear increase in mean annually integrated uf.MeHg mass load within the shallow portion of the treatment cells (between inlets and checks) during both study years, but this was followed by a decrease within the deep portion of the treatment cells (between the check and outlets) (fig. 15*F*). This decrease within the deep cell of the treatment wetlands was more pronounced for the p.MeHg fraction (fig. 15*D*) than for the f.MeHg fraction (fig. 15*B*), suggesting particulate trapping within the deep cells. In control wetlands, Year 2 exhibited a clear increase between the inlets and outlets for all three MeHg fractions, while no such increase was observed during Year 1. Again, this likely reflects the difference in hydrologic management for the control wetlands between Year 1 and Year 2, and the direct effect of increasing MeHg export in flow-through as opposed to fill-and-maintain approaches.

The average MeHg/THg annual load ratios (expressed as a percentage) for the unfiltered fractions (uf.MeHg/uf.THg) are given in table 9. For control wetlands, the MeHg/THg load ratio was similar between the inlet and outlet during Year 1, but more than doubled from the inlets to the outlets during Year 2, which was related to the management of the control wetlands in a flow-through mode from September through December, before switching back to fill-and-maintain management for the remainder of the Year 2 flooded period. For the treatment wetlands, there was a doubling of the MeHg/THg load ratio during Year 1 between the inlets and the check weirs in the shallow cells, but virtually no increase between the inlets and check weirs during Year 2. In both years, there was a substantial decrease between the check weirs and the outlets in the deep cells, indicative of preferential MeHg removal over THg removal in the deep cells.

Table 9. Mean annual unfiltered surface water MeHg/THg load ratios from the Cosumnes River Preserve mercury study for water control structures (WCS), by year. Results are expressed as a percentage and the standard deviation of the mean value is given in parentheses ( ).

Wetland type, WCS	Year 1		Year 2	
Control, Inlet	12	(3)	12	(2)
Control, Outlet	11	(1)	26	(3)
Treatment, Inlet	10	(1)	14	(1)
Treatment, Check	22	(4)	16	(1)
Treatment, Outlet	14	(3)	11	(2)

An alternative way to consider the loads data is to calculate the difference in mass loading between WCS to calculate the net removal or production (either new production or net flux from the sediment to the water column) of a given Hg fraction between any two WCS in a given study cell or the wetlands as a whole. To directly compare control wetlands (one shallow cell) to treatment wetlands (the combined shallow and deep cells) the difference in annually integrated mass loading between outlets and inlets (OUT-IN) was calculated, and the averages for all four control wetlands and treatment wetlands are graphically summarized in figure 16. On average, there was a small net increase in f.THg

in the control wetlands (44–57 mg) and a much larger net increase in f.THg in the treatment wetlands (139–322 mg), over both years (fig. 16*A*). A similar trend was seen for f.MeHg, with a comparatively smaller net increase in the control wetlands (2–13 mg) and a larger average increase in the treatment wetlands (18–37 mg), over both years (fig. 16*B*). There was no net increase in either the control wetlands or the treatment wetlands during Year 1 for either p.THg or p.MeHg (figs. 16*C* and 16*D*). In contrast, during Year 2 there were net increases for both p.THg and p.MeHg in both the control wetlands and the treatment cells.

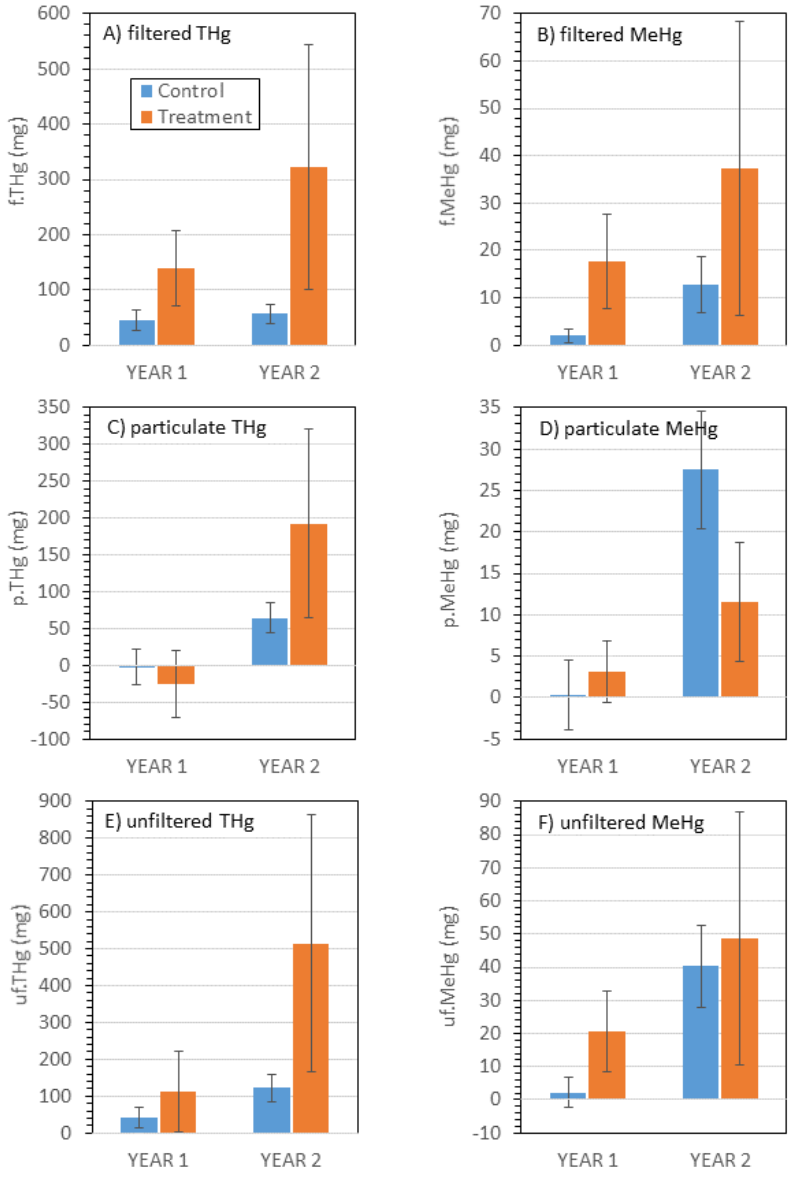

Figure 16. Bar plots (*A–F*) of mean annually integrated net change between inlets and outlets for THg and MeHg mass loads within control and treatment wetlands of the Cosumnes River Preserve mercury study. Hg fractions represent *A*, filter-passing THg; *B*, filter-passing MeHg; *C*, particulate THg; *D*, particulate MeHg; *E*, unfiltered THg; and *F,* unfiltered MeHg. Error bars reflect standard errors. mg, milligram.

Summing f.THg and p.THg to calculate the original whole water uf.THg annually integrated mass loads, the following average (±standard error) net changes for OUT-IN were observed for uf.THg (fig. 16*E*): (a) control wetlands had a net increase from inlets to outlets of 42±29 mg (35±23 percent relative to inlet) during Year 1 and a net increase of 122±37 mg (275±67 percent relative to inlet) during Year 2; (b) treatment wetlands (shallow and deep combined) had a net increase from inlets to outlets of 113±110 mg (95±68 percent relative to inlet) during Year 1 and a net increase of 515±348 mg (385±245 percent relative to inlet) during Year 2.

Similarly, summing f.MeHg and p.MeHg to calculate the original whole water uf.MeHg annually integrated mass loads, the following average (±standard error) net changes for OUT-IN were observed for uf.MeHg (fig. 16*F*): (a) control wetlands had no appreciable production (new production or from a shift from particulates or from sediment flux) or loss of MeHg from inlets to outlets with a net change of 2±5 mg (38±37 percent relative to inlet) during Year 1. In contrast, during Year 2 there was a substantial net increase of 40±12 mg (783±212 percent relative to inlet); (b) treatment wetlands (shallow and deep combined) had a net increase from inlets to outlets of 21±12 mg (132±79 percent relative to inlet) during Year 1 and a net increase of 49±38 mg (243±160 percnet relative to inlet) during Year 2, which was similar to the net OUT-IN for the control wetlands during Year 2.

While a visual comparison of the means for the control wetlands versus the treatment wetlands would suggest that the latter often had higher annually integrated values of the various Hg fractions shown in figure 16, in fact, differences in OUT-IN for control wetlands versus treatment wetlands were not statistically significant in any case (as assessed with MODEL D). However, this largely reflected the low number of annually-integrated observations (n=16) inherent in the annual mass loads dataset and the often large standard errors for the treatment wetland, which was driven by large variations in the Hg loads among deep cells.

Within treatment wetlands, we can calculate both the difference in annual load between the check weir and the inlet (CHK-IN) for the shallow cells, and the difference between the outlet and the check weir (OUT-CHK) for the deep cells. To examine how the flow-through treatment wetlands operated on average, the mean (n=4) annually integrated within-cell changes in load for the various Hg fractions are graphically presented in fig. 17 for both the shallow and deep cells of the treatment wetlands. For f.THg (fig. 17*A*), there was a clear increase within the shallow cells during both years, followed by either no increase (Year 1) or a slight further increase (Year 2) in the deep cells. For f.MeHg (fig. 17*B*), there was also a clear net increase within the shallow cells during both years, followed by a decrease in the deep cells during both years. There was also a clear increase in p.THg (fig. 17*C*) during Year 1 and in p.MeHg (fig. 17*D*) during both years within the shallow cells, which was followed by a clear decrease in both p.THg and p.MeHg within the deep cells for both study years.

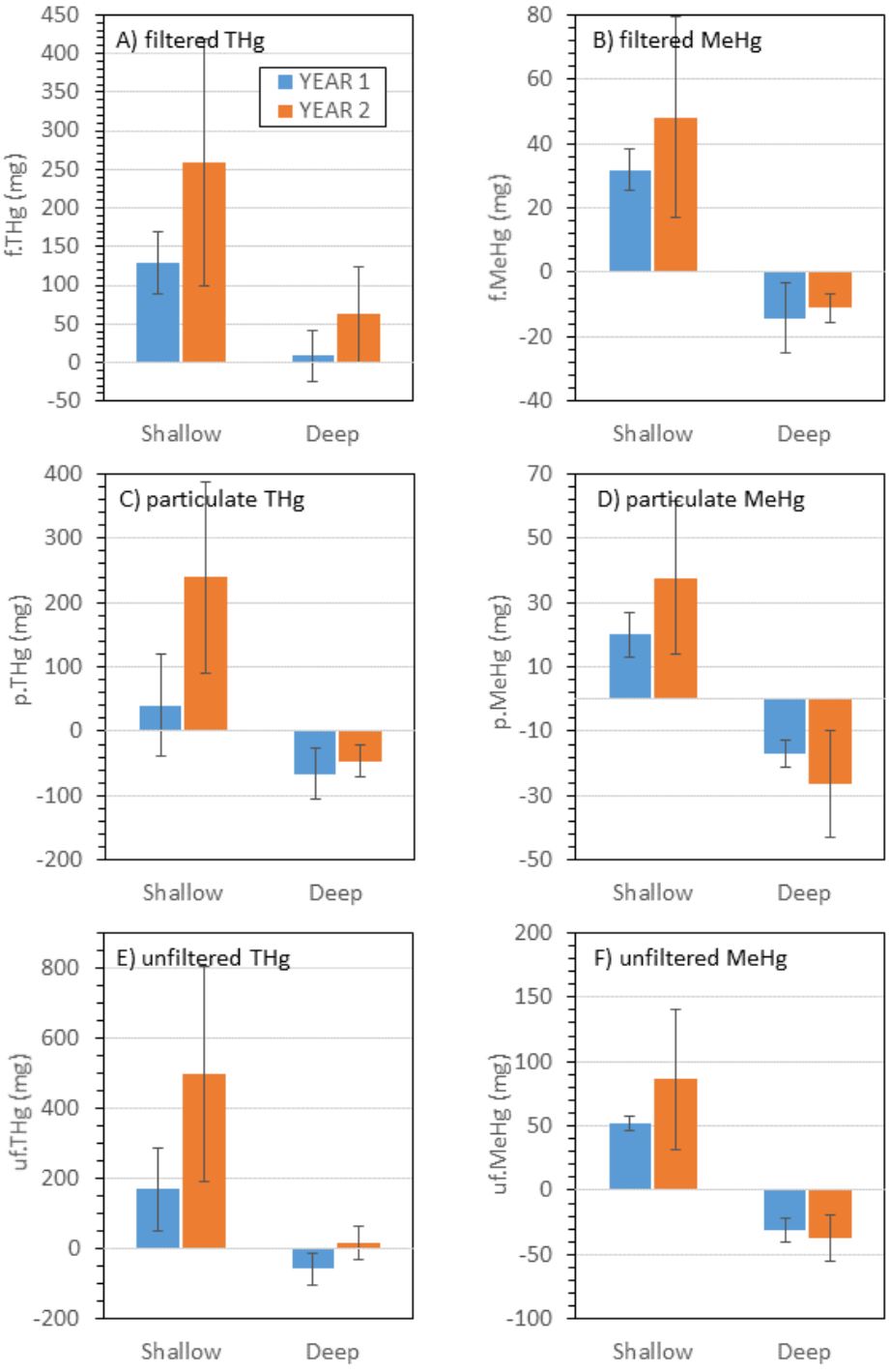

Figure 17. Bar plots of mean annually integrated net change for THg and MeHg mass loads in the shallow cells between the check weir and the inlet and deep cells between the outlet and the check weir of treatment wetlands of the Cosumnes River Preserve mercury study, by study year. Hg fractions represent *A*, filter-passing THg; *B*, filter-passing MeHg; *C*, particulate THg; *D*, particulate MeHg; *E*, unfiltered THg; and *F,* unfiltered MeHg. Error bars reflect standard errors. mg, milligram.

The sum of f.THg and p.THg loads yields an original whole water uf.THg load to determine the annually integrated within-cell changes in mass load. The following average (± standard error) net annual changes were thus observed for uf.THg (fig. 17*E*): (a) shallow cells had a net increase from inlets to check weirs of 170±118 mg (128±81 percent relative to inlet) during Year 1 and a net increase of 499±307 mg (375±215 percent relative to inlet) during Year 2; (b) deep cells had a net decrease from check weirs to outlets of 57±46 mg (13±9 percent relative to the check weir load) during Year 1 and exhibited no effective gain or loss (-16±47 mg; (2±7 percent relative to check weir load) during Year 2.

Summing f.MeHg and p.MeHg to calculate the original whole water uf.MeHg annually integrated within-cell changes in mass load, the following average (± standard error) net annual changes were observed for uf.MeHg (fig. 17*F*): (a) shallow cells had a net increase from inlets to check weirs of 52±5 mg (293±95 percent relative to inlet) during Year 1 and a net increase of 86±55 mg (430±224 percent relative to inlet) during Year 2; (b) deep cells had a net decrease from check weirs to outlets of 31 ± 9 mg (43±13 percent relative to the check weir load) during Year 1 and a net decrease of 37±18 mg; (39±7 percent relative to check weir load) during Year 2.

Summarizing the within-cell net changes in annual loads for uf.THg, for both years of data combined (*n*=8), we observed the following: (a) Within control wetlands, uf.THg loads increased 82±27 mg between inlets and outlets; (b) Within flow-through treatment wetlands, uf.THg loads increased 314±185 mg between inlets and outlets; (c) Within the shallow cell of the treatment wetlands, uf.THg loads increased 334±165 mg between inlets and check weirs; (d) Within the deep cells of the treatment wetlands, uf.THg loads exhibited no net increase or decrease (-21±33 mg) between check weirs and outlets.

Summarizing the within-cell net changes in annual loads for uf.MeHg, for both years of data combined (*n*=8), we observed the following: (a) Within control wetlands, uf.MeHg loads increased 21±9 mg between inlets and outlets; (b) Within flow-through treatment wetlands, uf.MeHg loads increased 35±19 mg between inlets and outlets; (c) Within the shallow portion of the treatment wetlands, uf.MeHg loads increased 69±26 mg between inlets and check weirs; (d) Within the deep cells of the treatment wetlands, uf.MeHg loads decreased 34±9 mg between check weirs and outlets. Thus, for the full treatment wetland, the deep cells removed approximately 50 percent of the uf.MeHg generated in the upstream shallow cells, under flow-through conditions. Further, while the mean annual MeHg/THg load ratio within the control wetlands increased 7±3 percent (from 12±2 percent to19±3 percent) between inlets and outlets, there was essentially no change in the MeHg/THg load ratio for the treatment wetlands (shallow and deep combined=0±2 percent) between inlets and outlets. In fact, the 7±3 percent increase in the MeHg/THg load ratio observed within the shallow cell portion of the treatment wetlands was fully offset by a 7±2 percent decrease between the check weir and the outlets in the deep cells.

Particulate Trapping in the Deep Cells

We investigated the efficiency of MeHg removal as a function of particulate settling and trapping in the deep cells using three independent approaches: (a) loads calculations based on the particulate mass load at the outlets minus the particulate mass load at the check weir as detailed above for p.THg and p.MeHg; (b) long-term (seasonal) particulate flux using 60 felt covered deposition pads per cell; (c) short-term (24 hour) particulate flux using the settling traps and elevators. The results from these three approaches are described below and compared.

Particulate Trapping via TSS Loads Analysis

Particulate loads were calculated from TSS concentration data (appendices 3–5) associated with p.THg and p.MeHg filters collected at the various WCS. Particulate trapping within the deep cells was then calculated for each study year as the net change in annually integrated TSS loads between the check weir and the outlet (OUT-CHK) (table 10). There were large differences observed both among deep cells and between study years, with some cells releasing a higher load at the outlets than what came into the deep cell from the check weir, resulting in net particulate production (positive values) within the deep cell (D07 during Year 1, D17 and D18 during Year 2). This net production of particulate material primarily reflected levee erosion that was observed in some areas and potentially net within-cell production of phytoplankton, which was also observed to be quite dense in some cells during various periods. In contrast, there were two cases where deep cells trapped in excess of 3300 kg of particulate material annually (D17 during Year 1 and D01 during Year 2). Combining data from both years and all cells (*n*=8), the deep cells exhibited net trapping of particulates (average±standard error), both on an absolute mass basis (-769±593 kg) and on an areal basis (-38.3±28.8 g/m^2).

Table 10. Annually integrated particulate net loss or production within the deep cells of the Cosumnes River Preserve mercury study, by study year.

[The data reflects net particulate trapping (negative values) or generation (positive values) within the individual deep cells, as calculated from the change in annually integrated total suspended solids loads beteen the check weir and the outlet (OUT–CHK). Results are presented in units of absolute mass in kilograms (kg) and on a cell area normalized basis in grams per square meter (g/m2). The average (AVG) and standard error (SE) are given for the 4 deep cells]

DEEP cell	Year 1		Year 2	
	Mass Load OUT-CHK (kg)	Areal Load OUT-CHK (g/m2)	Mass Load OUT-CHK (kg)	Areal Load OUT-CHK (g/m2)
D01	-488	-26.4	-3,386	-183.9
D07	48	2.6	-287	-15.8
D17	-3,314	-136.5	852	35.9
D18	-440	-19.1	866	37.5
AVG	-1,049	-44.9	-489	-31.8
S.E.	765	37.4	1,003	52.2

Long-Term Seasonal Particulate Flux–Felt Pads

The second approach to assessing the capacity of the deep cells to trap particulates, and thus reduce THg and MeHg export form the flow-through wetlands, involved the deployment of the 240 sediment deposition pads (60 per deep cell) during Year 1 (figs. 6, 7 and 18). The results of this effort are summarized on table 11. The amount of Year 1 seasonal deposition measured with this approach was quite large across all four deep cells with an average±standard error of 30,850±1,583 kilograms (kg) by mass and 1,444±75 grams per square meter (g/m^2) by area. These values were 11-fold to 95-fold greater than the amount of particulates trapped as calculated OUT-CHK loads for the three deep cells where net particle trapping was measured during Year 1 (D01, D17 and D18; table 10). We conclude that the felt pad approach significantly overestimated the particulate trapping potential of the deep cells, because of a combination of levee erosion in some places and wind-driven particulate resuspension, which can redistribute surface sediment without significantly contributing to a net change in within-cell particulate mass. During many field sampling events, the effect of high wind events on deep cell turbidity was apparent, particularly in the later afternoon. Figure 19 shows a photo of one such event

and illustrates the turbidity in deep cell D07 and the comparative lack of turbidity in the adjacent shallow cell S07. The physical processes of wind-driven benthic resuspension and levee erosion are implied. Figure 18 also shows areas within cells that have elevated regions of particulate deposition, which tend to be most concentrated along the interior edges (deposition pads located closest to levee walls). Because of these observations, we conclude that the particulate deposition data generated from this long-term seasonal flux approach with 240 settling pads overestimates particulate trapping, and associated THg and MeHg removal within the deep cells.

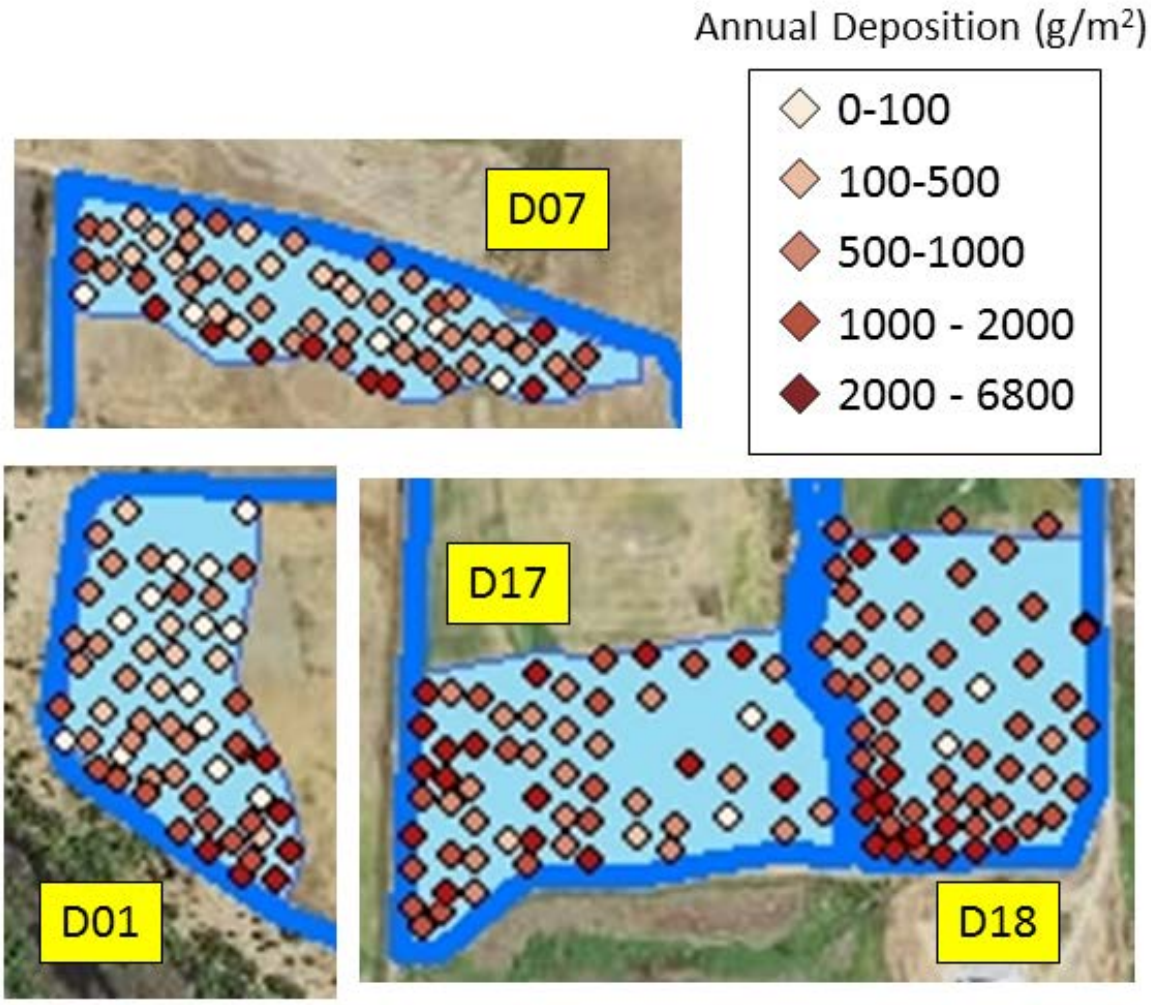

Figure 18. Maps depicting annual particulate deposition (areal basis) within the four deep cells of the Cosumnes River Preserve mercury study, as measured with long-term (seasonal) deposition pads during study Year 1. g/m^2, grams per square meter.

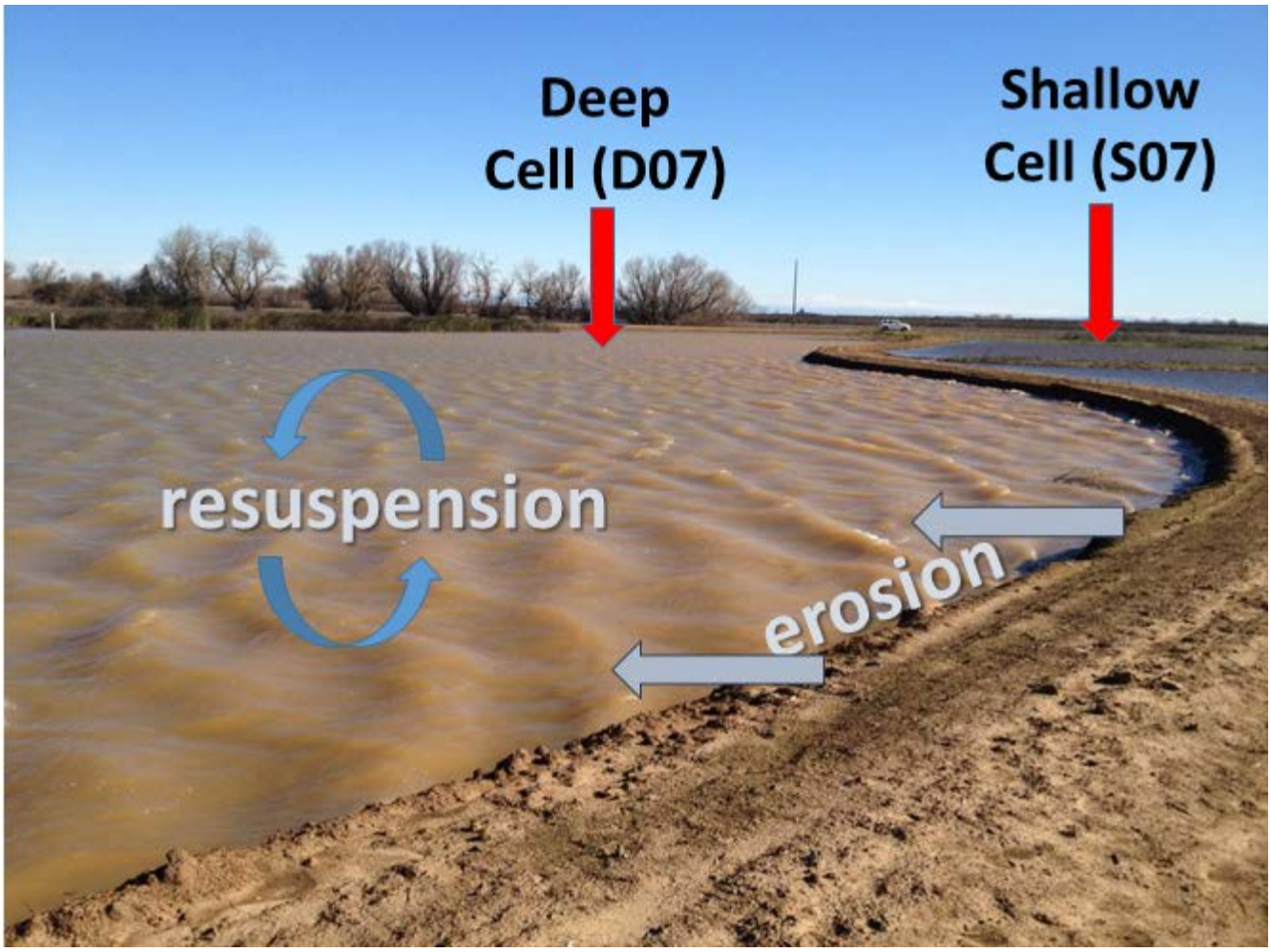

Figure 19. Photograph showing an example of turbidity within deep cell D07 of the Cosumnes River Preserve mercury study on a windy afternoon. The photograph was taken from the check levee separating shallow cell S07 from deep cell D07. The much less turbid (blue) water is apparent within S07 in the upper right portion of the photo. Wind-driven waves are apparent within the deep cell, and the physical process of wind-driven benthic resuspension and levee erosion are implied.

Table 11. Annual particulate deposition within the deep cells of the Cosumnes River Preserve mercury study as assessed by Year 1 deployment of settling pads.

[The data reflects particulate deposition on settling pads for the full flooded period of Year 1 (flood up: mid-Sept. 2014 through drawdown: mid-May 2015) within the individual deep cells. Results are presented in units of absolute mass and on a cell-area normalized basis; standard error (SE) is in parenthesis. kg, kilogram; g/m^2, grams per square meter; AVG, average]

Deep cell	Deposition, by mass (kg)		Deposition, by area (g/m^2)	
D01	22,894	(3,025)	1,243	(164)
D07	22,120	(2,652)	1,215	(146)
D17	36,708	(3,487)	1,512	(144)
D18	41,675	(3,431)	1,807	(149)
AVG	30,850	(1,583)	1,444	(75)

Short Term (24 hour) Particulate Flux–Settling Traps

The third approach to assessing the capacity of the deep cells to trap particulates involved short-term (24 hour) particulate flux measurement conducted three times per year, during both study years, using sediment traps and elevators (figs. 7 and 8). Figure 20 depicts the mean daily particulate flux measurements for each study cell during all six sampling events. Deep cell D17 consistently exhibited the highest particulate flux, with measured rates at or exceeding 20 grams per square meter per day ($g/m^2/d$). Cell D01 exhibited nearly as high of a particulate flux during the fall (November 2015) of Year 2, but lower flux rates during the winter (February 2016) and spring (May 2016). To calculate annually integrated rates (full flooding period) for each year, the daily rates between each sampling event were interpolated within a given study year. For the period prior the fall sampling, the daily flux was assumed to be equal to the value measured during November of that year. For the period after the spring sampling, the daily flux was assumed to be constant with the rate measured during the spring of that year. Daily rates for the full flooded period were then summed to calculate the annually integrated particulate flux, based on these short-term measurements (table 12). The calculated annually integrated particulate flux to the benthos for Year 1 (average±standard error, 27,457±5,780 kg by mass, 1,193±40 g/m^2 by area) was very similar to that measured with the long-term depositional pad approach (table 11). For Year 2, the average annual flux calculated via the short-term settling traps was almost double that for Year 1 (table 12), with the flux in cell D17 exceeding 5 kg/m^2. The grand average for both years and all cells combined was 39,141±16,081 kg per cell by mass and 1,752±674 g/m^2 by area. As with the long-term depositional pads, these values far exceed those calculated by considering particulate OUT-CHK loads by a factor of 50-fold (comparing the grand averages for the two study years). We thus conclude that within-cell physical processes affecting particulate settling, resuspension and levee erosion make these short-term (24 hour flux) measurements not useful for the purposes of calculating the p.THg and p.MeHg trapping efficiency of the deep cells.

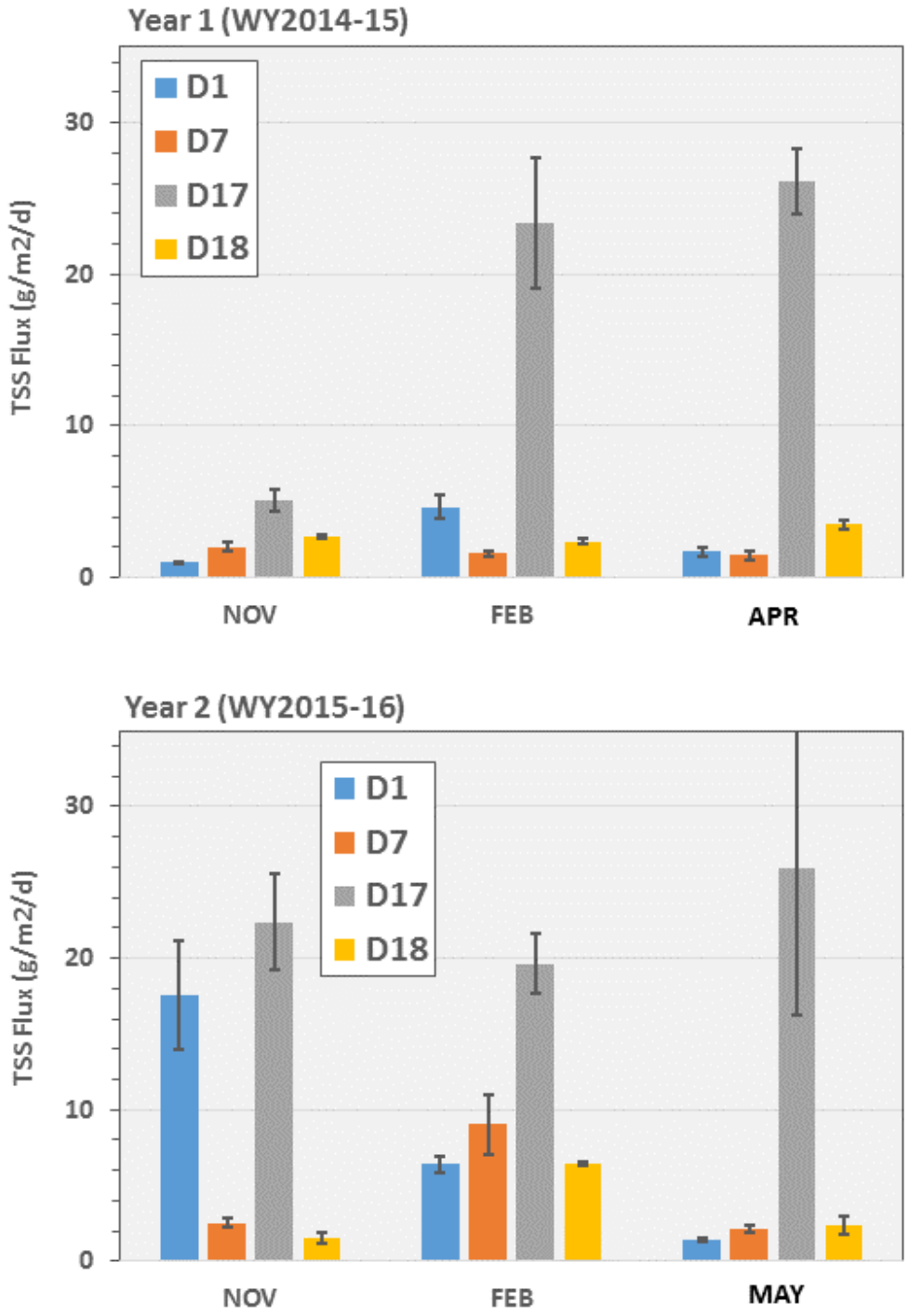

Figure 20. Bar plots of daily total suspended solid (TSS) flux in the Cosumnes River Preserve mercury study as measured in short-term (24 hours) settling traps for both study years. Bars represent the mean and standard error (number of samples=4) for each deep cell and each sampling event (month indicated) during *A*, Year 1 and *B*, Year 2. WY, water year; g/m^2/d, grams per square meter per day.

Table 12. Annually integrated particulate flux to the benthos within the deep cells of the Cosumnes River Preserve mercury study, as measured with short-term (24 hour) settling traps, for both study years.

[Results are presented in units of absolute mass in kilograms (kg) flux per cell and on a cell area normalized basis in grams per square meter (g/m^2). For each cell the mean (±standard error) is given for four particulate trapping (elevator) stations per cell. The average (AVG) and propagated standard error (in parenthesis) is given for all deep cells, for each year]

Deep cell	Year 1				Year 2			
	Particulate mass flux per cell (kg)		Particulate areal flux (g/m^2)		Particulate mass flux per cell (kg)		Particulate areal flux (g/m^2)	
D01	9,595	(2,702)	521	(147)	41,711	(11,663)	2,265	(633)
D07	6,766	(2,017)	372	(111)	20,524	(6,536)	1,127	(359)
D17	80,208	(22,803)	3,303	(939)	122,093	(58,061)	5,028	(2391)
D18	13,259	(1,810)	575	(78)	18,975	(7,288)	823	(316)
AVG	27,457	(5,780)	1,193	(240)	50,826	(15,006)	2,311	(630)

Particulate Total Mercury and Methylmercury Removal in the Deep Cells

Based on the above analysis of our three independent approaches to measure net particulate flux to the benthos and trapping within the deep cells, we conclude that the loads calculation approach OUT-CHK is the best of the three, and that the other two significantly overestimate particulate flux to the benthos because of wind-driven resuspension and possibly levee erosion. Based on this conclusion, we used the loads calculation OUT-CHK approach to calculate annually integrated within-cell changes (removal or apparent production) in p.THg and p.MeHg (table 13) for the deep cell. The highly and persistently turbid cell D17 removed the most p.THg and p.MeHg during Year 1, while the much less turbid cell D01 removed the most p.THg and p.MeHg during Year 2. For both years and all cells combined (n=8), the annual net removal of p.THg by the deep cells was -56±22 mg per cell by mass and -2.65±0.97 $\mu g/m^2$ by area, and net removal of p.MeHg by the deep cells was -22±8 mg per cell by mass and -1.08±0.45 $\mu g/m^2$ by area.

Table 13. Annually integrated change in particulate total mercury (THg) within the deep cells of the Cosumnes River Preserve mercury study, as calculated from loads between the check weir and outlet (OUT-CHK), for both study years.

[Results are presented in units of change in absolute mass in milligrams (mg) per cell and change in area normalized mass in micrograms per square meter ($\mu g/m^2$) for particulate total mercury (p.THg) and methylmercury (p.MeHg). Positive values reflect a net increase in p.THg between the check weir and outlet. Negative values reflect net removal of p.THg between the check weir and outlet.. The average (AVG) and standard error (SE) is given for all deep cells combined, for each year]

Deep cell	Change in p.THg, by mass (mg)		Change in p.THg, by area ($\mu g/m^2$)		Change in p.MeHg, by mass (mg)		Change in p.MeHg, by area ($\mu g/m^2$)	
	Year 1	Year 2	Year 1	Year 2	Year 1	Year 2	Year 1	Year 2
D01	-66	-105	-3.58	-5.70	-20	-76	-1.08	-4.13
D07	-4	-28	-0.22	-1.54	-6	-9	-0.33	-0.49
D17	-176	-65	-7.25	-2.68	-25	-11	-1.03	-0.45
D18	-17	12	-0.74	0.52	-17	-9	-0.74	-0.39
AVG	-66	-47	-2.95	-2.35	-17	-26	-0.79	-1.37
(SE)	39	25	1.61	1.30	4	17	0.17	0.92

Methylmercury Loss via Photodemethylation

Field measurements of surface water light profiles taken in the interior of the deep cells (n=16, near the short-term particulate flux elevators) and at WCS outlets of treatment and control wetlands (n=16) were well described with an exponential decay function (all significant regressions with R^2 >0.8). The resulting calculated light extinction coefficients (K_{ext}) ranged from 0.020/cm to 0.091/cm. When attenuation was calculated for each cell, PAR transmission was found to be reduced by approximately 50 percent within the top 40 cm of surface water for cells D01, D07 and D18, and reduced 50 percent in the top 20 cm of surface water in the highly and persistently turbid cell D17.

Cell and monthly averaged DOC and turbidity data was used to calculate cell and month specific k_{ext} coefficients according to equation 11, which was derived explicitly from data collected as part of this study. The resulting k_{ext} values were then used in conjunction with monthly averaged f.MeHg concentrations in equation 9 to calculate cell and month specific rates of photodemethylation, which are graphically depicted in figure 21. There is a clear seasonal trend with the lowest demethylation rates occurring during the winter period of lowest incident sunlight, followed by increasing rates during the spring. There is also a clear trend among cells during the spring, with photodemethylation rates being the highest in cell D01 (the least turbid deep cell) and lowest in D17 (the most turbid deep cell). The monthly rates are then integrated for the full flooded season and the results for individual cells, by study year, are provided in table 14. For both years and all deep cells combined, the mean (±standard error) annually integrated MeHg lost via photodegradation within the deep cells was 6.84±0.20 mg by mass and 0.33±0.01 µg/m^2 by area.

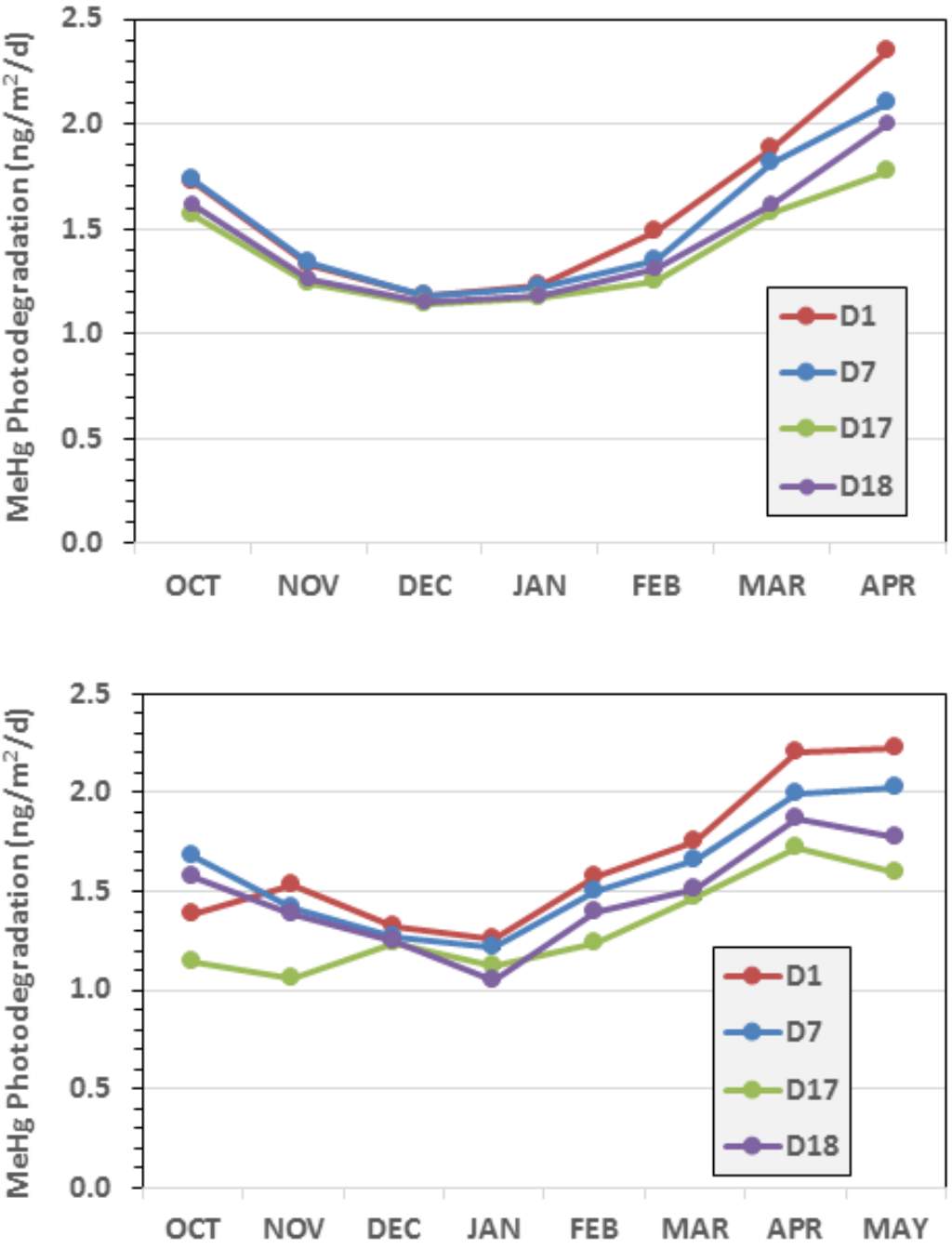

Figure 21. Time series plots of areal methylmercury (MeHg) photodegradation monthly average rates in nanograms per square meter per day (ng/m^2/d) for the deep cells within the Cosumnes River Preserve mercury study during *A*, Year 1 (October 2014–2015); and *B*, Year 2 (October 2015–May 2016).

Table 14. Annually integrated photodemethylation rates for the deep cells in the Cosumnes River Preserve mercury study, during both Study Years.

[Year 1 (Oct. 1, 2014–April 30, 2015) and Year 2 (Oct. 1, 2015–May 15, 2015). Results are presented in units of absolute mass lost in milligrams (mg) and on a cell area normalized basis in micrograms per square meter (μg/m^2) The average (AVG) and standard error (SE) are given for the four deep cells]

Deep cell	MeHg lost, mass basis (mg)		MeHg lost, areal basis (μg/m^2)	
	Year 1	Year 2	Year 1	Year 2
D01	6.26	6.82	0.34	0.37
D07	5.95	6.52	0.33	0.36
D17	7.18	7.23	0.30	0.30
D18	7.11	7.67	0.31	0.33
AVG	6.63	7.06	0.32	0.34
(SE)	(0.31)	(0.25)	(0.01)	(0.02)

Methylmercury Loss via Benthic Microbial Demethylation

Microbial MeHg degradation potential (MDP) rates in the surface sediment (top 2 cm) were assessed with stable isotope Me^{201}Hg bottle incubations during three periods per year of study (fall [November], winter [February], and spring [April/May]), as described in the Methods section. Mean MDP rates for each deep cell and sampling event are depicted in figure 22, which shows that deep cell D01 consistently exhibited the the highest MDP rates, and that Year 2 MDP rates exceeded those for Year 1 in cell D01. To calculate how much MeHg was potentially degraded annually (for the full flooding period) in the surface sediment interval, the daily MDP rates between each sampling event were first interpolated within a given study year. For the period prior to the fall sampling, the daily rate was assumed to be equal to the value measured during November of that year. For the period after the spring sampling, the daily rate was assumed to be constant with the rate measured during the spring of that year. These daily rates were then added for the full flooded period, for each cell. The resulting potential mass of MeHg removed annually via microbial MeHg degradation is summarized for each deep cell in table 15. The highest benthic MeHg degradation was in cell D01 during both years, and the average across all four deep cells was twice as much during Year 2 (217±12 μg/m^2) as compared to Year 1 (91±8 μg/m^2). For both years and all deep cells combined, the mean (± standard error) annually integrated potential (assuming measured rates from each season reflect seasonal rates, n=3) for MeHg degraded within the deep cells surface sediment was 3,041±137 mg by mass and 154±7 μg/m^2 by area.

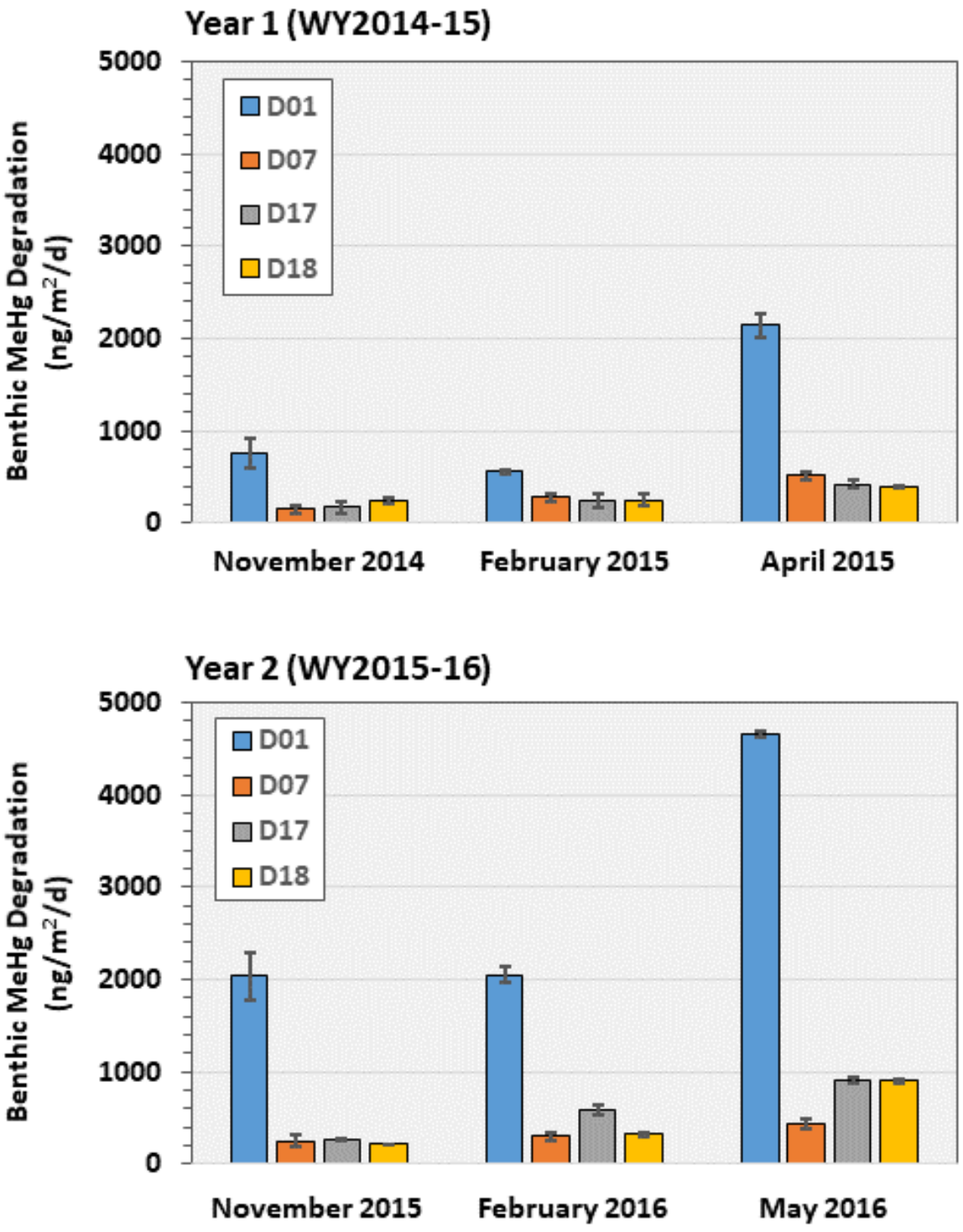

Figure 22. Bar plots of benthic MeHg degradation potential (MDP) rates in the Cosumnes River Preserve mercury study, as measured with 7-day $Me^{201}Hg$ amendment bottle incubations. Bars represent the mean and standard error for 3 locations sampled within each deep cell and each sampling event (month indicated) during *A*, Year 1; and *B*, Year 2.

Table 15. Annually integrated methylmercury degradation potential in surface sediment of the deep cells of the Cosumnes River Preserve mercury study, for both study years.

[Results are presented as the mean (± standard error) of 3 sampling sites per cell, in units of absolute mass in milligrams (mg) of MeHg degraded, and on a cell area normalized basis in micrograms per square meter (µg/m^2), based on 7-day microbial degradation potential (MDP) rate bottle incubations. The average (AVG) and propogated standard error is given for all deep cells, for each year]

Deep cell	MeHg degraded, by mass (mg)				MeHg degraded, by area (µg/m^2)			
	Year 1		Year 2		Year 1		Year 2	
D01	3,640	(465)	10,843	(834)	198	(25)	589	(45)
D07	1,007	(193)	1,283	(218)	55	(11)	70	(12)
D17	1,249	(342)	2,887	(187)	51	(14)	119	(80
D18	1,335	(223)	2,088	(102)	58	(10)	91	(4)
AVG	1,808	(162)	4,275	(222)	91	(8)	217	(12)

Stable isotope (or radioisotope) amendment experiments conducted to assess potential rates of benthic microbial processes such as MeHg degradation have been extensively used, because they provide a robust tool for comparisons across sites or over time (Marvin-DiPasquale and Oremland 1998; Marvin-DiPasquale and others, 2000; Marvin-DiPasquale and others, 2003). However, such amendment and incubation experiments can only provide potential rates, as a number of experimental variables affect the rates measured (for example, isotope amendment amount and chemical form, incubation time, and incubation temperature). Thus, the MDP rates measured in this study (fig. 22) and the annually integrated amount of MeHg degraded in the surface sediment calculated from them (table 15), cannot be taken as absolute MeHg degradation. Instead, they are most useful for comparing relative differences among sites and sampling events for the potential for MeHg degradation.

To help get a better understanding as to whether the surface sediment within the deep cells were net zones of MeHg degradation, or instead net zones of MeHg production, we also tracked the change in concentration associated with the ambient MeHg pool in the same bottle incubations that were used to measure MDP rates. Those result are depicted in fig. 23, and demonstrate that under the conditions of incubation (7 days, anaerobic conditions, incubated at ±1°C of average field temperature) nearly all deep cells and dates were net MeHg-producing during Year 1 and all were net MeHg-producing during Year 2. In fact, there were only three examples (13 percent of all site/date specific incubations) for which the average change in the ambient MeHg pool was negative (net MeHg degrading), all during Year 1 (D07 in November, D18 in February, D01 in April). To calculate annually integrated sediment net MeHg production or degradation based on these measured changes in the ambient MeHg pool, daily rates of change between sampling events were interpolated between each measured rate (fig. 23). For the period prior the the fall sampling, the daily rate was assumed to be equal to the value measured during November of that year. For the period after the spring sampling, the daily rate was assumed to be constant with the rate measured during the spring of that year. These daily rates were then added for the full flooded period, for each cell and each study year. The resulting net annual change in the ambient MeHg pool is summarized for each deep cell in table 16. The annually integrated values were all net positive, suggesting that the surface sediment layer of the deep cells is net MeHg producing, as opposed to net MeHg degrading. As was seen with MPD rates, the values for net change in the ambient MeHg pool was in cell D01 during both years, and the average across all four deep cells was almost 9-fold higher during Year 2 (203±12 µg/m^2) as compared to Year 1 (24±4 µg/m^2), indicating that microbial activity overall was more active in the second year after construction of the deep cells. This may partially be the result a full season of vegetative growth during the dry season between Year 1 and Year 2. While this vegetation was sparse and mowed down prior to flood up, it was not removed.

Comparatively, during Year 1, the freshly dug deep cells had very little labile organic matter in them prior to flood up. For both years and all cells combined, the mean (± standard error) annually integrated net change in the ambient MeHg pool within the deep cells surface sediment was 2,260±118 mg by mass and 114±6 µg/m^2 by area.

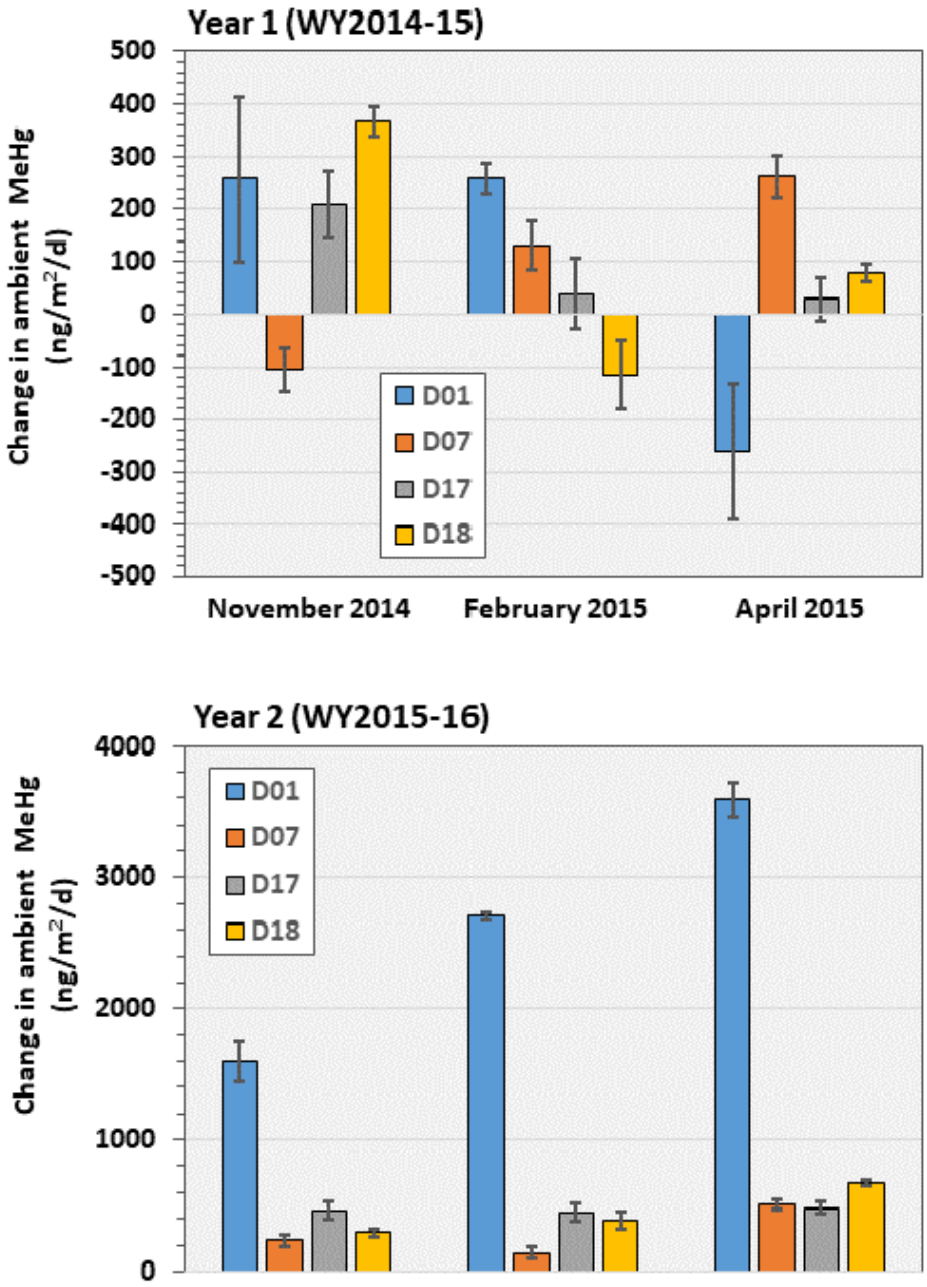

Figure 23. Bar plots of the net daily rate of change in the ambient MeHg pool in the Cosumnes River Preserve mercury study, as measured with 7-day Me^{201}Hg amendment bottle incubations. Bars represent the mean and standard error for 3 locations sampled within each deep cell and each sampling event (month indicated) during *A*, Year 1; and *B*, Year 2. Positive values reflect net MeHg production and negative values reflect net MeHg degradation.

Table 16. Annually integrated net change in ambient methylmercury pools in surface sediment of the deep cells of the Cosumnes River Preserve mercury study, for both study years.

[Results are presented as the mean (± standard error) of 3 sampling sites per cell, in units of absolute mass in milligrams (mg) of MeHg degraded, and on a cell area normalized basis in micrograms per square meter (µg/m^2), based on 7-day microbial degradation potential (MDP) rate bottle incubations. The average (AVG) and propagated standard error is given for all deep cells, for each year]

Deep cell	MeHg net change, by mass (mg)				MeHg net change, by area (µg/m^2)			
	Year 1		Year 2		Year 1		Year 2	
D01	645	(267)	10,233	(670)	35	(15)	556	(36)
D07	176	(37)	1,050	(473)	10	(2)	58	(26)
D17	585	(225)	2,571	(194)	24	(9)	106	(8)
D18	670	(101)	2,148	(222)	29	(4)	93	(10)
AVG	519	(91)	4,001	(218)	24	(4)	203	(12)

Methylmercury Benthic Diffusive Flux Estimates

Annually integrated estimates of MeHg benthic flux are summarized for each deep cell and study Year in table 17. Three estimates of bentic flux are provided for each deep cell/Year combination, based on the 25 percent quartile (Q.25 percent), 50 percent quartile (Q.50 percent, median), and 75 percent quartile (Q.75 percent) results of the non-parametric analysis of previously published sediment porewater partitioning coefficient (k_d) data used to estimate (back-calculate) porewater MeHg concentrations. As the statisitically derived values of k_d increase (representing preferential binding of MeHg to the particulate phase) the values of benthic flux decrease. Both positive (out of sediment) and negative (into sediment) values of benthic flux were estimated (table 17) based on the 25–75 percent inner-quartile range of k_d values used in the calculations. The Q.50 percent (median) value is primarily used on the cell specific and grand average box models presented below.

Table 17. Annually integrated methylmercury benthic diffusive flux in deep cells of the Cosumnes River Preserve mercury study, for both study years.

[MeHg benthic flux (F) results are presented on a cell area normalized basis in micrograms per square meter (µg/m^2) for the full flooded season of Year 1 (WY2014–15) and Year 2 (WY2015–16). Three estimates of F are given for each deep cell and Year combination, corresponding to the 25 percent quartile (Q.25%), 50 percent quartile (Q.50%), and 75 percent quartile (Q.75%) results of the non-parametric analysis of previously published sediment porewater partitioning coefficient (kd) data. Positive values of F indicate MeHg flux out of the sediment, while negative values of F indicate MeHg flux into the sediment]

Deep cell	F,Q.25% (µg/m^2)		F,Q.50% (µg/m^2)		F,Q.75% (µg/m^2)	
	Year 1	Year 2	Year 1	Year 2	Year 1	Year 2
D01	4.17E-01	1.25E+00	-6.13E-03	1.59E-01	-1.63E-01	-2.45E-01
D07	5.37E-02	1.59E-01	-5.09E-02	-3.31E-02	-8.95E-02	-1.04E-01
D17	1.15E-01	1.13E-01	-4.99E-03	-3.69E-03	-4.92E-02	-4.69E-02
D18	1.16E-01	7.71E-02	2.96E-03	-2.43E-02	-3.90E-02	-6.17E-02
AVG	1.75E-01	4.01E-01	-1.48E-02	2.45E-02	-8.51E-02	-1.15E-01

Deep Cell MeHg Budget

A MeHg budget was constructed for each of the deep cells, based on (a) the amount of uf.MeHg entering the deep cell through the check weir, (b) the amount of p.MeHg removed via particulate trapping as calculated with the loads [OUT-CHK] approach, (c) the amount of f.MeHg removed via photodegradation, (d) the amount of uf.MeHg exiting the deep cell through the outlet weir, and (e) unexplained MeHg loss or production. While MeHg degradation in the surface sediment was considered a potential loss term, the conclusion that the surface sediment layer was net MeHg-producing (based on observed changes in the ambient MeHg pool during incubation experiments) warranted eliminating net MeHg degradation in the sediment as a significant loss term for consideration. The budget constructed used annually integrated values for each of the model terms. Because of differences in the surface area (18,211 to 24,281 m^2) and volume (10.0 to 14.0 acre feet, table 1) among deep cells, the annual budgets were constructed using area-normalized concentration data ($\mu g/m^2$).

The approach to the deep cell MeHg budget is presented in a step-wise fashion. We first examine how much MeHg enters and exits into the deep cells throught the check weirs and outlets, respectively, and at the composition of the uf.MeHg with respect to f.MeHg and p.MeHg fractions. Table 18 summarizes this data, with MeHg loads (table 7) being normalized to the individual cell area.

Table 18. Annually integrated MeHg loads, normalized to area, entering and exiting the deep cells of the Cosumnes River Preserve mercury study, by fraction type and percentage.

[Unfiltered, filtered and particulate methylmercury (uf.MeHg, f.MeHg and p.MeHg) load data is provided for all four deep cells in micrograms per square meter ($\mu g/m^2$) at the check weir (CHK) and outlet (OUT) water control structures, normalized to deep cell specific area. Percentage (%) is also provided for f.MeHg and p.MeHg. The average (AVG) and standard error (S.E.) are given for the 4 deep cells for each study year, and for both study years combined]

Cell	CHK					OUT				
	uf.MeHg ($\mu g/m^2$)	f.MeHg ($\mu g/m^2$)	p.MeHg ($\mu g/m^2$)	f.MeHg (%)	p.MeHg (%)	uf.MeHg ($\mu g/m^2$)	f.MeHg ($\mu g/m^2$)	p.MeHg ($\mu g/m^2$)	f.MeHg (%)	p.MeHg (%)
Year 1										
D01	4.06	2.08	1.98	51	49	3.85	2.94	0.91	76	24
D07	5.09	3.33	1.76	65	35	2.81	1.35	1.46	48	52
D17	2.84	1.21	1.63	43	57	1.18	0.58	0.61	49	51
D18	2.75	1.61	1.14	59	41	1.04	0.65	0.39	63	37
AVG	3.68	2.06	1.63	54	46	2.22	1.38	0.84	59	41
S.E.	0.56	0.46	0.18	5	5	0.68	0.55	0.23	7	7
Year 2										
D01	14.88	8.74	6.14	59	41	10.10	8.09	2.01	80	20
D07	2.31	1.43	0.88	62	38	1.59	1.21	0.38	76	24
D17	2.39	1.52	0.86	64	36	0.99	0.58	0.41	58	42
D18	1.82	1.04	0.78	57	43	1.21	0.82	0.39	68	32
AVG	5.35	3.18	2.17	60	40	3.47	2.68	0.80	71	29
S.E.	3.18	1.86	1.32	2	2	2.21	1.81	0.40	5	5
Years 1 & 2										
AVG	4.52	2.62	1.90	57	43	2.85	2.03	0.82	65	35
S.E.	1.53	0.91	0.63	3	3	1.10	0.91	0.22	4	4

One noteworthy observation from the data presented in table 18, is the relative shift in the proportions of f.MeHg and p.MeHg from water coming in at the check and exiting at the outlets. Specifically, for both study years individually and combined, the percentage of f.MeHg increased from check to outlet, while the percentage of p.MeHg decreased. This could reflect a proportionally more effective removal of p.MeHg, compared to f.MeHg, or reflect a physical shift in the partitioning of MeHg between the particulate and aqueous phase, or both, within the deep cell.

The next step in the budget construction involves calculating the amount and percent of change (decrease or increase) for each MeHg fraction within the deep cell, summarized in table 19.

Table 19. Annually integrated net MeHg loss within the deep cells of the Cosumnes River Preserve mercury study, by fraction type and percentage.

[Results reflect the difference in annual load between deep cell outlets and check weirs [OUT-CHK] for unfiltered, filtered and particulate methylmercury (uf.MeHg, f.MeHg and p.MeHg), normalized to area in micrograms per square meter ($\mu g/m^2$) for all four deep cells. The percentage (%) of each fraction removed, relative to the incoming load at the check weir for that fraction [%REMOVED: [OUT-CHK]/[CHK]x100), is given, as is the percentage of the f.MeHg and p.MeHg removed relative to the uf.MeHg (rt uf.MeHg) load incoming load at the check weir. The average (AVG) and standard error (S.E.) are given for the 4 deep cells for each study year, and for both study years combined]

Cell	[OUT-CHK]			% Removed (relative to specific fraction load at CHK)			% Removed (relative to uf.MeHg load at CHK)	
	uf.MeHg ($\mu g/m^2$)	f.MeHg ($\mu g/m^2$)	p.MeHg ($\mu g/m^2$)	uf.MeHg (%)	f.MeHg (%)	p.MeHg (%)	f.MeHg (%)	p.MeHg (%)
Year 1								
D01	-0.22	0.86	-1.07	-5	41	-54	21	-26
D07	-2.28	-1.98	-0.30	-45	-59	-17	-39	-6
D17	-1.65	-0.63	-1.02	-58	-52	-63	-22	-36
D18	-1.71	-0.96	-0.75	-62	-60	-66	-35	-27
AVG	-1.46	-1.19[a]	-0.79	-43	-57[a]	-50	-32[a]	-24
S.E.	0.44	0.35[a]	0.18	13	2[a]	11	4[a]	6
Year 2								
D01	-4.78	-0.65	-4.13	-32	-7	-67	-4	-28
D07	-0.71	-0.22	-0.49	-31	-15	-56	-10	-21
D17	-1.40	-0.95	-0.45	-59	-62	-52	-40	-19
D18	-0.61	-0.22	-0.39	-33	-21	-50	-12	-21
AVG	-1.88	-0.51	-1.37	-39	-26	-56	-16	-22
S.E.	0.98	0.18	0.92	7	12	4	8	2
Years 1 & 2								
AVG	-1.67	-0.80[a]	-1.08	-41	-40[a]	-53	-23[a]	-23
S.E.	0.50	0.21[a]	0.45	7	8[a]	6	5[a]	3

[a]Data for Year 1, cell D01 (highlighted in red) was excluded from the calculation.

The above analysis (summarized in table 19) shows that uf.MeHg, f.MeHg, and p.MeHg were all reduced within each deep cell during both years, with the sole exception of f.MeHg in cell D01 during Year 1. For this exception (highlighted in red), f.MeHg increased 41 percent and 21 percent relative to the f.MeHg and uf.MeHg loads coming into D01 through the check weir. This outlier data

was excluded, for the purposes of calculating individual year and Year 1 and Year 2 combined averages. Across all cells and for both years combined, uf.MeHg decreased 41±7 percent, f.MeHg decreased 40±8 percent relative to incoming f.MeHg load and 23±5 percent relative to incoming uf.MeHg load, and p.MeHg decreased 53±6 percent relative to incoming p.MeHg load and 23±3 percent relative to incoming uf.MeHg load.

To quantify the effect on photodemethylation within the deeps cell on the reduction of f.MeHg load and uf.MeHg load entering the deep cell, the relevant data is summarized in table 20. Areal rates of photdemethylation provided in table 14 were used in the calculation of percent loss reported in table 20.

Table 20. Annually integrated percent MeHg loss within the deep cells of the Cosumnes River Preserve mercury study via photodegradation.

[Results reflect the relative percentage (%) loss of MeHg because of photodemehtylation (rates from table 14) relative to the following loads: (a) filtered methylmercury (f.MeHg) inputs at the check weir (CHK), (b) unfiltered methylmercury (uf.MeHg) inputs at the CHK, (c) total within cell decrease in f.MeHg (OUT-CHK), and (d) total within cell decrease in uf.MeHg [OUT-CHK]. The average (AVG) and standard error (S.E.) are given for the 4 deep cells for each study year, and for both study years combined]

	Photodegradation			
Cell	Relative to f.MeHg at CHK (%)	Relative to uf.MeHg at CHK (%)	Relative to f.MeHg OUT-CHK (%)	Relative to uf.MeHg OUT-CHK (%)
Year 1				
D01	16	8	-40	157
D07	10	6	17	14
D17	24	10	47	18
D18	19	11	32	18
AVG	17	9	32[a]	17[a]
S.E.	3	1	8[a]	1[a]
Year 2				
D01	4	2	57	8
D07	25	16	163	50
D17	20	12	31	21
D18	32	18	153	55
AVG	20	12	101	33
S.E.	6	3	33	11
Years 1 and 2				
AVG	19	11	71[a]	26[a]
S.E.	3	2	21[a]	7[a]

[a]Data for Year 1, cell D01 (highlighted in red) was excluded from the calculation.

The data in table 20 indicates that across all cells and both years, the photodegradation of MeHg can account for a 19±3 percent loss of the f.MeHg load or a 11±2 percent loss of the uf.MeHg load coming into the deep cell from the check weir. Relative to the mean annual total decrease in f.MeHg and uf.MeHg within the deep cells (calculated from OUT-CHK), photodegradation can account for 71±21 percent and 26±7 percent, respectively. This suggests that not all of the decrease in f.MeHg within the deep cells may be directly attributable to photodemethylation.

The repartitioning of f.MeHg onto the particulate fraction may in some cases account for a portion of this total decrease in within-cell f.MeHg loss, as calculated from OUT-CHK. While k_d partitioning coefficients were not significantly different between the deep cell check weir and outet, while comparing all WCS Types and controlling for Year and SEASON (MODEL A.1, appendix 3), there LSM k_d values were higher at the outlet compared to the check. This trend suggest a general shift in MeHg from the filter-passing pool to the particle-associated pool, and is thus consistant with potential particle scavenging on f.MeHg in the deep cells. However, the significant spatial trend was a shift from the particulate to the filter-passing (decreasing k_d values) between inlet WCS and either the outlet of the control wetlands or the check weir associated with outflows from the shallow cells of treatment wetlands.

MeHg Box Models

A simple MeHg box model was constructed for each deep cell by Year (figs. 24–27) and for the grand mean of all deep cells and both study years (fig. 28). Data for these models includes: (a) uf.MeHg into the deep cell based on check load (table 18); (b) uf.MeHg exiting the deep cell based on the oulet load (table 18); (c) uf.MeHg lost within the deep cells based on OUT-CHK (table 19); (d) p.MeHg within-cell decrease from OUT-CHK (table 19); and (e) f.MeHg loss via Photodemethylation (table 14).

For all box models, we assume the uf.MeHg load coming into the deep cell from the check represents 100 percent. For the grand mean budget (fig. 28), the annual load at the check weir is 4.52 ± 1.53 µg/m^2. Relative to this amount, there was an overall decrease in uf.MeHg within the deep cell of 37 percent and the export through the outlet weir of 63 percent. The p.MeHg loss via particulate trapping represents 24 percent of the uf.MeHg load coming in from the check (table 19). The f.MeHg loss via photodemethylation represents 7 percent of the uf.MeHg load coming in from the check (table 20). Not accounting for any diffusive or advective flux of f.MeHg to or from the sediment, the sum of the measured loss of p.MeHg (assumed particulate trapping) plus the loss of f.MeHg from photodemethylation equals 31 percent out of the 37 percent of the uf.MeHg removed by the deep cell. This means that there is an unexplained 6 percent deficit (potential loss) of MeHg in the deep cell budget, which is well within acceptable error for this level of mass balance analysis.

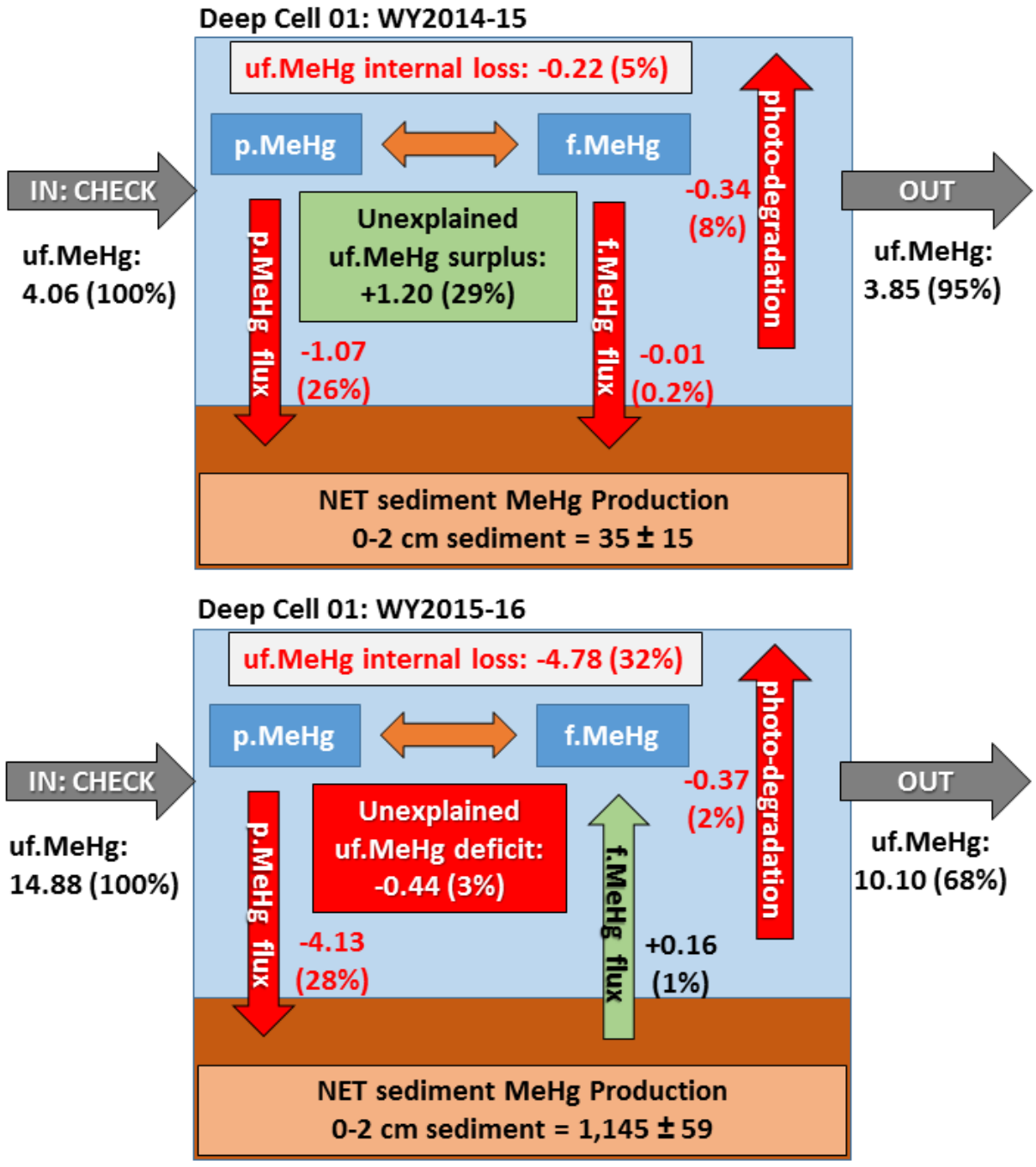

Figure 24. Box model of MeHg mass loading and within-cell loss (or production) for deep cell D01 of the Cosumnes River Preserve mercury study during Year 1 (WY 2014–15) and Year 2 (WY 2015–16) sampling seasons. Units are expressed on an areal normalized basis in micrograms per square meter (µg/m^2) and the percentage in parentheses ( ) are relative to the uf.MeHg input to the deep cell. The net internal loss (OUT-CHECK) in uf.MeHg is given in the grey box at the top. Internal loss and production terms are depicted in red and green arrows, respectively. The unexplained MeHg budget surplus or deficit is given in the center (green or red) box.

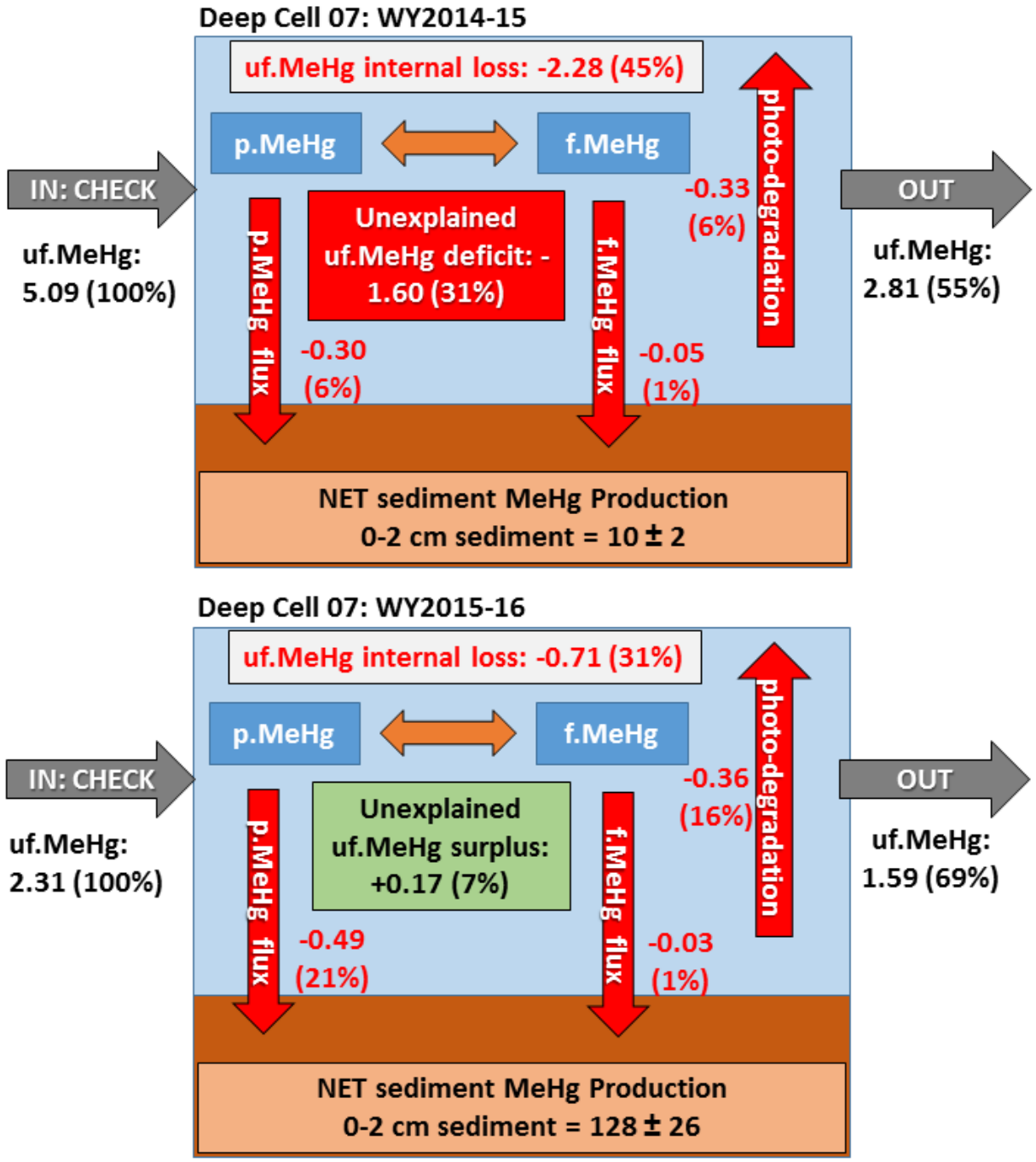

Figure 25. Box model of MeHg mass loading and within-cell loss (or production) for deep cell D07 of the Cosumnes River Preserve mercury study during Year 1 (WY 2014–15) and Year 2 (WY 2015–16) sampling seasons. Units are expressed on an areal normalized basis in micrograms per square meter (µg/m^2) and the percentage in parentheses ( ) are relative to the uf.MeHg input to the deep cell. The net internal loss (OUT-CHECK) in uf.MeHg is given in the grey box at the top. Internal loss and production terms are depicted in red and green arrows, respectively. The unexplained MeHg budget surplus or deficit is given in the center (green or red) box.

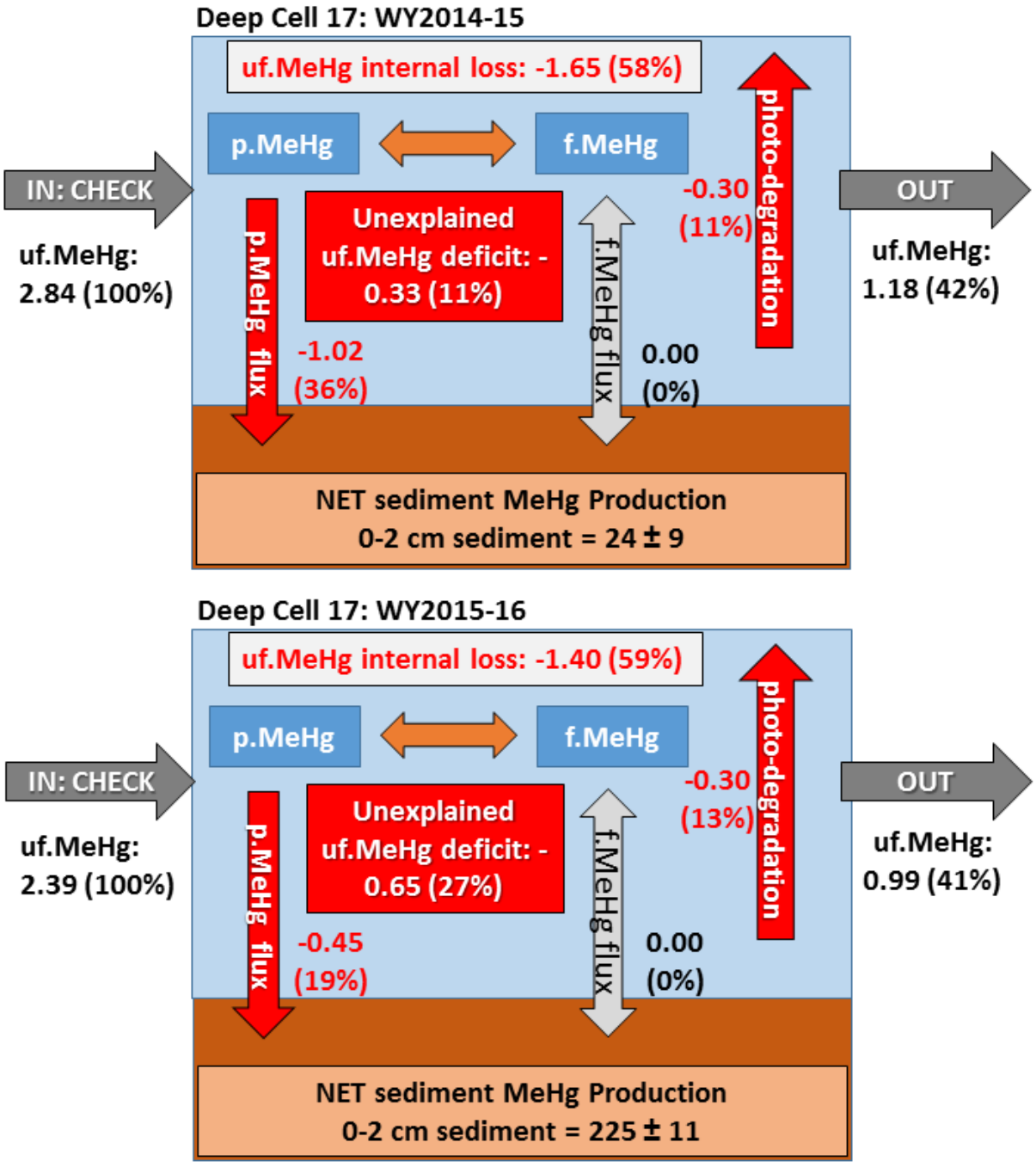

Figure 26. Box model of MeHg mass loading and within-cell loss (or production) for deep cell D17 of the Cosumnes River Preserve mercury study during Year 1 (WY 2014–15) and Year 2 (WY 2015–16) sampling seasons. Units are expressed on an areal normalized basis in micrograms per square meter (μg/m^2) and the percentage in parentheses ( ) are relative to the uf.MeHg input to the deep cell. The net internal loss (OUT-CHECK) in uf.MeHg is given in the grey box at the top. Internal loss and production terms are depicted in red and green arrows, respectively. The unexplained MeHg budget surplus or deficit is given in the center (green or red) box.

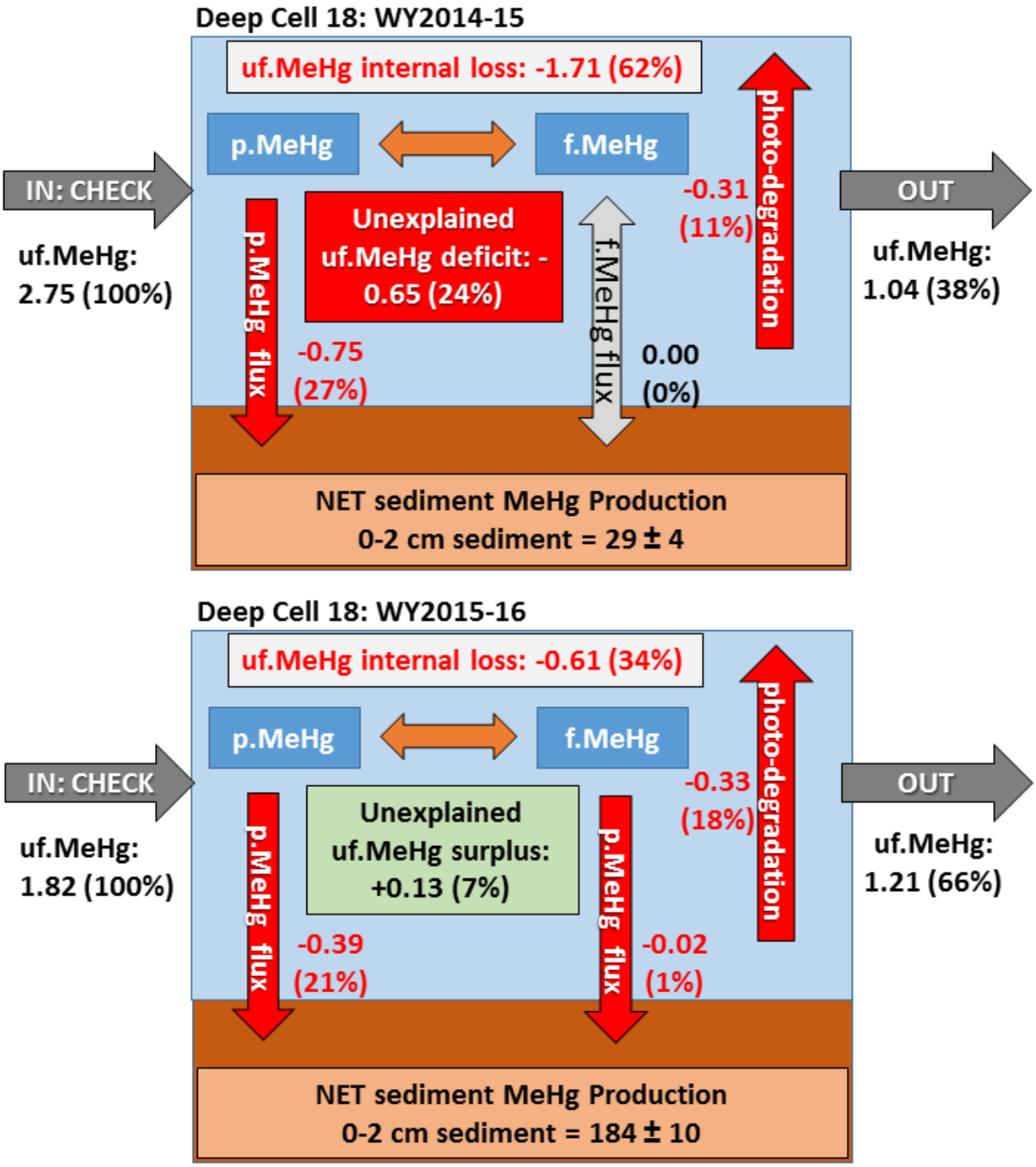

Figure 27. Box model of MeHg mass loading and within-cell loss (or production) for deep cell D18 of the Cosumnes River Preserve mercury study during Year 1 (WY 2014–15) and Year 2 (WY 2015–16) sampling seasons. Units are expressed on an areal normalized basis in micrograms per square meter (µg/m^2) and the percentage in parentheses ( ) are relative to the uf.MeHg input to the deep cell. The net internal loss (OUT-CHECK) in uf.MeHg is given in the grey box at the top. Internal loss and production terms are depicted in red and green arrows, respectively. The unexplained MeHg budget surplus or deficit is given in the center (green or red) box.

Based on the literature derived median k_d value (1706 L/kg) used to calculate porewater MeHg concentrations, the estimated MeHg diffusive benthic flux for the mean box model was essentially zero (0.00±0.02 µg/m^2) (fig. 28). Alternatively, using the literature derived 25–75 percent.IQ values to bound k_d (606–5188 L/kg), MeHg diffusive benthic flux estimates range from +0.29±0.14 µg/m^2 [+6 percent, out of the sediment] to -0.10 ± 0.03 µg/m^2 [-2 percent, into the sediment], resulting in an unexplained MeHg deficit ranging from 12 percent to 4 percent relative to the incoming uf.MeHg load, which is still well within the acceptable range of error. This suggests that the diffusive flux of f.MeHg, either into or out of the sediment, is likely only playing a minor role in the overall net balance of MeHg within the deep cells.

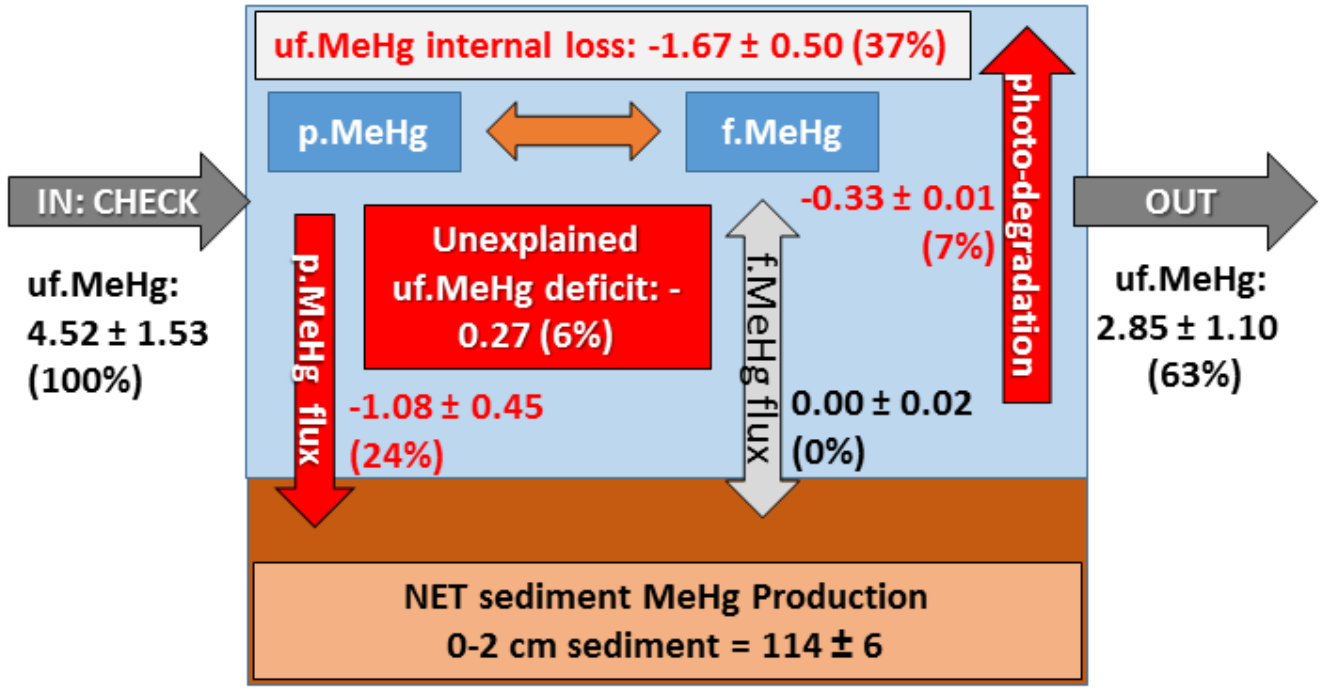

Figure 28. Box model of MeHg mass loading and within-cell loss (or production) for all deep cells (D01, D07, D17, and D18) of the Cosumnes River Preserve mercury study over both sampling seasons (WY 2014–15 and WY 2015–16) combined. Units are expressed on an areal normalized basis in micrograms per square meter (µg/m^2) and the percentage in parentheses ( ) are relative to the uf.MeHg input to the deep cell. The net internal loss (OUT-CHECK) in uf.MeHg is given in the grey box at the top. Internal loss and production (PROD) terms (boxes and arrows) are depicted in red and green respectively. Error terms represent standard errors. Internal loss terms (particle settling and photdegradation) are depicted with red arrows. Benthic flux of f.MeHg is shown as grey two headed arrow (zero flux). The unexplained MeHg budget deficit is given in the center red box.

The MeHg box models constructed for the four individual deep cells (fig. 24–27) provide a further measure of the variability among individual wetlands (spatially) and temporally (between years). Across all eight models (4 deep cells x 2 Years), we can summarize the following observations:

- Net MeHg loss within the deep cell ranged from 5 to 62 percent (median: 39 percent) across all eight box models, with the lowest removal seen in Cell D01 during Year 1 and the highest (62 percent) seen in Cell D18 during Year 1.
- Particulate MeHg flux to the benthos was consistently the largest MeHg removal term and ranged from 6 to 36 percent (median 24 percent) of the uf.MeHg coming into the deep cell.
- Photodegradation was the second most important MeHg loss term across all eight models, ranging from 2 to 18 percent (median 11 percent) of the uf.MeHg coming into the deep cell.
- Estimated MeHg flux across the sediment water interface ranged from -1.1 percent (out of sediment) to 1.4 percent (into sediment) (median 0.2 percent), relative to the uf.MeHg load coming into the deep cell, suggesting that this loss (or production) term is comparatively minor.
- All eight individual budgets resulted in net benthic MeHg production on an annually integrated bases, based upon changes in the ambient MeHg pool during 7-day bottle incubations.
- The unexplained portion of each budget ranged from 29 percent in excess of the incoming uf.MeHg load (Cell D01/Year 1) to a 31 percent deficit, relative to the incoming uf.MeHg load (Cell D07/Year 1), with a median of 7 percent.

Mercury Bioccumulation Studies

We analyzed THg concentrations in 1712 mosquitofish, including 1586 fish retrieved from the 64 cages over 2 years, 80 reference fish representing the source population, and an additional 46 fish caged in 3 locations within the wetland's source-water canals in 2015. At the time of fish introduction into cages (30 days prior to retrieval), THg concentrations in reference mosquitofish from the stock population were very low at 0.04±0.004 µg/g d.w. (n=50 reference fish) in 2015 and 0.03±0.002 µg/g d.w. (n=30 reference fish) in 2016. At the time of fish retrieval in 2015, THg concentrations in mosquitofish caged in the wetland's source water canals were 0.10±0.005 µg/g d.w. (n=46 reference fish).

When comparing among wetland types (control vs. treatment), there was not a significant interaction between type × sub-site × year ($F_{3,42.02}$=0.15, p=0.93), and therefore this 3-way interaction was dropped from the mercury model. The interactions for type × year ($F_{1,45.01}$=4.22, p=0.05) and type × sub-site ($F_{3,45.11}$=6.02, p=0.002) were significant in the subsequent model; therefore we conducted two separate models for each year to focus on the wetland type effect.

In 2015, THg concentrations in mosquitofish at retrieval decreased as a function of fish mass at introduction ($F_{1,631.20}$=4.57, p=0.03) and increased with the change in fish mass after introduction ($F_{1,640.60}$=4.21, p=0.04). However, there was a significant interaction between type × sub-site ($F_{3,18.00}$=3.85, p=0.03), which precluded interpretation of the main effects of wetland type ($F_{1,5.98}$=3.98, p=0.09) and sub-site ($F_{3,18.10}$=3.05, p=0.06). Therefore, we performed Tukey pair-wise tests and found that the only significant difference in fish THg concentrations was within the experimental wetlands between the inlet of the shallow cell and the inlet of the deep cell (fig. 29), as was seen for aqueous uf.MeHg concentrations as well (fig. 11*B*, appendix 6*B*).

In 2016, THg concentrations in mosquitofish at retrieval increased with mass at introduction ($F_{1,890.40}$=10.65, p=0.001) and there was no relation with the change in mass after introduction ($F_{1,895.00}$=0.10, p=0.75). There were no significant effects of wetland type ($F_{1,5.96}$=1.68, p=0.24), sub-site ($F_{3,18.04}$=0.87, p=0.47), or the type × sub-site interaction ($F_{3,18.03}$=2.57, p=0.09; fig. 29) on THg concentrations in mosquitofish.

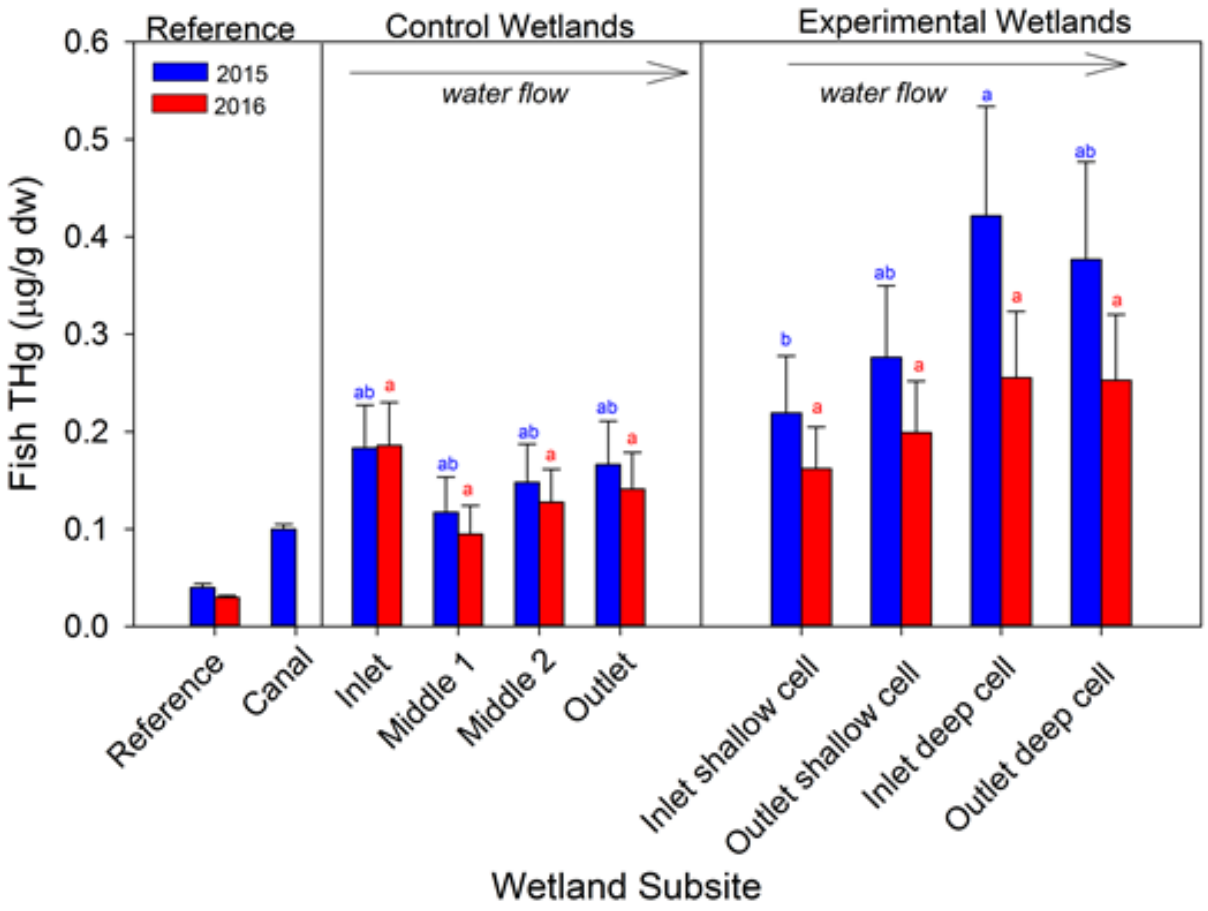

Figure 29. Geometric means for mosquitofish THg concentrations in micrograms per gram dry weight (µg/g dw) among cage locations (sub-site) within control and treatment wetlands of the Cosumnes River Preserve mercury study during the spring deployment (MAR-MAY), for Year 1 and Year 2. THg concentrations in reference fish representing the fish source population at the time of fish introduction each year and fish caged for 30 days at 3 sites within a source water canal in 2015 are also shown. Letters above bars denote ranking and significant differences among sub-sites within each year assessed separately. Bars sharing the same letter within a year are not significantly different. Red is 2015 data and blue is 2016 data. The arrow shows the direction of water flow within the control and experimental wetlands. Error bars reflect standard errors.

Fish Body Mass

We also examined whether fish body mass differed among wetland types (control vs. treatment). There was not a significant interaction between type × sub-site × year ($F_{3,42.22}$=0.21, p=0.89), and therefore this 3-way interaction was dropped from the mass model. The interactions for type × year ($F_{1,45.24}$=0.01, p=0.99) and year × sub-site ($F_{3,45.17}$=0.48, p=0.69) were not significant in the subsequent model and therefore were also dropped from the final model. In the final mass model the change in fish mass after introduction into cages increased with mass at introduction as expected ($F_{1,1527.00}$=127.61, p<0.0001) and differed between years ($F_{1,50.98}$=8.20, p=0.01). There was a significant interaction between type × sub-site ($F_{3,49.46}$=2.79, p=0.05), which precluded interpretation of the main effects of wetland type ($F_{1,6.00}$=0.25, p=0.63) and sub-site ($F_{3,49.46}$=8.15, p<0.001). Therefore, we performed Tukey pair-wise tests and found that the main differences in fish body mass occurred in the control wetland between the inlet and outlet and in the experimental wetland between the inlet of the shallow cell and both the outlet of the shallow cell and inlet of the deep cell (fig. 30).

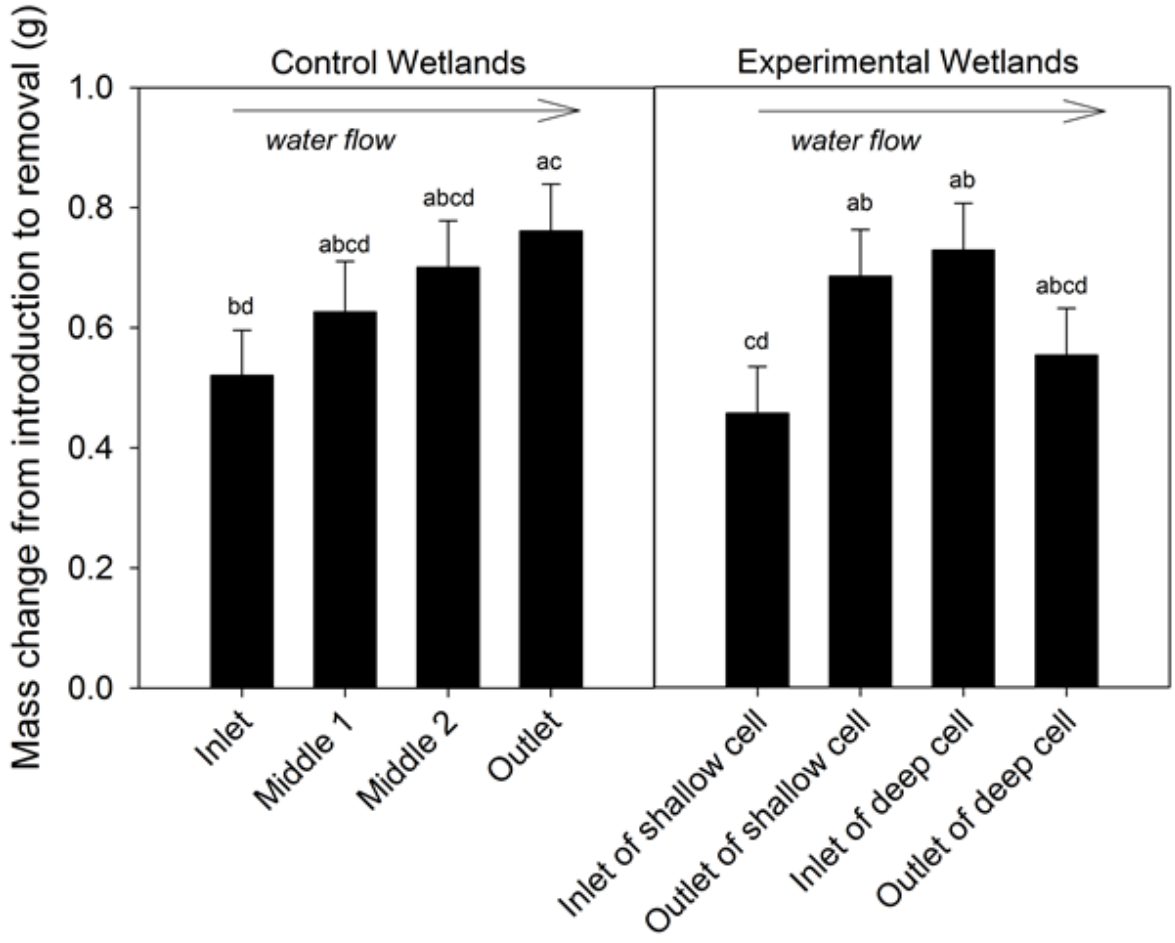

Figure 30. Change in mosquitofish body mass in grams (g) from the time of introduction to retrieval 30 days later among cage locations (sub-site) within control and treatment wetlands of the Cosumnes River Preserve mercury study during Year 1 and Year 2. Letters above bars denote ranking and significant differences among sub-sites, with bars sharing the same letter being not significantly different. Deployment during spring months (MAR–MAY).

In general, mosquitofish gained more mass the further into the wetland along the water flows path that they were caged, such that fish mass gain was highest at the control wetlands outlets and in the middle of the experimental wetlands. Mosquitofish THg concentrations were higher in experimental wetlands than in control wetlands during 2015, likely because of an associated increase in MeHg availability immediately following wetland construction activities. Although mosquitofish THg concentrations were higher during the year following wetland construction (2015), fish THg concentrations declined significantly in the treatment wetlands during the second year of study (2016), and in 2016 fish THg concentrations in treatment wetlands were no different than those of fish in the control wetlands. However, by Year 2 of the study, we still did not detect an effect of the deep cell reducing THg concentrations in fish compared to the shallow wetland cell upstream. We will continue to track the experiment's progress in year 3 of study, which we recently obtained funding from USGS to continue.

Ancillary Data and Results

Hydrology

Appendix 7 summizes cell specific hydrology, including dates of initiation for flood up and drawdown, the period of time a cell was considered full and how long it was maintained under flow-through conditions, and the hydraulic residence time (HRT). No differences were observed between Year 1 and Year 2, and the annual average HRT during flooding ranged from 27 days in shallow cells of treatment wetlands (flow-through), to 38 days in control wetlands (fill-and-maintain), and 51 days in deep cells of treatment wetlands.

Excitation Emissions Spectra

Fluorescence spectrometry provides information about the processes occurring within the wetland cells that affect DOM concentration and character (Coble 1996; Hansen and others, 2016). Each region of the excitation-emissions (EEM) spectra relates to specific structures within the DOM, for instance the region around ex360-em370 (FDOM) is used extensively as an indicator of DOC concentration because of relatively stable humic substance fluoresce in that region (Downing and others, 2009), whereas proteins and many DOM degradation intermediates fluoresce in the region around ex270–280 and em300–340 (peak B and peak T) making that area of the EEM spectra a good indicator of actively cycling organic materials (Coble 1996; Hansen and others, 2016). DOM character is an important factor in MeHg production (Graham and others, 2012; Moreau and others, 2015) and presumabely MeHg degradation as well. Thus, understanding how DOM changes can provide valuable information related to MeHg production and degradation.

Although EEMs can provide valuable indicators of source and processing, the ability to track changes in DOM within a (semi-)closed system, like impounded wetlands, using intensity ratios can provide more sensitive characterization of DOM and inform the processes that are affecting it—and the substances that interact with it—such as THg and MeHg. For instance, higher fluorescence in the peak N region was associated with higher MeHg concentrations in impounded wetlands and rice fields (Fleck and others, 2014).

When comparing the EEM intensity ratios of water exiting the shallow cells to the source water at the inlets (fig. 31*A*), there are clear region-specific responses indicating changes in DOM source and processing occurring within the shallow wetland cell. Although the ratios reflect an increase in DOM fluorescence across the entire spectra as DOM concentration increased (>1 across the EEM spectra), the greatest increases (~2.5 times) were focused in the spectral regions near peaks M and N and the deep

ultraviolet excitation wavelengths (fig. 31A). The focused increase in these specific regions indicates enhanced production of fresh organic material, likely of microbial origin (Coble 1996; Fleck and others, 2014). In contrast, the EEM intensity ratios at the outlet relative to the check weir (fig. 31*B*) indicate that as the water passes through the deep cell there is little additional change in the DOM character except for a focused decrease occurring in the peak Z region, which indicates photodegradation of the DOM and MeHg with passage through the deep cell (Fleck and others, 2014). These data support a doubling of microbially-generated DOM contributed by the shallow cell to the flow at the check weir, whereas passage through the deep cell suggest a loss (~40 percent) of DOM because of photodegradation with minimal changes to the microbial DOM pool. In combination, the whole field spectra ratios suggest a net doubling of microbially-derived (peak M and N) DOM and net increase (~40 percent) of photosensitive (peak Z) DOM from inlet to outlet (fig. 31*C*). If the relations between DOM spectra and MeHg are similar to previous work, this would suggest a similar trend would be likely for MeHg (Fleck and others, 2014). The use of EEM Intensity ratios may help provide a powerful screening tool that can aid the identification of enhanced MeHg production in different wetland types and aid the identification of time periods where MeHg production and photodegradation are most active.

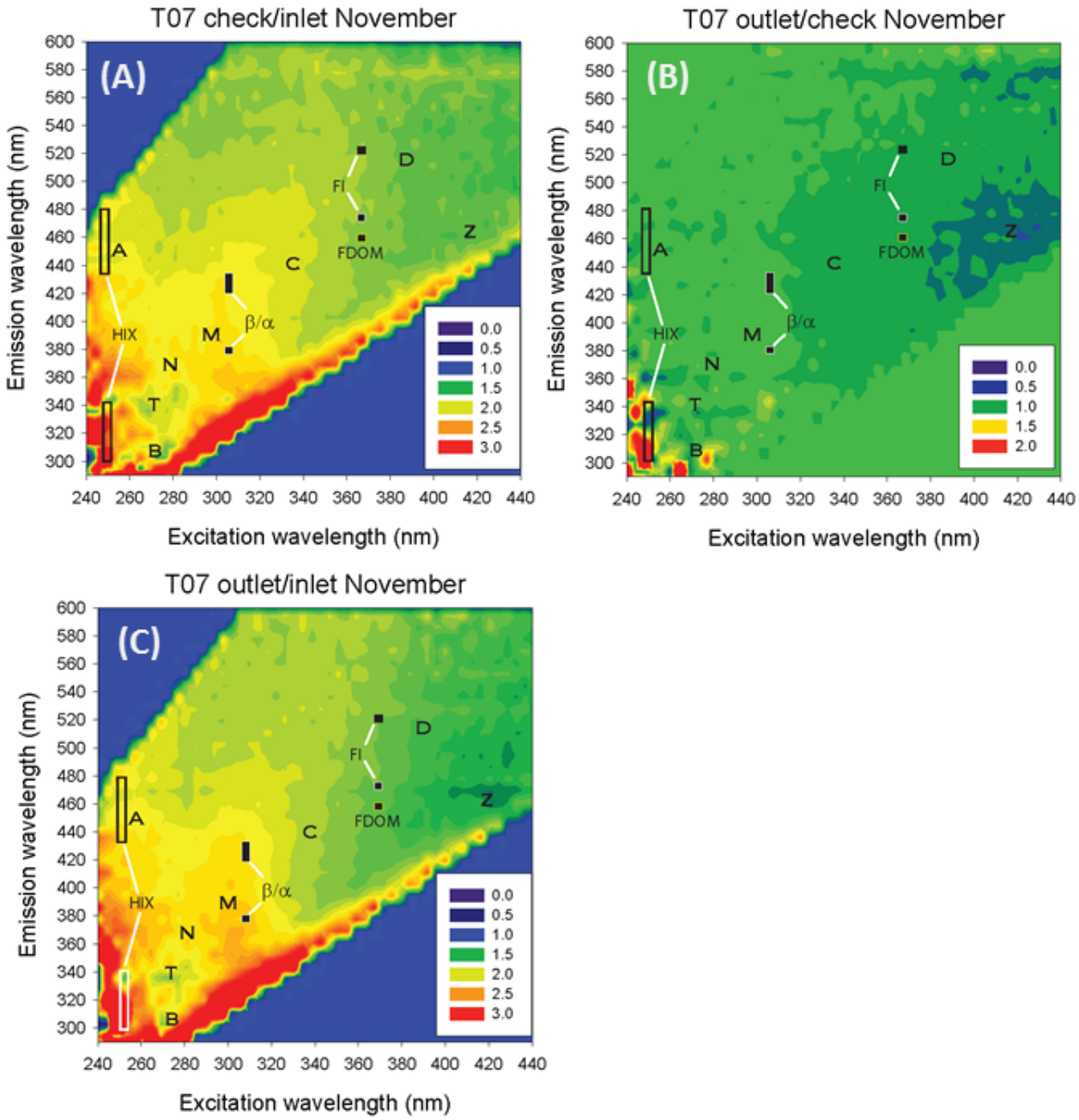

Figure 31. Excitation-Emissions (EEM) Spectra ratio plots for water control structure (WCS) comparisons in treatment wetland T07 of the Cosumnes River Preserve mercury study. The plots reflect the ratio of pairs of EEM spectra from natural water samples collected at the inlet, check and outlet WCS associated with treatment wetland T07. The ratios reflect the change in DOM fluorescence as the water passes through *A*, the shallow cell; *B*, the deep cell; and *C,* the entire field in combination. The letters on each plot reflect specific excitation–emission regions representative of known organic composition (see Fleck and others, 2014), and are used as points of comparison among the plots.

Water Isotopes

Surface water isotopic data (δ^2H and $\delta^{18}O$) provided important information with respect to relative residence times and preferential flow paths within each study cell. The δ^2H versus $\delta^{18}O$ data for the current study (fig. 32) plotted below the GMWL and LMWL (as expected), representative of evaporating water bodies. Isotopic values over the entire study area ranged from −58.11 to −35.19 ‰ with a median of -46.43‰ for δ^2H and −7.82 to −2.33‰ with a median of -5.67‰ for $\delta^{18}O$. Deuterium excess (d-excess=$\delta^2H - 8 \times \delta^{18}O$), an indicator of kinetic fractionation during evaporation, ranged from −22.3 to 6.69‰ with a median of -0.57‰. Lower d-excess values indicating greater evaporation. Surprisingly, the lowest d-excess values were observed in shallow cells of the flow-through treatment wetlands indicating hydrologically-trapped pools of water within the shallow cells.

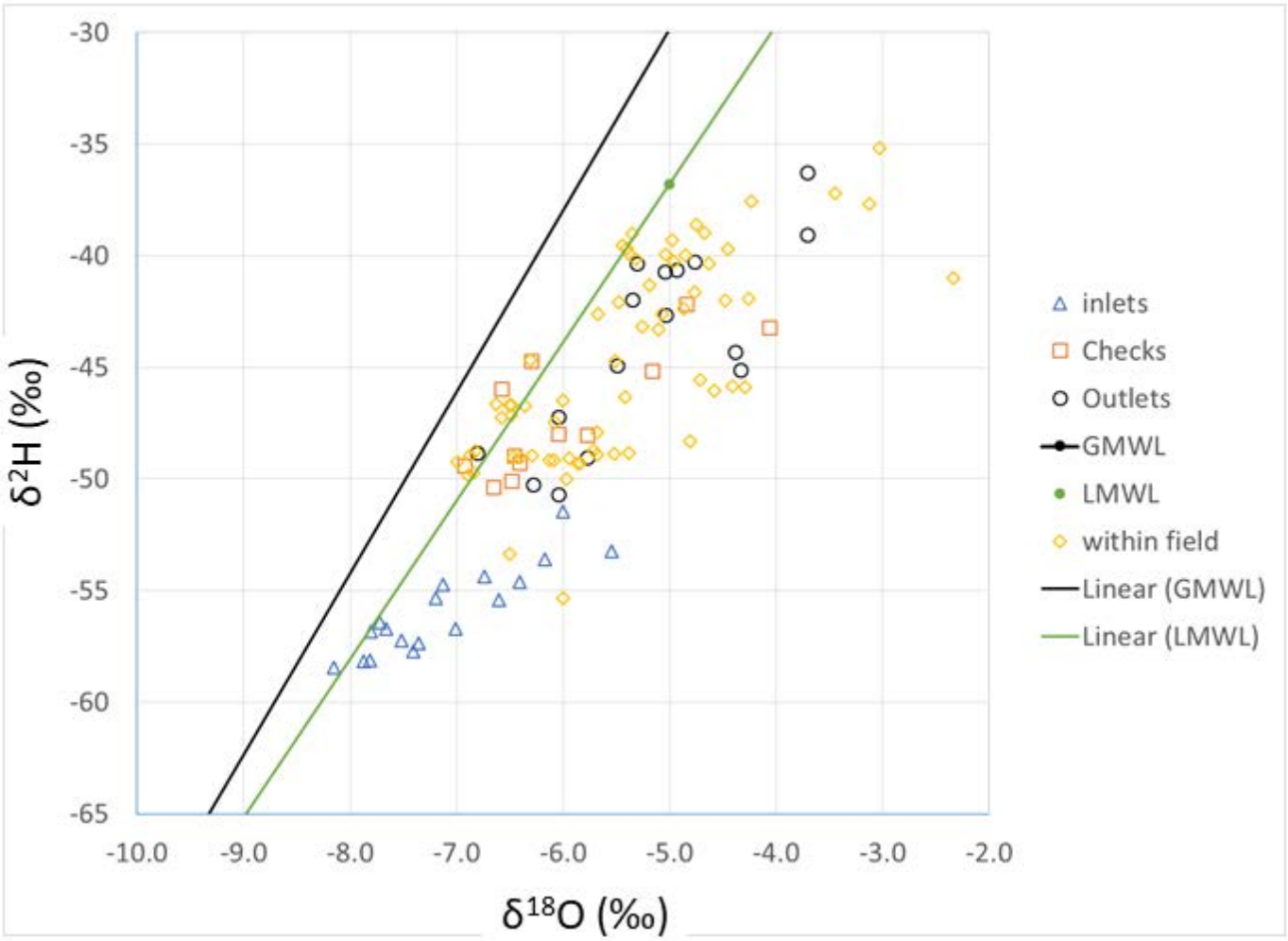

Figure 32. Plot of surface water δ^2H versus $\delta^{18}O$ isotopic data from the Cosumnes River Preserve mercury study. The δ^2H-$\delta^{18}O$ plot shows the Global Meteoric Water Line (GMWL, black line), the local meteoric water line (LMWL, green line), and data from this study by water control structure (WCS) type collected during February 8th and 19th, 2016; and within-field samples collected during February 23–24, 2016.

The contour maps of d-excess shown in fig. 33 illustrate the spatial variability in water residence times across the cells. The general observation that the shallow cells of the flow-through treatment wetlands have more prounounced preferential flow paths (S1, S7, S17 and to a degree S18) than do control wetlands (C02, C09, C13, C06) was expected. However, the observed differences in evaporation among control wetlands (fig. 33) was not expected, and likely reflect differences in hydrologic management such as the periodic pulsed refilling of C09 as compared with the more continuous trickle (maintain) employed for C13. Further, the influence of changing inlet source water isotopic signatures over time cannot be ruled out as having played a role in observed patterns. Finally, the d-excess spatial patterns also suggest preferred pathways for water flow in both shallow cells, but less so in the deep cells. Deep cell isotopic distributions appear more well mixed (recirculating flow) than shallow cell isotopic distributions (both control and treatment), which implies an effective surface area of the treatment wetlands' deep cells.

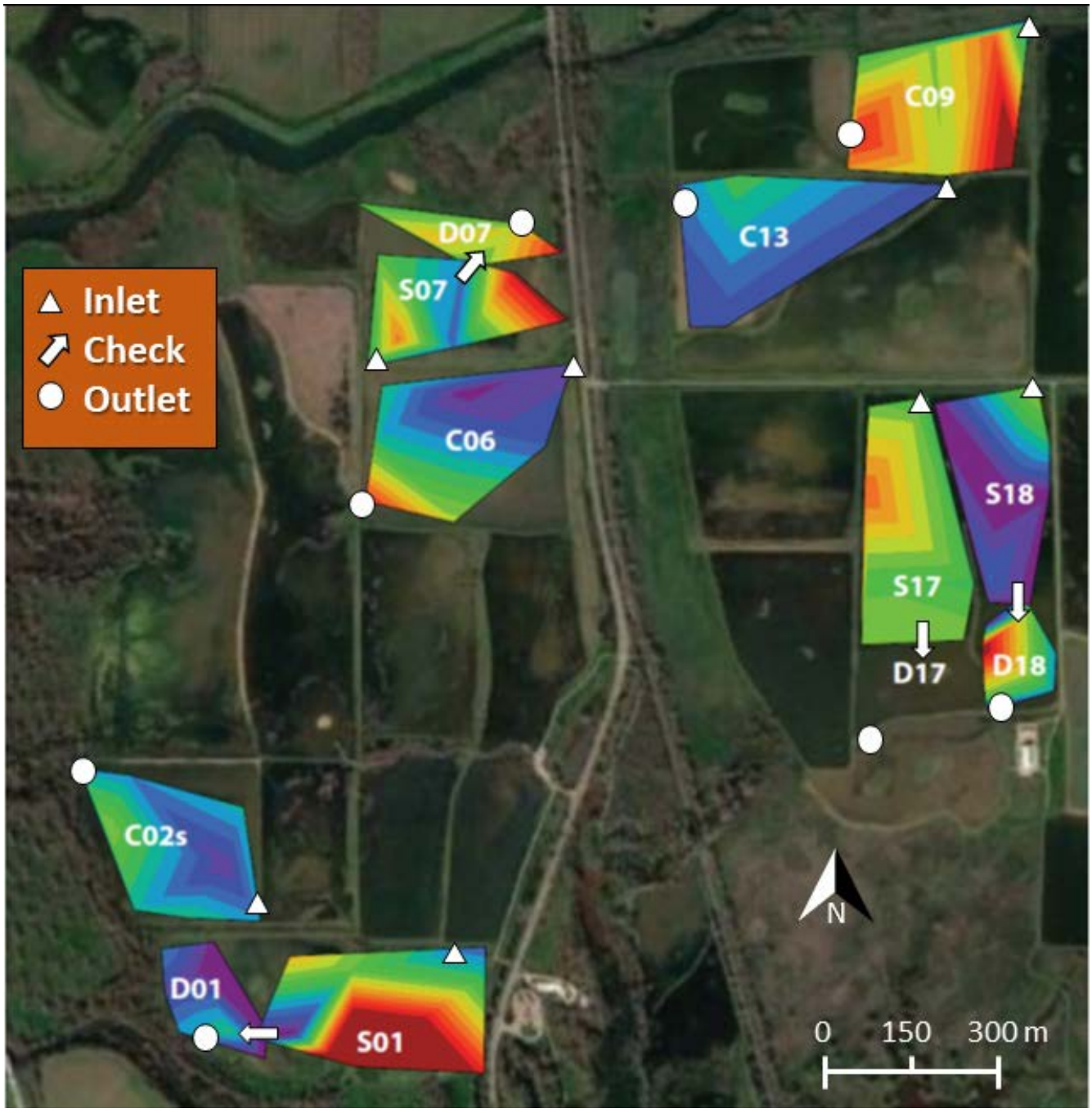

Figure 33. Contour maps of surface water δ-excess during February 2016 of the Cosumnes River Preserve mercury study. Isotopically depleted zones (blue end of the color spectrum) indicate comparatively fresh water zones, while less isotopically depleted areas (red end of the spectrum) indicate zones of evaporation and slower flow. These maps were used to identify relative residence times to locate preferential flow paths. Inlets, outlets and check weirs are identified, along with the flow direction (as per check weir arrow direction). Samples for D17 were lost, and thus no data exists for that cell. Base image retrieved from Google Earth..

These measurements of water flow (for example, plumbing) illustrate that flow paths can develop in shallow fields that limit the effective area of influence on load calculations, and thus also generate heterogeneity in surface water conditions. For example, freshwater inputs appear to have flowed strongly from inlets to check weirs in treatment wetlands bypassing a significant portion the landscape, which thus may have led to more, or less, export depending on the relative influence of wetland benthic fluxes. In contrast, deep cells appear more well mixed, with similar residence times among them. Mercury cycling processes within deep cells are thus appropriately extrapolated to the scale of the entire cell whereas the shallow cells may experience a bias because of differences in the effective and estimated water volumes contributing to the flow out of the cells. For shallow flow-through treatment cells, long residence times were observed in various sections of all fields, and export waters at the check were fairly fresh, indicating shorter residence times than the areal-average. Finally, deep cells showed limited evidence of evaporation from inlet to outlet, perhaps due in part to active wind-driven advective mixing throughout the cells.

Surface Sediment Characterization

Differences among cell type (control, treatment-shallow, treatment-deep) for surface sediment parameters were examined during 4 sampling events: a) before floodup in Year 1 (September 2014), b) 2 months after floodup in Year 1 (November 2014), c) end of flood season before drawdown in Year 1 (April 2015), and d) end of flood season before drawdown in Year 2 (May 2016). While controlling for sampling event, no significant differences were observed among cell types, except for lower organic matter (measured as %LOI) concentrations in the excavated deep cells compared to treatment shallow and control wetland types (appendix 8). In addition, sediment MeHg concentration and percentage of MeHg was significantly higher during all three sampling events conducted during flooded conditions compared to the pre-floodup conditions during September 2014, while controlling for cell type. However, there were significant Cell Type x EVENT interactions in the case of both parameters (appendix 8).

Significant differences among individual deep cells were observed for multiple sediment parameters (appendix 9). Most importantly, sediment THg and MeHg concentration and ambient MeHg production rates, were all significantly elevated in cell D01 (the cell location physically closest to the Cosumnes River) compared to the other three deep cells, while controlling for both Year and SEASON. The approach to pre-flooding vegetation management (discing or mowing) in the control wetlands and shallow portion of the treatment wetlands exhibited no significant effect on surface sediment Hg concentrations or speciation, but did show a small but significant difference in organic content (measured as %LOI), with higher concentrations for the mowed treatment compared to the disced treatment, while controlling for sampling event (appendix 10).

Conclusion

The current project provided a very detailed examination of a potentially promising wetland management option—the construction of deep cells along established flow paths—that could be employed to reduce MeHg export from, and bioaccumulation in, seasonal wetlands of the delta. We begin our concluding remarks by recasting the project's original hypothesis in terms of explicit statements of what we observed (or did not observe). We then conclude with some reflections on how various aspects of what we learned, challenges we encountered, and how these might inform next steps:

Hypotheses Revisited

- HYP.1: The presence of open-water deep cells *did* lower net MeHg and THg export from the deep cell of the treatment wetlands, compared to the shallow cell of the treatment wetlands. In part because of their higher hydrologic flow rates, treatment wetlands overall (shallow cells + deep cells) *did not* exhibit lower MeHg export compared to the control wetlands. The efficacy of the deep cells in reducing MeHg export an average of 37 percent (n=8) and ranged from 5 to 62 percent across individual sites and both years (n=8). Evidence of active processes of removal were documented, including an average 7 percent loss through photodemethylation and a 24 percent loss through particulate settling. Calculated at the whole field scale for treatment wetlands, the 69±26 mg of MeHg exported annually by shallow treatment cells, was reduced by 34±9 mg across both years, leading to a full 50 percent reduction in potential export by deepwater cells under flow-through conditions (net export=35±19 mg MeHg).
- HYP.2: The presence of deep-water cells *did not* reduce THg bioaccumulation in caged fish at the outlet of the deep-water cell, neither relative to the outlet of the shallow wetland cell upstream of the deep-water cell nor relative to the outlet of the control wetlands. Hydrologic flow path analysis and similarities in water conditions (for example, aqueous MeHg concentrations) between check and outlet concentrations imply active advective mixing, and thus it is not surprising that Hg bioaccumulation was similar within the well-mixed cell. It is important to note that bioaccumulation was only measured in spring (March to May), at a point when aqueous MeHg concentrations were not significantly different between check and outlet locations.
- HYP.3: The hydrologic flow-through management conditions tested in this study *did not* result in lower surface water MeHg concentrations in shallow flow-through treatment wetlands, compared to the fill-and-maintain control wetlands. Concentrations of all aqueous Hg species were found to be higher at wetland outlets, compared to wetland inlets, across all wetlands regardless of hydraulic residence time.
- HYP.4: The hydrologic flow-through management conditions tested in this study *did* result in increased surface water MeHg and THg loads from the shallow portion of the flow-through treatment wetlands, compared to the fill-and-maintain control wetlands. Hydrologic loads drove the aqueous Hg load patterns far more than differences in concentrations of different Hg species.
- HYP.5: The hydrologic flow-through management conditions tested in this study *did not* result in lower fish THg concentrations in the shallow treatment cells upstream of the deep-water treatment cells, or relative to the control wetlands.

Reflections on Lessons Learned, Challenges Encountered and Going Forward

This unique landscape manipulation study, designed to answer key questions related to minimizing MeHg export and bioaccumulation, has generated a valuable and detailed geochemical dataset for both Hg and non-mercury metrics, including key water quality parameters and process-based rate measurements. As with any complex field study, there were a number of surprising results and lessons learned. The bulleted text below attempts to interweave comments on lessons learned and problems encountered with thoughts on next steps. In doing so the authors hope to help guide and stimulate the thinking of both resource managers and scientists to move these ideas and potential implementation studies forward.

Key Lessons Learned

- The deep cells effectively worked in terms of lowering MeHg export load under flow-through conditions, although variation in efficiency and the relative importance of various removal mechanisms varied appreciably. More study is required to better understand what drives this cell-to-cell variability.
- The hypothesized decrease in fish bioaccumulation as a function of flow-through management did not work out. It is not totally clear why this is, but not having sufficiently high flow rates is suspected. Increasing flow rates even further to achieve some measureable decrease in bioaccumulation in a future study may not be practical or even desirable, because of other BLM considerations. See BLM Addendum (McQuillen, CVWQRB Agreement 13-504-255 Addendum).
- Particulate cycling within the deep cell setting is much more dynamic, complicated, and difficult to measure than we had anticipated. However, the implication is that this dynamic process likely plays a key role in the relative efficiency of MeHg removal in the deep cells. The data collected strongly suggests that there are often large shifts in MeHg and THg partitioning between the dissolved phase within the deep cells, which can change both temporally and spatially, likely because of changing particulate concentrations, composition and other geochemical conditions. Better understanding these processes will be valuable to any future studies of deep cell effectiveness for Hg trapping.
- The unexplained proportion of the MeHg loads budget, relative to inputs, varied widely (±30 percent) among the four cells over two years (n=8). Future studies should work to narrow this unaccounted for fraction by continuing to focus on understanding internal processes.

Key Challenges

- Measurements of particulate vertical flux in the deep cells. While considerable resources and time were spent trying to get reasonable short- and long-term vertical flux rates for particulates (and associated p.MeHg and p.THg), internal processes such as wind driven resuspension and levee erosion within these shallow ponded settings largely frustrated these efforts. Instead of using this hard won data, we needed to rely on the simple changes in particulate concentrations between inlets and outlets to inform our MeHg load budgets for the deep cells.
- Establishing, maintaining and documenting consistent targeted flow regimes. This is always challenging for many reasons. The time and resources necessary for maintaining precisely targeted conditions needed for a highly quantitative process level study of this type is always going to be more demanding than might typically be the case under normal wetland management regimes.

New Question Raised

- We saw the biggest concentrations and loads in MeHg in the period soon after flood up. It is suspected that some of this is because of the release of old MeHg baked into the sediment since the end of the last wet season. What is the balance of new MeHg production versus the release of previously preserved MeHg during the period immediately following flood up?
- How does this early flood season spike affect MeHg uptake into the base of the food web? That is an important question not addressed in the current study, as the fish cage experiments were conducted during the late flooded period (March to May).

- Deep cell stabilization timeframe: We observed some fairly large differences in Hg dynamics between Year 1 and Year 2 in some of the deep cells (particularly D01). It was anticipated that during the first year following the deep cell construction that we might see conditions reflecting the recent site disturbance. While we have a hint that this is true because of the Year 2 data collected, we really have no clear sense of how long it takes for one of these newly created deep cells to reach something approaching a stable condition. One full flooded season? Two? Ten? This points to the importance of maintaining at least some baseline monitoring program at the CRP associated with these unique deep cells, which allow quantification of loads and process measurements.
- What are the roles, importance, and underlying mechanisms involved in particulate resuspension events and how they affect Hg partitioning and removal in the deep cell setting?
- If there is a movement towards a single hydrologic management regime that reflects something more like the fill-and-trickle design described in Thoughts for Next Phase Studies and Improved Study Design below, is there a scenario where this can be employed while at the same time still decreasing the amount of bioaccumulation that occurs (in both the deep and shallow cells)? This is an open question. However, one management variable that could be manipulated to achieve this goal would be how vegetation is managed in both the shallow and deep cells prior to flood up. Bioaccumulation studies (fish cages, wild populations and base of food web) will all need to be critical components of answering these questions in any future work in this area.

Thoughts for Next Phase Studies and Improved Study Design

- More replication of wetland cells with a more simplified design that employs a single hydrologic flow regime for both control and treatment wetlands; see 'Fill-and-trickle' below.
- Fill-and-trickle: A key concern of wetland managers often has to do with water conservation and usage costs. However, some amount of water flow is also important to any quantitative hydrologic study researching Hg export and bioaccumulation using the deep cell design. In the current study, we employed two different hydrologic management modes, which made field site management, field sampling, and data analysis both more interesting and challenging. A simpler approach in the future would be to employ a singular fill-and-trickle management to both treatment and control wetland. This regime would use a little more flow (low and constant) than the current fill-and-maintain mode, while also using lower flows rates relative to those employed on the treatment wetlands.
- Treatment Wetland Design: The design of next generation deep cells should employ a number of changes that would make the implementation by managers more practical and likely. A primary step in this direction would be eliminating the check levee separating the shallow and deep cell, which would greatly reduce initial construction costs and long-term maintenance. This design change would result in a more gradual slope between shallow and deep ends of the wetland cell. It would also potentially decrease field sampling and analytical cost as it removes 1/5 of the WCS (check levee weir) used in the current design.
- Deep Cell Location and Depth: One thing that was surprising in the current study was the big differences we observed among the four deep cells, in terms of Hg concentrations and transformations. Cell D01 in particular was quite different from the other three in that it had much higher uf.MeHg loads into the deep cell (in Year 2), as well as higher potential rates of microbial MeHg degradation. Cell D01 was closest to the Cosumnes River, a situation that might have played a role. It is possible that the distribution of historic floodplain deposits and their relative amount of Hg contamination may have played a role here. Thus, understanding the

relation of deep cell depth and its placement along a flowpath relative to any areas or subsurface zones of known elevated mercury contamination, will be important things to consider for any similar implementation studies or BLM actions going forwards.

- Assessing MeHg benthic flux: Of the three main loss terms measured in the current study, loss to the benthos, not directly related to particulate flux, proved to be the one with the most uncertainty. While the bottle incubations conducted were instructive for examining potential rates of MeHg degradation and the change in the ambient Hg pool to assess NET MeHg production/degradation, they were not able to supply relevant information on the physical flux of f.MeHg between the benthos and overlying water. Instead, we relied on some crude estimates of diffusion, calculated from sediment kd values statistically gleaned from the published literature and used to back-calculate (estimate) porewater f.MeHg concentrations. Future studies would do well to collect and measure porewater MeHg concentrations directly (or employ benthic flux chambers), which will provide much more reliable measurements of this potentially important parameter. While our estimate did suggest the f.MeHg flux between the benthos and surface water is small relative to the input of all uf.MeHg to the deep cell, there is some degree of uncertainty regarding these estimates. In addition, for most cells we did have minor to moderate (-3 to 31 percent) unexplained contributions to MeHg loads that potentially could be explained by benthic flux if our current estimates are too far off.
- Bioaccumulation studies—Seasonal Considerations: In the current study we saw the biggest MeHg concentrations and loads during the period following flood up (SEP-NOV). However, fish cage studies were conducted during the late flood period (MAR-MAY) when MeHg concentrations in the water were comparatively low and no strong treatment affect was observed in the fish cage studies. Thus, there is no information on food web bioaccumulation during the early- and mid-flooding periods that would be informed by all of the non-biota work that is also being done on those seasonal time steps. Future studies should consider having at least some parallel bioaccumulation research that complements the non-biotic field work that is happening during these flood up periods.
- Bioaccumulation studies—Base of Foodweb: One approach that could be done in parallel with the non-biological field work, and is less resource intensive than the fish cages, would be to collect base of foodweb organisms via plankton tows, light traps, and such to help better define the seasonal changes that might be happening at that lower trophic level alongside the seasonal changes we see for non-biotic parameters.
- In the current study, we put some limited effort towards better characterizing spatial and temporal changes in the DOC pool quality, using some fairly sophisticated approaches (for example, EEM spectra, see fig. 31). Since we know that DOC is of critical importance in Hg cycling and the information that we did collect suggests big changes in DOC quality moving from the shallow to the deep portions of the treatment wetlands, future work might more fully employ these techniques and leverage their information to better understand what drives Hg partitioning and removal within the deep cell setting.

Acknowledgments

This project was supported by funding through the U.S. Environmental Protection Agency (EPA 319(h), CA State Agreement# 13-504-255) and the California Department of Fish and Game (Grant# E1483002), with in-kind federal matching funds from the following U.S. Geological Survey programs: Toxics, National Research Program, and the CA Water Science Center . The authors would like to thank the team of USGS field and laboratory staff that made this study possible, including: Jennifer L. Agee, Le H. Kieu, Evangelos Kakouros, Michelle Arias, Melissa Mooradian, Vivian Underhill, Renee Wang, Sara Peek (Menlo Park, CA); Erica Schmidt (CA-WSC, Sacramento, CA); Matt Toney, Mark Herzog, Alex Hartman, Breanne Cooney, Sarah Peterson (WERC, Dixon, CA) and others (FERC, Corvalis, OR). The authors would also like to following BLM staff who contributed to the field preparation and maintanance: Mariah Brumbaugh, Mark Ackerman, and Jeff Babcock, as well as Sara Sweet of the Nature Conservancy, with assistance in CRP collection and sampling permits. Review of this report by Janis Cooke (CVRWQCB) and Peter Weiss-Penzias (UCSC) greatly improved this document.

References Cited

Ackerman, J.T., and Eagles-Smith, C.A., 2010, Agricultural wetlands as potential hotspots for mercury bioaccumulation—Experimental evidence using caged fish: Environmental Science and Technology, v. 44, no. 4, p. 1,451–1,457.

American Public Health Association, 1981a, Section 209 C—Total Nonfiltrable Residue Dried at 103–105 ºC., *in* Franson, M.A.H., ed., Standard methods for the examination of water and wastewater, 15th Edition: Washington, D.C., American Public Health Association, American Water Works Association, Water Pollution Control Federation.

American Public Health Association, 1981b, Section 209 G—Volatile and Fixed Matter in Nonfilterable Residue and in Solid and Semisolid Samples, *in* Franson, M.A.H., ed., Standard methods for the examination of water and wastewater, 15th Edition: Washington, D.C., American Public Health Association, American Water Works Association, Water Pollution Control Federation.

Bachand, P.A.M., Bachand, S.M., Fleck, J.A., Anderson, F., and Windham-Myers, L., 2014, Differentiating transpiration from evaporation in seasonal agricultural wetlands and the link to advective fluxes in the root zone: Science of the Total Environment, v. 484, p. 232–248.

Chalmers, A., Marvin-DiPasquale, M.C., Degnan, J.R., Coles, J., Agee, J.L., and Luce, D., 2013, Characterization of mercury contamination in the Androscoggin River, Coos County, New Hampshire: U.S. Geological Survey Open-File Report 2013-1076, 58 p., also available at https://pubs.er.usgs.gov/publication/ofr20131076.

Coble, P.G., 1996, Characterization of marine and terrestrial DOM in seawater using excitation–emission matrix spectroscopy: Marine Chemistry, v. 51, no. 4, p. 325–346.

Craig, H., 1961, Isotopic variations in meteoric waters: Science, v.133, no 3465, p. 1,702−1,703.

DeWild, J.F., Olson, M.L., and Olund, S.D., 2002, Determination of methyl mercury by aqueous phase ethylation, followed by gas chromatographic separation with cold vapor atomic fluorescence detection: U.S. Geological Survey Open-File Report 2001-445, 14 p., also available at https://pubs.er.usgs.gov/publication/ofr2001445.

Downing, B.D., Bergamaschi, B.A., Kendall, C., Kraus, T.E., Dennis, K.J., Carter, J.A., and Von Dessonneck, T.S., 2016, Using continuous underway isotope measurements to map water residence time in hydrodynamically complex tidal environments: Environmental Science and Technology, v. 50, no. 24, p. 13,387–13,396.

Downing, B.D, Boss, E., Bergamaschi, B.A, Fleck, J.A., Lionberger, M.A., Ganju, N.K., Schoellhamer, D.H., and Fujii, R., 2009, Quantifying fluxes and characterizing compositional changes of dissolved organic matter in aquatic systems in situ using combined acoustic and optical measurements: Limnology and Oceanography—Methods, v. 7, no. 1, p. 119–131.

Eagles-Smith, C.A., Ackerman, J.T., Fleck, J., Windham-Myers, L., McQuillen, H., and Heim, W., 2014, Wetland management and rice farming strategies to decrease methylmercury bioaccumulation and loads from the Cosumnes River Preserve, California: U.S. Geological Survey Open-File Report 2014-1172, 42 p., also available at https://pubs.er.usgs.gov/publication/ofr20141172.

Fleck, J.A., Gill, G., Bergamaschi, B.A., Kraus, T.E.C., Downing, B.D., and Alpers, C.N., 2014, Concurrent photolytic degradation of aqueous methylmercury and dissolved organic matter: Science of the Total Environment, v. 484, p. 263–275.

Fleming, E.J., Mack, E.E., Green, P.G., and Nelson, D.C., 2006, Mercury methylation from unexpected sources—Molybdate-inhibited freshwater sediments and an iron-reducing bacterium: Applied and Environmental Microbiology, v. 72, no. 1, p. 457–464.

Gasper, J.D., Aiken, G.R., and Ryan, J.N., 2007, A critical review of three methods used for the measurement of mercury (Hg^{2+})-dissolved organic matter stability constants: Applied Geochemistry, v. 22, no. 8, p. 1,583–1,597.
Gill, G.A., Bloom, N.S., Capellino, S., Driscoll, C.T., Dobbs, C., McShae, L., Mason, R., and Rudd, J.W.M., 1999, Sediment-water fluxes of mercury in Lavaca Bay, Texas: Environmental Science and Technology, v. 33, no. 5, p. 663–669.
Gilmour, C.C., Henry, E.A., and Mitchell, R., 1992, Sulfate stimulation of mercury methylation in freshwater sediments: Environmental Science and Technology, v. 26, no. 11, p. 2281–2287.
Graham, A.M., Aiken, G.R., and Gilmour, C.C., 2012, Dissolved organic matter enhances microbial mercury methylation under sulfidic conditions: Environmental Science and Technology, v. 46, no. 5, p. 2,715–2,723.
Hansen, A.M., Fleck, J.A., Downing, B.D., Kraus, T., von Dessonneck, T., and Bergamschi. B.A., in press, Procedures for the measurement of absorbance and fluorescence from dissolved organic matter using the Horiba Scientific AquaLog® Fluorometer: U.S. Geological Survey Open-File Report 2018-1096, will be available at https://pubs.er.usgs.gov/publication/ofr20181092.
Hansen, A.M., Kraus, T.E.C., Pellerin, B.A., Fleck, J.A., Downing, B.D., and Bergamaschi, B.A., 2016, Optical properties of di
ssolved organic matter (DOM)—Effects of biological and photolytic degradation: Limnology and Oceanography, v. 61, no. 3, p. 1,015–1,032.
Heald, C.C., ed., 2002, Cameron hydraulic data book: Flowserve Corporation.
Jeffres, C.A., Opperman, J.J., and Moyle, P.B., 2008, Ephemeral floodplain habitats provide best growth conditions for juvenile Chinook salmon in a California river: Environmental Biology of Fishes, v. 83, no. 4, p. 449–458.
Kendall, C., Silva, S.R., and Kelly, V.J., 2001, Carbon and nitrogen isotopic compositions of particulate organic matter in four large river systems across the United States: Hydrological Processes, v. 15, no. 7, p. 1,301–1,346.
Kerin, E.J., Gilmour, C.C., Roden, E., Suzuki, M.T., Coates, J.D., and Mason, R.P., 2006, Mercury methylation by dissimilatory iron-reducing bacteria: Applied and Environmental Microbiology, v. 72, no. 12, p. 7,919–7,921.
Lerman, A., 1979, Geochemical processes—Water and sediment environments: New York, John Wiley and Sons, 481 p.
Lewis, M.E., and Brigham, M.E., 2004, Low Level Mercury (ver. 1.0): U.S. Geological Survey Techniques of Water-Resources Investigations, book 9, chap. A5., sec. 5.6.4.B, October 2004, accessed March 1, 2017, at https://water.usgs.gov/owq/FieldManual/chapter5/pdf/5.6.4.B_v1.0.pdf.
Lutz, M.A., Brigham, M.E., and Marvin-DiPasquale, M., 2008, Procedures for collecting and processing streambed sediment and pore water for analysis of mercury as part of the National Water-Quality Assessment Program: U.S. Geological Survey Open-File Report 2008-1279, 69 p., also available at https://pubs.er.usgs.gov/publication/ofr20081279.
Marvin-DiPasquale, M., Agee, J., Bouse, R., and Jaffe, B., 2003, Microbial cycling of mercury in contaminated pelagic and wetland sediments of San Pablo Bay, California: Environmental Geology, v. 43, no. 3, p. 260–267.
Marvin-DiPasquale, M., Agee, J., McGowan, C., Oremland, R.S., Thomas, M., Krabbenhoft, D., and Gilmour, C., 2000, Methyl-mercury degradation pathways—A comparison among three mercury-impacted ecosystems: Environmental Science and Technology, v. 34, no. 23, p. 4,908–4,916.
Marvin-DiPasquale, M., and Agee, J.L., 2003, Microbial mercury cycling in sediments of the San Francisco Bay-Delta: Estuaries, v. 26, no. 6, p. 1,517–1,528.

Marvin-DiPasquale, M., Agee, J.L., Kakouros, E., Kieu, L.H., Fleck, J.A., and Alpers, C.N., 2011, The effects of sediment and mercury mobilization in the South Yuba River and Humbug Creek confluence area, Nevada County, California—Concentrations, speciation and environmental fate—Part 2—Laboratory Experiments: U.S. Geological Survey Open-File Report 2010-1325-B, 53 p., also available at https://pubs.er.usgs.gov/publication/ofr20101325B.

Marvin-DiPasquale, M., Alpers, C.N., and Fleck, J.A., 2009, Mercury, methylmercury, and other constituents in sediment and water from seasonal and permanent wetlands in the Cache Creek Settling Basin and Yolo Bypass, Yolo County, California, 2005−06: U.S. Geological Survey Open-File Report 2009-1182, 69 p., also available at https://pubs.er.usgs.gov/publication/ofr20091182.

Marvin-DiPasquale, M.C., and Oremland, R.S., 1998, Bacterial methylmercury degradation in Florida Everglades peat sediment: Environmental Science and Technology, v. 32, no. 17, p. 2,556–2,563.

Marvin-DiPasquale, M., Stewart, R., Fisher, N.S., Pickhardt, P., Mason, R.P., Heyes, A., and Winham-Myers, L., 2007, Evaluation of mercury transformations and trophic transfer in the San Francisco Bay/Delta—Identifying critical processes for the ecosystem restoration program—Final Report for Project # ERP-02-P40: Submitted to the California Bay-Delta Authority (CBDA), Sacramento, California.

Marvin-DiPasquale, M., Windham-Myers, L., Agee, J.L., Kakouros, E., Kieu, L.H., Fleck, J., Alpers, C.N., and Stricker, C.A., 2014, Methylmercury production in sediment from agricultural and non-agricultural wetlands in the Yolo Bypass, California, USA: Science of the Total Environment, v. 484, p. 288–299.

Marvin-DiPasquale, M., Lutz, M.A., Brigham, M.E., Krabbenhoft, D.P., Aiken, G.R., Orem, W.H., and Hall, B.D., 2009, Mercury cycling in stream ecosystems. 2. Benthic methylmercury production and bed sediment—pore water partitioning: Environmental Science and Technology, v. 43, no. 8, p. 2,726–2,732.

Matthes, W.J., Jr., Sholar, C.J., and George, J.R., 1992, Quality-assurance plan for the analysis of fluvial sediment by laboratories of the U.S. Geological Survey: U.S. Geological Survey Open-File Report 91-467, 31 p., also available at https://pubs.er.usgs.gov/publication/ofr91467.

McCord, S.A., and Heim, W.A., 2015, Identification and prioritization of management practices to reduce methylmercury exports from wetlands and irrigated agricultural lands: Environmental Management, v. 55, no. 2, p. 725–740.

Moreau, J.W., Gionfriddo, C.M., Krabbenhoft, D.P., Ogorek, J.M., DeWild, J.F., Aiken, G.R., and Roden, E.E., 2015, The effect of natural organic matter on mercury methylation by Desulfobulbus propionicus 1pr3, Frontiers in Microbiol, v. 6, art. 1389, 15 p.

Olund, S.D., DeWild, J.F., Olson, M.L., and Tate, M.T., 2004, Methods for the preparation and analysis of solids and suspended solids for total mercury: U.S. Geological Survey Techniques and Methods, book 5, chap. A8, accessed March 15, 2017, at https://pubs.usgs.gov/tm/2005/tm5A8/.

Potter, B.B., and Wimsatt, J.C., 2005, Method 415.3 Determination of total organic carbon and specific UV absorbance at 254 nm in source water and drinking water: U.S. Environmental Protection Agency Document #: EPA/600/R-05/055, rev. 1.1

Poulin, B.A., Ryan, J.N., and Aiken, G.R., 2014, Effects of iron on optical properties of dissolved organic matter: Environmental Science and Technology, v. 48, no. 17, p. 10,098–10,106.

Rouleau, C., and Block, M., 1997, Fast and high-yield synthesis of radioactive (CH3Hg)-Hg-203(II): Applied Organometallic Chemistry, vol. 11, no. 9, p. 751–753.

Schwankl, L.J., Prichard, T.L., and Hanson, B.R., 2007, Measuring applied water in surface-irrigated orchards: University of California, Davis, Agricultural and Natural Resources Publication 8230, 10 p.

Seavy, N.E., Viers, J.H., and Wood, J.K., 2009, Riparian bird response to vegetation structure—A multiscale analysis using LiDAR measurements of canopy height: Ecological Applications, v. 19, no. 7, p. 1,848–1,857.
Seber, G.A.F., 1982, The estimation of animal abundance and related parameters (2d ed): London, Charles Griffin and Company, 654 p.
Strickland, J.D.H., and Parsons, T.R., 1972, A practical handbook of seawater analysis: Ottawa, Canada, Fisheries Research Board of Canada, 310 p.
U.S. Bureau of Reclamation, 2001, Water measurement manual—A water resources technical publication: United States Department of Interior, Bureau of Reclamation.
U.S. Environmental Protection Agency, 2001, Method 1630: Methyl mercury in water by distillation, aqueous ethylation, purge and trap, and CVAFS: U.S. Environmental Protection Agency, 45 p.
U.S. Environmental Protection Agency, 2002, Method 1631, Revision E—Mercury in water by oxidation, purge and trap, and cold vapor atomic fluorescence spectrometry: U.S. Environmental Protection Agency, 38 p.
U.S. Environmental Protection Agency, 2005, EPA Method 415.3 Rev 1.1—Determination of total organic carbon and specific UV absorbance at 254 nm in source water and drinking water: U.S. Environmental Protection Agency.
U.S. Environmental Protection Agency, 2007a, Method 9056A—Determination of inorganic anions by ion chromatography (Rev. 1.0): U.S. Environmental Protection Agency, 19 p.
U.S. Environmental Protection Agency, 2007b, Method 7473—Mercury in solids and solutions by thermal decomposition, amalgamation, and atomic absorption spectrophotometry: U.S. Environmental Protection Agency 17 p.
University of California Agriculture and Natural Resources, 2016, Weather, models, & degree-days: University of California Agriculture and Natural Resources web page, accessed November 7, 2016, at http://ipm.ucanr.edu/WEATHER/index.html.
Weishaar, J.L., Aiken, G.R., Bergamaschi, B.A., Fram, M.S., and Fujii, R., 2003, Evaluation of specific ultraviolet absorbance as an indicator of the chemical composition and reactivity of dissolved organic carbon: Environmental Science and Technology, v. 37, no. 20, p. 4,702–4,708.
Wiener, J.G., Gilmour, C.C., and Krabbenhoft, D.P., 2003, Mercury strategy for the bay-delta ecosystem—A unifying framework for science, adaptive management, and ecological restoration: La Crosse, Wis., University of Wisconsin-La Crosse, 60 p.
Windham-Myers, L., Fleck, J.A., Ackerman, J.T., Marvin-DiPasquale, M., Stricker, C.A., Heim, W.A., Bachand, P.A., Eagles-Smith, C.A., Gill, G., Stephenson, M., and Alpers, C.N., 2014a, Mercury cycling in agricultural and managed wetlands—A synthesis of methylmercury production, hydrologic export, and bioaccumulation from an integrated field study: Science of the Total Environment, v. 484, p. 221–231.
Windham-Myers, L., Marvin-DiPasquale, M., Kakouros, E., Agee, J.L., Kieu, L.H., Stricker, C.A., Fleck, J.A., and Ackerman, J.T., 2014b, Mercury cycling in agricultural and managed wetlands of California, USA— Seasonal influences of vegetation on mercury methylation, storage, and transport: Science of the Total Environment, v. 484: 308–318.
Windham-Myers, L., Marvin-DiPasquale, M., Krabbenhoft, D.P., Agee, J.L., Cox, M.H., Heredia-Middleton, P., Coates, C., and Kakouros, E., 2009, Experimental removal of wetland emergent vegetation leads to decreased methylmercury production in surface sediment: Journal of Geophysical Research—Biogeosciences, v.114, no. G2.

Wood, M.L., Foe, C., Cooke, J., and Louie, S.J., 2010, Sacramento-San Joaquin Delta Estuary TMDL for Methylmercury—Staff Report: Sacramento, Calif., Regional Water Quality Control Board—Central Valley Region.

YSI, 2012, EXO User Manual—Advanced Water Quality Monitoring Platform: Yellow Springs, Ohio, YSI Incorporated, 153 p.

Zillioux, E.J., Porcella, D.B. and Benoit, J.M., 1993, Mercury cycling and effects in freshwater wetland ecosystems: Environmental Toxicology and Chemistry, v. 12, no. 12, p. 2,245–2,264.

Appendixies 1–10.

Appendixes 1–10 are presented as Excel table files, and are available for download on the report index page at https://doi.org/10.3133/ofr20181092.

- Appendix 1. Summary of Quality Assurance Results Associated with Surface Water and Sediment Parameters.
- Appendix 2. Surface Water Total Mercury and Methylmercury Data, by Field ID, WCS, and Date.
- Appendix 3. MODEL A.1: Least Squares Mixed Model Results for Surface Water Parameters, Comparing Differences among Study Year, Season and WCS Type.
- Appendix 4. MODEL B: Least Squares Mixed Model Results for Surface Water Parameters, Comparing Differences among WCS Type, by Season.
- Appendix 5. MODEL C: Least Squares Mixed Model Results for Surface Water Parameters, Comparing Differences among WCS Type, by Year.
- Appendix 6. MODEL A.2: Least Squares Mixed Model Results for Surface Water Filtered, Particulate, and Unifiltered THg and MeHg Concentrations and MeHg Daily Loads
- Appendix 7. Summary of Hydrology, by Cell and Study Year.
- Appendix 8. MODEL E: Least Squares Mixed Model Results for Surface Sediment Parameters, Comparing Treatment versus Control Sites and Sampling Events.
- Appendix 9. MODEL F: Least Squares Mixed Model Results for Deep Cell Sediment Parameters, by Cell.ID, Year, Season.
- Appendix 10. MODEL G: Least Squares Mixed Model Results for Surface Sediment Parameters, Comparing Vegetation Management Rractices (Disced versus Mowed) and Sampling Event in Control and Shallow Treatment Cells.

ISSN 2331-1258 (online)
https://doi.org/10.3133/ofr20181092